Numerical investigation of discrete breather dynamical properties in several ordered and disordered nonlinear lattices.

Panagiotis Maniadis

Department of Physics

University of Crete

November 30, 2001

PHD Thesis

supervised by professor G.P. Tsironis

Αριθμητική μελέτη δυναμικών ιδιοτήτων των διακριτών Breather σε πλέγματα περιοδικά και μη.

Παναγιώτης Μανιαδής.

Τμήμα Φυσικής

Πανεπιστήμιο Κρήτης

30/11/2001

Διδακτορική διατριβή

Επιβλέπων καθηγητής Γ. Π. Τσιρώνης.

Πρόλογος.

Τις τελευταίες δεκαετίες και λόγω της γρήγορης εξέλιξης των ηλεκτρονικών υπολογιστών κατέστη δυνατή η παρατήρηση και η έρευνα φυσικών φαινομένων τα οποία δεν μπορούσαν να μελετηθούν πριν. Η πολυπλοκότητα στις εξισώσεις που περιγράφουν μη γραμμικά συστήματα συχνά ωθεί τους ερευνητές στην απλοποίηση του μοντέλου με την διαγραφή όρων σχετικά μικρών ή στην αριθμητική επίλυση με την χρήση ηλεκτρονικών υπολογιστών. Η αριθμητική μελέτη ενός προβλήματος έχει το πλεονέκτημα ότι μπορεί να πραγματοποιηθεί πάντα, ακόμα και σε περιπτώσεις όπου έχει αποδειχθεί ότι η λύση δεν μπορεί να γραφεί με βάση γνωστές συναρτήσεις και άρα είναι το μόνο εργαλείο διαθέσιμο για την μελέτη μιας μεγάλης κατηγορίας προβλημάτων.

Κατά την τελευταία δεκαετία, μεγάλος αριθμός ερευνητών έδειξαν ενδιαφέρον για μια νέα ανακάλυψη, τις ενδογενώς εντοπισμένες ταλαντώσεις ή διακριτούς breather. Η παρούσα διατριβή ξεκίνησε το 1997 με κύριο στόχο την μελέτη και την κατανόηση του νέου αυτού φαινομένου. Κατά την διάρκεια της μελέτης εμφανίστηκαν νέα και ενδιαφέροντα προβλήματα. Λόγω της πολυπλοκότητας του συστήματος, το κύριο μέρος της δουλειάς είναι βασισμένο σε αριθμητική μελέτη και λύσεις προερχόμενες από προσομοιώσεις σε ηλεκτρονικό υπολογιστή.

Η ύπαρξη διακριτών breather είναι ένα γενικό φαινόμενο. Μπορούν να εμφανιστούν σε πάρα πολλά φυσικά συστήματα όπως σε μόρια, μοριακούς κρυστάλλους, επαφές Josephson, δίκτια δεσμών υδρογόνου και άλλα, όπου η μη γραμμικότητα είναι παρούσα στις αλληλεπιδράσεις. Η ύπαρξη τους σε ένα σύστημα μπορεί να επηρεάσει αρκετές από τις φυσικές του ιδιότητες όπως τις ηλεκτρονικές διεγέρσεις, τις θερμοδυναμικές ιδιότητες, τις ταλαντωτικές ιδιοκαταστάσεις, την διάδοση ενέργειας και άλλες. Σε αρκετές περιπτώσεις οι διακριτοί breather μπορούν να κινηθούν και να μεταφέρουν ενέργεια ανάμεσα σε διαφορετικά μέρη του συστήματος. Το ενδιαφέρον μας εστιάζεται στην κατανόηση των ιδιοτήτων των εντοπισμένων αυτών ταλαντώσεων και για το λόγο αυτό ερευνάμε αρκετά διαφορετικά φυσικά μοντέλα στα οποία μπορούν

να δημιουργηθούν. Συγκεκριμένα μελετάμε την ύπαρξη, την ευστάθεια, την ευκινησία και την αλληλεπίδραση τους με άλλες διεγέρσεις στα μοντέλα αυτά.

Η σειρά με την οποία παρουσιάζονται τα προβλήματα που μελετήσαμε είναι η ακόλουθη: Το κεφάλαιο 0 είναι μια γενική εισαγωγή. Στο κεφάλαιο 1 γίνεται μια λεπτομερής εισαγωγή στον τομέα των διακριτών breather. Στο ίδιο κεφάλαιο παρουσιάζεται το θεώρημα MacKay-Aubry για την ύπαρξη και οι αριθμητικές μέθοδοι για την κατασκευή και την μελέτη της ευστάθειας. Παρουσιάζονται επίσης φυσικά συστήματα στα οποία οι διακριτοί breather έχουν παρατηρηθεί πειραματικά. Στο κεφάλαιο 2 παρουσιάζεται ένα απλό σύστημα στο οποίο υπάρχουν διακριτοί breather. Στο σύστημα αυτό συγκρίνουμε τα αριθμητικά αποτελέσματα με τα προσεγγιστικά που προκύπτουν με την χρήση της προσέγγισης στρεφόμενου κύματος (rotating wave approximation). Στο κεφάλαιο 3 μελετάμε την επίδραση που επιφέρει η ύπαρξη αλληλεπίδρασης με δεύτερους γείτονες. Στο κεφάλαιο 4 αναλύουμε την ευστάθεια και την ευκινησία των διακριτών breather σε σχεδόν μονοδιάστατα και διδιάστατα συστήματα. Στο κεφάλαιο 5 μελετάμε την αλληλεπίδραση ανάμεσα σε breather και τοπολογικά σολιτόνια σε συστήματα με ασθενείς δεσμούς υδρογόνου. Στο κεφάλαιο 6 μελετάμε την ύπαρξη και την ευστάθεια διακριτών breather σε συστήματα με ισχυρούς δεσμούς υδρογόνου. Στο κεφάλαιο 7 μελετάμε την επίδραση στην λύση που επιφέρει η ύπαρξη ατελειών στο σύστημα. Ερευνάμε επίσης τις αλληλεπιδράσεις των κινούμενων διακριτών breather με τις ατέλειες αυτές.

Πριν προχωρήσουμε παρακάτω θα ήθελα να ευχαριστήσω τον επιβλέποντα καθηγητή της παρούσας εργασίας Γ. Π. Τσιρώνη για την ευκαιρία που μου προσέφερε να συνεργαστούμε. Καθ' όλη τη διάρκεια της εργασίας ήταν υπομονετικός και πάντα διαθέσιμος να προσφέρει συμβουλές και οδηγίες όπου χρειάστηκε. Μου προσέφερε επίσης την δυνατότητα να γνωρίσω διαπρεπείς επιστήμονες από όλον τον κόσμο, να συζητήσω μαζί τους και σε μερικές περιπτώσεις να συνεργαστούμε με αυτούς εδώ στο πανεπιστήμιο Κρήτης αλλά και την δυνατότητα να επισκευτώ αρκετούς από αυτούς σε άλλα ερευνητικά ιδρύματα.

Θα ήθελα ακόμα να ευχαριστήσω τον καθηγητή Serge Aubry ο οποίος μας ενέπνευσε το ενδιαφέρων για την μελέτη των διακριτών breather και υπήρξε μια ανεξάντλητη πηγή πληροφοριών γύρω από το θέμα, πάντα διαθέσιμος για συζήτηση και με αρκετές καινούργιες και ενδιαφέρουσες ιδέες. Θα ήθελα τα τον ευχαριστήσω επίσης για την φιλοξενία που μου προσέφερε κατά τις επισκέψεις μου στο C.E.A. Saclay τον Ιανουάριο του 1998 και του 2000.

Θα ήθελα επίσης να ευχαριστήσω τον καθηγητή Alex. V. Zolotaryuk, καθώς και τους Γ. Καλόσακα, Γ. Κοπιδάκη, Ν. Βουλγαράκη, Μ. Ελευθερίου, Jose Luis Marin Espanol και αρκετούς άλλους για την βοήθεια που μου προσέφεραν.

0.1 Περίληψη.

Μη γραμμικά κύματα παρατηρήθηκαν για πρώτη φορά από τον J. Scott Russell το 1845 και αναφέρονται στο άρθρο "Report of the British Association for the Advancement of Science". Ο Russell παρατήρησε ένα μοναχικό κύμα το οποίο κινούνταν χωρίς διασπορά, κατά μήκος ενός ρηχού καναλιού με νερό. Στην αναφορά του γράφει ότι ακολούθησε το μοναχικό κύμα για πολλά μίλια κατά μήκος του καναλιού όπου διαδίδονταν χωρίς απώλειες. Η μαθηματική απόδειξη της ύπαρξης κυμάτων αυτής της μορφής διατυπώθηκε το 1895 από τους D.J. Korteweger και G. de Vries. Οπως αποδείχθηκε, η μη γραμμική υδροδυναμική εξίσωση που πρότειναν για την περιγραφή της διάδοσης κυμάτων σε ρηχό νερά, επιδέχονταν λύσεις απομονωμένων και εντοπισμένων κυμάτων της ίδιας μορφής με αυτά που παρατήρησε ο Russell. Τα μοναχικά αυτά κύματα ονομάστηκαν "Σολιτόνια".

Το 1955 οι E. Fermi, J. R. Pasta και S. M. Ulam μελέτησαν την ισοκατανομή της ενέργειας ανάμεσα σε 64 σωματίδια συζευγμένα με μια μη γραμμική αλληλεπίδραση. αντίθετα με ότι πίστευαν, ανακάλυψαν ότι ξεκινώντας με ένα σωματίδιο διεγερμένο αρχικά, η ενέργεια μεταδίδονταν σε όλες τις ιδιοκαταστάσεις του συστήματος αλλά μετά από κάπιο χρονικό διάστημα, το σύστημα επανέρχονταν στην αρχική κατάσταση. Η αρχική κατάσταση έμοιαζε ευσταθής και το σύστημα δεν μπορούσε να οδηγηθεί σε θερμοδυναμική ισορροπία.

Η ανακάλυψη των Fermi, Pasta και Ulam για την σχέση ανάμεσα σε εντοπισμένες λύσεις και τις θερμοδυναμικές ιδιότητες ενός συστήματος δημιούργησε αρκετό ενδιαφέρον για την μελέτη των σολιτονίων. Απομονωμένα κύματα σολιτονικής μορφής έχουν βρεθεί θεωρητικά αλλά και πειραματικά σε πάρα πολλά συστήματα και σε διαφορετικούς επιστημονικούς κλάδους όπως η υδροδυναμική, η οπτική, η φυσική στοιχειωδών σωματιδίων, η ηλεκτροδυναμική, η φυσική στερεάς κατάστασης και η βιολογία. Πολλά σολιτονικά μοντέλα έχουν προταθεί για την περιγραφή ασυνήθηστης συμπεριφοράς συστημάτων όπου είναι αισθητή η παρουσία μη γραμμικότητας.

Η δουλειά του Henry Poincare αποτέλεσε ένα άλλο σταθμό στην ανάπτυξη της θεωρίας της μη γραμμικής δυναμικής. Κατά την μελέτη του για την ευστάθεια του ηλιακού συστήματος, ανακάλυψε πάρα πολλά μαθηματικά εργαλεία και καθιέρωσε την γεωμετρική και τοπολογική αντιμετώπιση των μη γραμμικών συστημάτων. Η δουλειά του αναπτύχθηκε εκτενώς από τους Lorenz, Feigenbaum, Kolmogorov, Arnold, Moser, Lyapunov και πολλούς άλλους και οδήγησε στην ανακάλυψη του χάους και την δημιουργία της θεωρίας της μη γραμμικής δυναμικής

Μια σχετικά νέα ανακάλυψη στην θεωρία της μη γραμμικής δυναμικής είναι η ανακάλυψη των ενδογενώς εντοπισμένες ταλαντώσεις ή διακριτών breather. Αρχικά παρατηρήθηκαν το 1988 από τους A.J. Sievers και S. Takeno ως εντοπισμένες χωρικά και περιοδικές χρονικά ταλαντώσεις σε συστήματα συζευγμένων ταλαντωτών. Το 1994 οι R.S. MacKay και S. Aubry απέδειξαν ότι οι διακριτοί breather υπάρχουν ως ακριβείς λύσεις σε μια μεγάλη κατηγορία συστημάτων συζευγμένων μη γραμμικών ταλαντωτών. Το θεώρημα που απέδειξαν έδινε παράλληλα και μια αριθμητική τεχνική για την κατασκευή και μελέτη των ταλαντώσεων αυτών.

Μεγάλο ενδιαφέρον για περετέρω μελέτη δημιουργήθηκε μετά από την πρώτη αυτή παρατήρηση. Οι διακριτοι breather αποδείχθηκε αριθμητικά ότι είναι γραμμικώς ευσταθείς λύσεις με μεγάλο χρόνο ζωής σε αρκετά συστήματα και μπορούν να επηρεάσουν τις θερμοδυναμικές και άλλες ιδιότητες. Εχει επίσης βρεθεί ότι κάτω από τις κατάλληλες συνθήκες μπορούν να κινούντε και άρα μπορούν να μεταφέρουν ενέργεια ανάμεσα σε διαφορετικά μέρη του ίδιου συστήματος. Τα τελευταία δύο χρόνια μάλιστα υπάρχουν αρκετές πειραματικές παρατηρήσεις που επιβεβαιώνουν την ύπαρξη τους σε συστήματα όπως πλέγματα επαφών Josephson, συζευγμένων κυματοδηγών και άλλα. Είναι φανερό λοιπόν ότι μπορούν να εμφανιστούν σε κάθε μη γραμμικό και διακριτό σύστημα.

Εχει αποδειχθεί ότι οι διακριτοί breather υπάρχουν σε συστήματα συζευγμένων ταλαντωτών, είναι εκθετικά εντοπισμένοι στον χώρο και περιοδικοί στον χρόνο. Επειδή οι ταλαντωτές είναι μη γραμμικοί, εκτός από την κύρια συχνότητα

ω_b, στην ανάλυση Fourier των ταλαντώσεων εμφανίζονται και όλες οι αρμονικές $n\omega_b$. Για την μελέτη της ευστάθειας τους χρησιμοποιήθηκε η "θεωρία Floquet για την μελέτη ευστάθειας περιοδικών τροχιών". Με την χρήση της θεωρίας αυτής έχει βρεθεί ότι στα περισσότερα συστήματα υπάρχουν ευσταθείς breather, η ευστάθεια όμως εξαρτάται από την συχνότητα και τις παραμέτρους του συστήματος. Η γραμμική ευσράθεια σημαίνει ότι μπόρουν να διατηρηθούν στο σύστημα για μεγάλα χρονικά διαστήματα και δεν καταστρέφονται όταν διαταράσονται με μικρές διαταραχές.

Εάν η συχνότητα ενός breather βρίσκεται μέσα στην ζώνη των γραμμικών φωνονίων του συστήματος τότε ο συντονισμός έχει σαν αποτέλεσμα την καταστροφή του breather και την διέγερση φωνονίων. Το αποτέλεσμα είναι το ίδιο όταν μία από τις αρμονικές της κύριας συχνότητας βρίσκεται σε συντονισμό με τα φωνόνια. Για την μελέτη του εντοπισμού και πως αυτός εξαρτάται από την συχνότητα χρησιμοποιούμε την προσέγγιση στρεφόμενου κύματος και την προσέγγιση ότι μόνο ένας ταλαντωτής είναι μη γραμμικός ενώ οι υπόλοιποι θεωρούνται γραμμικοί. Η προσέγγιση αυτή δικαιολογείται από το γεγονός ότι οι breather είναι εκθετικά εντοπισμένες λύσεις γύρω από έναν ταλαντωτή ο οποίος ταλαντώνεται με μεγάλο πλάτος ενώ οι υπόλοιποι ταλαντώνονται με μικρό πλάτος, στην γραμμική περιοχή του δυναμικού. Τα αποτελέσματα συμφωνούν αρκετά καλά με τα αριθμητικά όσο οι αρμονικές της κύριας συχνότητας βρίσκονται μακριά από την ζώνη των φωνονίων. Στα πλαίσια των δύο αυτών προσεγγίσεων μπορούμε να συγκρίνουμε τον εντοπισμό των breather με τον εντοπισμό που εμφανίζεται λόγω ύπαρξης ατελειών.

Παρ' ότι οι διακριτοί breathers υπάρχουν σε πολλά συστήματα, κάποιες από τις ιδιότητες τους, όπως η ευστάθεια και η ευκινησία, εξαρτώνται άμεσα από την γεωμετρία του εκάστοτε συστήματος αλλά και από τις λεπτομέρειες της μη γραμμικότητας. Ακόμα, οι επιτρεπόμενες συχνότητες που μπορεί να έχει ένας breather εξαρτώνται από τις λεπτομέρειες του μοντέλου. Για παράδειγμα, η ευστάθεια και η ευκινησία ενός breather αλλάζει όταν εισάγουμε ατέλειες στο σύστημα. Για την καλύτερη κατανόηση της επίδρασης που μπορούν να

έχουν στις φυσικές ιδιότητες του συστήματος, μελετάμε αρκετά μοντέλα με διαφορετική μη γραμμικότητα και (ή) διαφορετική πλεγματική γεωμετρία.

Η πειραματική παρατήρηση της ύπαρξης διακριτών breather σε συζευγμένες επαφές Josephson σε γεωμετρία σκάλας αλλά και η πιθανή ύπαρξη τους σε μακρομόρια τα οποία δεν μπορούν να θεωρηθούν μονοδιάστατα, μας ώθησε να μελετήσουμε σχεδόν μονοδιάστατες πλεγματικές γεωμετρίες και την επίδραση που έχουν στην ευστάθεια και την κινητικότητα τους. Οπως βρήκαμε η γεωμετρία του πλέγματος επηρεάζει και τις δύο αυτές ιδιότητες. Εάν δύο μονοδιάστατες αλυσίδες συζευκτούν παράλληλα η μια στην άλλη τότε η ευστάθεια και η κινητικότητα των breather αλλάζει. Οι απλοί breather γίνονται ασταθείς και ένας διπλός breather (όπου σωμάτια ταλαντώνονται με μεγάλο πλάτος και στις δύο αλυσίδες) γίνεται ευσταθής μετά από μια διακλάδωση τύπου διχάλας. Μετά την διακλάδωση ο διπλός breather είναι δυνατόν να κινηθεί ενώ οι απλοί breather εξαφανίζονται. Ακόμα η δυνατότητα ύπαρξης breather σε επιφάνειες ή σε λεπτά film μας ωθεί να μελετήσουμε διδιάστατα πλέγματα.

Παρόμοιες διακλαδώσεις, όπως στις σχεδόν μονοδιάστατες αλυσίδες, εμφανίζονται αν προσθέσουμε στο πλέγμα ατέλειες. Στην περίπτωση αυτή οι απλοί breather διακλαδίζονται με multibreathers που έχουν διεγερμένα τα σημεία στα οποία βρίσκονται οι ατέλειες. Μετά τις διακλαδώσεις, οι απλοί breather εξαφανίζονται μαζί με τους ασταθείς multibreather και παραμένουν οι ευσταθείς multibreather. Οι ατέλειες επηρεάζουν επίσης και την κινητικότητας των breather μιας και όπως βρήκαμε ένας κινούμενος breather δεν μπορεί να διασχίσει την περιοχή στην οποία βρίσκεται μια ατέλεια χωρίς να χάσει ενέργεια. Σε μερικές περιπτώσεις (ανάλογα με την συχνότητα του, την ταχύτητα του αλλά και την ατέλεια) μπορεί να απορροφηθεί από την ατέλεια ή να ανακλαστεί από αυτήν.

Ενα άλλο ενδιαφέρον πρόβλημα όπου η διακριτότητα και η μη γραμμικότητα έχουν κυρίαρχο ρόλο είναι στην περίπτωση δεσμών υδρογόνου. Για την περιγραφή τους έχουν προταθεί αρκετά μαθηματικά μοντέλα. Οπως δείξαμε, σε δύο από αυτά υπάρχουν διακριτοί breather. Σε αρκετές περιπτώσεις μάλιστα

οι breather αυτοί μπορούν να κινηθούν και άρα πιθανολογίται ότι σχετίζονται με την διάδοση πρωτονίων σε αυτού του τύπου τα συστήματα.

Αφού οι διακριτοί breather είναι ταλαντώσεις σε ένα μη γραμμικό μέσον, οι κινούμενοι breather μπορούν να θεωρηθούν ως μη γραμμικά κύματα. Ενδιαφέρον παρουσιάζει ο τρόπος με τον οποίο τα μη γραμμικά αυτά κύματα αλληλεπιδρούν με διαφορετικού τύπου μη γραμμικά κύματα που μπορούν να υπάρχουν στο ίδιο σύστημα όπως τα σολιτόνια τύπου kink. Υπάρχει μία ενεργός αλληλεπίδραση ανάμεσα στα δύο αυτά κύματα όταν βρίσκονται κοντά το ένα με το άλλο. Κατά την αλληλεπίδραση τους εμφανίζουν μία μεγάλη ποικιλία από διαφορετικές συμπεριφορές. Ανάλογα με την ενέργεια αλλά και τις παραμέτρους του μοντέλου το kink μπορεί να ανακλάσει τον breather ή να τον καταστρέψει διεγείροντας φωνόνια ή να τον απορροφήσει και να μετατρέψει την ενέργεια του σε κινητική ενέργεια. Σε άλλες περιπτώσεις τέλος, μπορεί να δημιουργηθεί μια δέσμια κατάσταση ανάμεσα στον breather και το kink με αποτέλεσμα ο breather να ταλαντώνεται σε μικρή απόσταση από το κέντρο του kink.

Preface.

During the last decades due to the rapid development of the electronic computers and of computer science, it became possible to observe and investigate several physical phenomena that was not possible to explore earlier. The complexity of the equations describing nonlinear systems often forces the researcher to simplify the model by removing terms which are relatively small or use numerical methods and computers. The numerical investigation of a problem has the advantage that it can be performed always even in cases where it can be proved that the solution cannot be expressed in terms of known functions and therefore it is the only tool we have to study a large variety of problems.

Within the last decade, increasing number of researchers got interested in a new discovery, viz. the intrinsic localized modes or discrete breathers. This thesis work was initiated in 1997 with main purpose to understand and explore this new phenomenon. The study of the subject yielded many new interesting problems. Due to the complexity of the systems we are studying, most of the work is based on numerical explorations and solutions obtained through computer simulations.

The existence of discrete breathers is a generic phenomenon. They can appear in many physical systems like molecules, molecular crystals, Josephson junctions, hydrogen bonded networks and other systems where nonlinearity is present in the interactions. When they appear in a system they can affect several of its physical properties such as electronic excitations, thermodynamical properties, vibrational modes, energy transfer properties and others. In several cases discrete breathers can be mobile and therefore they can transfer energy between different parts of the system. Our interest focus on understanding the properties of these localized excitations and for that reason we investigated several physical models where they can exist. In particular we investigate the stability, the mobility and the interactions with other excitations in these models.

The structure of this thesis is the following. Chapter 0 is a general introduction. Chapter 1 is an introduction to the field of intrinsic localized modes. In this chapter we present the MacKay-Aubry existence theorem, numerical methods for breather construction and the stability. We also present some physical systems where discrete breathers have been observed. In chapter 2 we introduce a simple model for discrete breather; in this model we compare exact numerical solutions with the solutions obtained using an approximate method ie. the rotating wave approximation (RWA). In chapter 3 we investigate the modifications due to interactions with second neighbors. In chapter 4 we analyze the stability and the mobility of discrete breathers in quasi-one dimensional systems as well as a two dimensional system. In chapter 5 we investigate the interaction of breathers with topological solitons in hydrogen-bonded networks with weak hydrogen bonds. In chapter 6 we investigate a model with strong hydrogen bonds and we examine the stability of the solutions obtained in this system. Finally in chapter 7 we examine the modifications on the solution in the case when there are impurities in the lattice. We also examine the interactions of mobile breathers with these impurities.

Before proceeding I would like to thank my advisor George Tsironis for the opportunity he gave me to work together. During all these years he has always been patient with me and was always available and ready to give me advice and instructions on how to proceed. He also gave me the opportunity to meet scientists from all over the world, to discus with them and even to work jointly with some of them here at University of Crete as well as visit some of them in other institutes.

I would also like to thank professor Serge Aubry. He was the one who initiate much of the interest in intrinsic localized modes and he has been an endless resource of information on the subject. He was always available for discussion and he had many new and interesting ideas. I also thank him for his hospitality during my visit in C.E.A. Saclay in January of 1998 and

January of 2000.

I also would like to thank professor Alex. V. Zolotaryuk, as well as George Kalosakas, George Kopidakis, Nikos Voulgarakis, Maria Eleftheriou, Jose Luis Marin Espanol and others for the help they offered me during my work.

Chapter 0

0.2 Summary.

Non-linear waves where observed by J. Scott Russell in 1845 and discussed it in the "Report of the British Association for the Advancement of Science". What Russell observed was a single solitary wave which was propagating without dispersion along a water channel. As he mention in his report the lonely wave could travel along the channel for miles without dissipation. The mathematical proof for the existence of such solitary waves came in 1895 by D.J. Korteweger and G. de Vries. They proposed a non-linear wave equation for the description of wave propagation in shallow water. As they discovered, the equation they proposed could sustain isolated localized traveling solution, the same type like the solitary wave observed by Russell. The lonely localized waves observed by Russell where called "Solitons".

In 1955 E. Fermi, J. R. Pasta and S. M. Ulam in their attempt to study the equipartition of energy between 64 particles, weakly coupled by a non-linear interaction, they discovered that starting with one particle excited, the energy distributed itself over the whole system modes but returned almost completely to the initial state. Thermodynamical equilibrium was not reached and the excitation seamed to be stable in that sense.

The discovery of Fermi, Pasta and Ulam for the importance of localized solution into the thermodynamical properties of a non-linear system, initiate lot of interest in the study of solitons. Soliton type propagating waves have been found theoretically and experimentally in a large variety of systems in several fields of science like hydrodynamics, optics, elementary particle physics, electromagnetism, condensed matter physics, and biology. Several soliton models have been proposed for the explanation of strange behavior in every system where the nonlinearity is present.

An other breakthrough in the non-linear science came with the work

of Henry Poincare. In his attempt to investigate the stability of the solar system, he discovered lots of mathematical as well as geometrical and topological tools for the study of non-linear systems. The work of Poincare was continued by Lorenz, Feigenbaum, Kolmogorov, Arnold, Moser, Lyapunov and many others and lead into the discovery of Chaos and the development of the theory of the non-linear dynamics.

A relatively new development in the theory of non-linear dynamical systems is the discovery of discrete breathers. They were initially observed in 1988 by A.J. Sievers and S. Takeno and they where described as spatially localized and time periodic solutions in systems of weakly coupled and non-linear oscillators. Discrete breathers where proven later (1994) by R.S. MacKay and S. Aubry, that they are exact solutions of a large variety of systems. Together with the existence proof the MacKay-Aubry theorem gave a numerical technique for the construction and study of these solutions.

Since then, lot of interest has been initiated into further study. Discrete breathers have been proven numerically to be long live and linearly stable solutions in many systems and they can affect their thermodynamical and other properties. It is also found that they can be mobile under certain conditions and therefore can play the role of energy carriers. In the last two years there are also experimental verifications for their existence in system like Josephson junctions and coupled wave-guides. It seems therefore that discrete breathers are present in every system as long as it is discrete and non-linear.

It has been shown that in systems of coupled non-linear oscillators, discrete breathers exist, are exponentially localized in space and periodic in time solutions. Since the oscillators are non-linear, apart of the main frequency ω_b, there are in the Fourier spectrum of the oscillation all the harmonics $n\omega_b$. Since they are periodic in time, their stability can be investigated using the Floquet stability analysis for periodic orbits. It has been found that they are linearly stable is most of the cases, depending on the

frequency and the other system parameters.The linear stability means that once they are created they remain in the system for a long time and they are not destroyed when they are perturbed by a small perturbation.

If the frequency of the breather lye inside the linear phonon spectrum, then the resonance with the phonons leads to the distraction of the breather and the excitation of small amplitude and extended phonons. Not only the basic frequency but also its harmonics when they are in resonance with the phonons lead to the same effect. For investigating the localization and its relation with the frequency of the breathers we use the rotating wave approximation and the approximation that only one oscillator is non-linear while the others are linear. The last approximation is valid because due to the exponential localization of the breather, only the central particles are oscillating with large amplitude while the others are oscillating in the linear part of the potential. The comparison of the approximate results with the numerically obtained solutions shows that they are in good agreement when the breather frequency harmonics are not close to the phonon band. In terms of these two approximations, we compare the discrete breathers with the well known linear impurity modes studied earlier and we find that the localization in both cases are related.

Although discrete breathers exist in many systems, properties such as the stability and the mobility depends on the geometry of the system as well as the details of the interactions. Even the aloud breather frequencies vary, depending on the details of the model. For example the stability and the mobility of a breather is altered when impurities are injected into the system. Therefore for the better understanding of the influence they can have in the physical properties of the system it is necessary to investigate several models with different interactions and (or) different lattice geometries.

The experimental observation of discrete breathers in Josephson Junction ladder and the possibility of the existence of discrete breathers in macromolecules which cannot be consider as one-dimensional, lead as to study

quasi one-dimensional lattice geometries and how they affect the stability and the mobility of DB. As it is found the lattice geometry affects their stability as well as the mobility. As soon as two one dimensional chains are linked with some inter-chain coupling the stability of the breathers is changed. Except of the stability, the mobility properties are different. The single breather becomes unstable and a double breather (which involves large amplitude oscillations in both chains) becomes stable through a pitch-fork bifurcation. After the bifurcation, the double breather it is possible to become mobile while the single breather vanishes. The possibility of the existence of discrete breathers in surfaces or in thin films, leads as to study their existence and their mobility in two dimensional lattices.

Similar bifurcations, like in the quasi-one-dimensional chain, occur when we introduce impurities into the system. In this case the single breather bifurcates with the multibreathers which have the impurity site excited. After each bifurcation, the single breather disappear together with one of the multibreathers while the other one becomes the dominant solution in the system. The impurities also modify the mobility of the breathers, since a single mobile breather cannot pas through the impurity without loss of energy, some times it is absorbed (depending on the energy of the breather and its velocity as well as the impurity) while other times it is reflected.

Another interesting problem where discreteness and nonlinearity is involved is the case of hydrogen bonds and several mathematical models have been proposed for their study. We consider two of them and we show that it they exhibit discrete breather solutions. Since in some cases they are also mobile, they can be associated with the proton transfer in chains of hydrogen bonds.

Discrete breathers are oscillations in a nonlinear medium, mobile breathers therefore can be consider as nonlinear waves. We investigate how these nonlinear waves interact with an other type of nonlinear waves that they can exist in the same systems like topological solitons ie. kinks. As we found

there is an effective attraction when a breather and a kink are close. The interactions of a kink with a mobile breather exhibit a large variety of different behaviors. Depending on the energy as well as in the model parameters, the kink acts in some cases as a wall reflecting the breather while in other cases it absorbs the breather and radiate its energy into phonons or transform it into kinetic energy. In other cases it has been observed that a bound state between them with the breather oscillating in a small distance from the center of the kink.

Contents

Chapter 1

Introduction.

Intrinsic localized (ILM's) modes or discrete breathers (DB) have been observed in several systems of coupled anharmonic oscillators. They spontaneously appear in numerical simulations as long lifetime periodic and localized structures [1]-[28]. The system where this kind of structures were initially introduced is a one dimensional lattice of particles, interacting with their neighbors through an anharmonic interaction. This system is widely known as Fermi-Pasta-Ulam (FPU) chain [7]. The system has the following Hamiltonian:

$$H = \sum_i \frac{1}{2} m_i \dot{u}_i^2 + C \sum_{<i;j>} W(u_i - u_j) \tag{1.1}$$

where m_i is the mass of the particle at lattice site i, u_i is the displacement of particle i from equilibrium, $W(u_i - u_j)$ is the interaction potential between the particle at lattice site i with the particle at lattice site j and C determines the strength of the coupling. The first summation is over all particles while the second summation is over all the neighbors of particle at site i. The symbol $< i; j >$ denotes summation over all the neighbors of particle at site i. The corresponding equation of motion for this system is:

$$m_i \ddot{u}_i = -C \sum_{<i;j>} W'(u_i - u_j) \tag{1.2}$$

where prime means derivative with respect to u_i.

Discrete breathers where also observed in lattices of anharmonic oscillators, coupled through an interaction potential, such as in Klein-Gordon lattices. The Hamiltonian and the equation of motion of such a system is respectively:

$$H = \sum_i \frac{1}{2} m_i \dot{u}_i^2 + V(u_i) + C \sum_{<i;j>} W(u_i - u_j) \tag{1.3}$$

$$m_i \ddot{u}_i = -V'(u_i) - C \sum_{<i;j>} W'(u_i - u_j), \tag{1.4}$$

where V is the anharmonic on-site potential. Nonlinear localization is a result of the interplay between the discreteness of the system combined with the nonlinearity. Discrete breathers are nonlinear structures that are typically exponentially localized in space and periodic in time. Fourier analysis shows that the presence of nonlinearity in the interaction or in the on-site potential results in non zero contribution of all the harmonics of the basic breather frequency.

One critical condition for the DB to exist is that the frequency of oscillation and its harmonics must be different from the phonon frequencies. The dispersion relation and phonons (or normal modes) of the system can be found if we make the small amplitude approximation on the system [106]. If the breather frequency is within the phonon band, then due to the resonance with the phonons, it will radiate, and as a result it will loose energy. Since all the harmonics have non-zero contribution, they must lie outside the phonon spectrum, otherwise they will excite phonons making the breather unstable.

In 1994 Serge Aubry and Robert McKay proved that discrete breathers exist and are linearly stable in Klein-Gordon systems (1.3). They proved a theorem which states that discrete breathers are exact solutions for a large variety of systems of coupled oscillators [8], [11]. In addition to existence, the theorem points to a breather construction method that enables as to find numerically DB solutions with typical numerical accuracy (10^{-15}) [11]-[19].

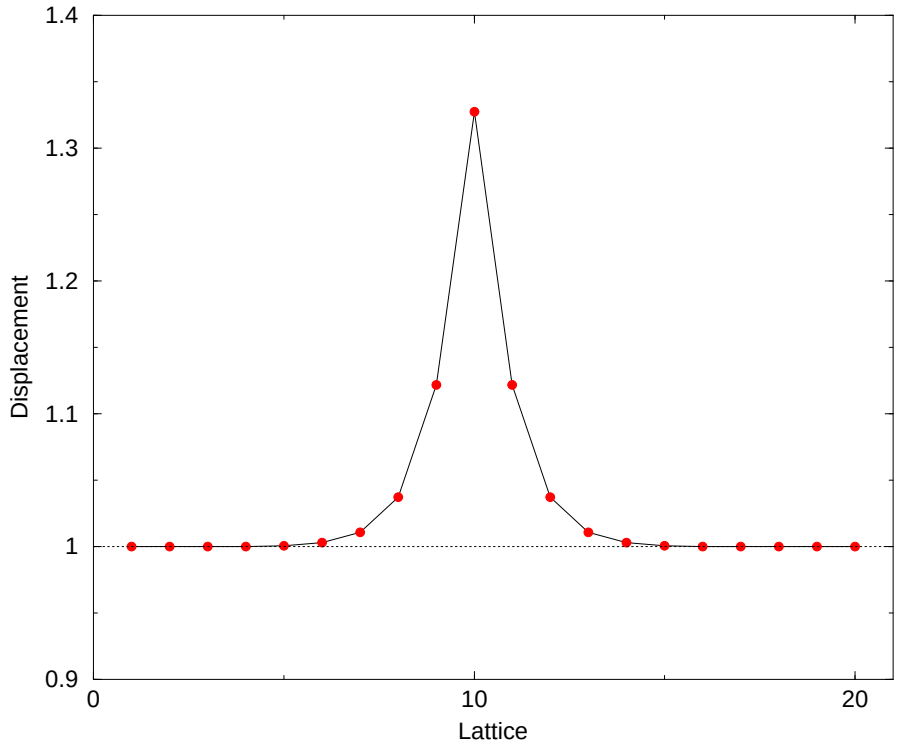

Figure 1.1: The single breather in the double well Φ^4 potential. The frequency is $\omega_b = 1.32$ and the coupling is $C = 0.131$.

Prior to the breather existence theorem, the study of intrinsic localized modes was based in approximate methods such as the rotating wave approximation. Numerical investigation was based on relaxation methods and the spontaneous and usually accidental creation of discrete breathers in numerical simulations. Breathers are known to exist in an integrable system in the strong coupling limit which can be described with a partial differential equation known as Sine-Gordon [6]. The breathers in the continuous Sine-Gordon equation are very fragile and they disappear under most perturbations of this equation. On the other hand breather solutions are proven to be very robust in discrete models [11]-[42].

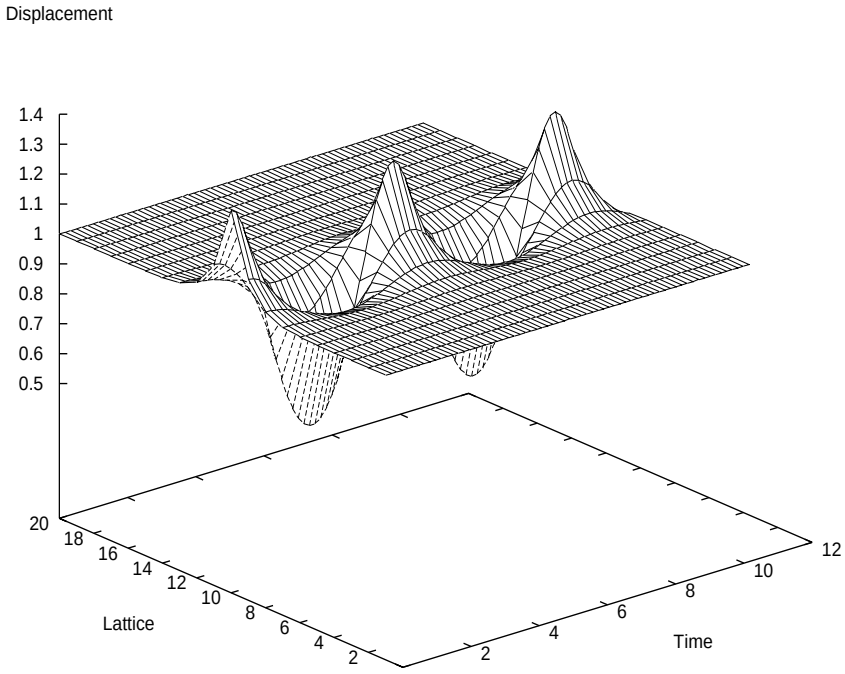

Figure 1.2: The time evolution of the breather shown in figure (1.1).

1.1 MacKay-Aubry theorem.

The existence of discrete breathers is connected with the so called "anti-integrable limit" or anticontinuous limit [9], [10],[57],[58]. The concept of anti-integrability was initially introduced for the standard map [57],[58] and it turns out to be a simple but powerful tool for finding infinitely many solutions in nonlinear systems. The method that have been used mostly up to now, is the one that starts from an integrable limit as also is done in the famous KAM (Kolmogorov-Arnold-Mozer) theorem [86],[87]. The new approach consists in choosing an "opposite" limit (which for that reason was initially named anti-integrable limit) where the system remains non-linear and exhibits chaotic, periodic or quasi-periodic solutions which can

be trivially analyzed. This method was first applied in systems of coupled nonlinear maps in the limit where the coupling goes to zero. In this limit the maps are not integrable. Later, when the same method was applied in systems of coupled oscillators in the limit of zero coupling ($C \to 0$), the term was changed to anticontinuous, since the single oscillator is integrable; furthermore this limit is the opposite to the one of strong coupling, where the system can be treated as a continuous medium.

In the anti-integrable limit each oscillator of equation (1.4) oscillates independently of the others. The motion of every independent oscillator can be described by the following Hamiltonian and the corresponding equation of motion:

$$H = \frac{1}{2} m\dot{u}^2 + V(u), \tag{1.5}$$

$$m\ddot{u} + V'(u) = 0, \tag{1.6}$$

where $V(u)$ is the anharmonic on-site potential. It is necessary for the potential to have at least one local minimum in order for periodic orbits to exist. These periodic orbits around the minimum at the anticontinuous limit are the trivial breather solutions of the system. A single oscillator is integrable due to energy conservation. All its periodic orbits can be expressed in the form $u(t) = g(\omega t + \alpha, \omega)$, where α is an arbitrary phase and $\omega = \omega(I)$ is the frequency which depends on the integrated action $I = \int_0^{2\pi/\omega} m\dot{u}^2 dt$ over one oscillation period.

Let us now consider the whole lattice. At the anticontinuous limit ($C = 0$), each oscillator can oscillate independently of the others. For an infinite lattice, there is an infinite group of different configurations, depending of the number of oscillators oscillating, their frequencies and their phases. For the proof of the theorem it is essential to consider only time reversible oscillations ie. the initial phase of every oscillator at $t = 0$ should be zero ($\dot{u}_i = 0$). For the classification of the breathers we introduce the coding sequence σ. For a given breather of frequency $\omega_b = \omega(I)$, depending on the initial phase of each oscillator, σ_i is defined as:

- $\sigma_i = 0$ when oscillator i is at rest.
- $\sigma_i = n$ when oscillator i is oscillating with frequency $\omega_i = n\omega_b$ and initial phase $\alpha_i = 0$.
- $\sigma_i = -n$ when oscillator i is oscillating with frequency $\omega_i = n\omega_b$ and initial phase $\alpha_i = \pi$.

We can now write the theorem from [8].

Theorem 1 *Consider a dynamical system (1.4) consisting of an array of anharmonic oscillators with a $\mathcal{C}^2$ potential, coupled between nearest neighbors by some arbitrary $\mathcal{C}^2$ potential with coefficient C. The frequency of a single oscillator versus its action is $\omega(I)$. The underlying lattice of the system can be of any finite dimension d.*

Let $\{u_n(t,0)\}$ be a time periodic solution with a given frequency ω_b which belongs to the set of values taken by $\omega(I)$ for the system of un-coupled oscillators ($C = 0$). Such a solution is labeled by the coding sequence $\{\sigma_n\}$.

Let us assume the non-resonance conditions:
(1) For $\sigma \neq 0$, $d\omega(I)/dI \neq 0$ for the corresponding determination of the periodic oscillation.
(2) For the oscillators at rest, $p\omega_b \neq \omega(0)$ for all integers p
Then there exists C_t positive nonzero such that this solution has a unique continuation $\{u_n(t,C)\}$ for $|C| < C_t$.

The proof of this theorem is given in [8] as an application of the implicit function theorem applied in the space of time symmetric loops described within the action angle representation. In [13] there is a proof based on the implicit function theorem, but in the original Lagrangian coordinates $\{u_i(t), \dot{u}_i(t)\}$. The second proof can be easily turned into an efficient numerical method for finding any of these solution. In addition, the Newton matrix involved by the implicit function theorem can be used for studying the linear stability of the obtained solutions.

1.2 Numerical methods.

The breather existence theorem provides us with a convenient numerical method for finding exact discrete breathers [8]- [19]. Due to the finite computer memory and computer time we are forced to study a finite system with N coupled oscillators. For the numerical calculation it is convenient to define the vector $\vec{X} = \{u_1, \ldots, u_N, \dot{u}_1, \ldots, \dot{u}_N\}^\dagger$, whose elements are the displacement and the velocity of every oscillator. For a given breather of frequency (ω_b) we define a nonlinear map $\vec{Y} = \mathbf{T}(\vec{X})$, which corresponds to the time evolution of the initial vector $\vec{X}(t = 0)$ over a breather period $(t_b = 2\pi/\omega)$ according to the equation of motion of the Klein-Gordon system (1.4),

$$\vec{X}(t = t_b) = \mathbf{T}(\vec{X}(t = 0)). \tag{1.7}$$

The breather solutions with period t_b are the fixed points of this map therefore $\vec{X}_b = \mathbf{T}(\vec{X}_b)$. To find the breather solutions is equivalent to finding the fixed points of $\mathbf{T}$. It is convenient to start from a known solution and using the map, try to find how this solution changes when one or more system parameters vary. The initial solution we take is the trivial breather solution at the anticontinuous limit $(C = 0)$. If we can vary the coupling by small steps δC, the breather will change in a continuous way. For small δC the new breather solution will differ from the initial one by a small vector $\vec{\Delta}$,

$$\vec{X}_{C+\delta C} = \vec{X}_C + \vec{\Delta}. \tag{1.8}$$

If we substitute this into equation (1.7) we have:

$$\begin{aligned} \vec{X}_b &= \mathbf{T}(\vec{X}_b) \Leftrightarrow \\ \vec{X} + \vec{\Delta} &= \mathbf{T}(\vec{X} + \vec{\Delta}) \Leftrightarrow \\ \vec{X} + \vec{\Delta} &= \mathbf{T}(\vec{X}) + \partial\mathbf{T} \times \vec{\Delta} \end{aligned} \tag{1.9}$$

where $\mathbf{M} = \partial\mathbf{T}$ is the tangent map of $\mathbf{T}$.

The tangent map can be calculated by integrating the linearized equations of (1.4).

$$m_i\ddot{\epsilon}_i = -V''(u_i)\epsilon_i - C\sum_{<i;j>} W''(u_i - u_j)(\epsilon_i - \epsilon_j), \tag{1.10}$$

where we have considered ϵ_i to be some small perturbation around the solution u_i. If we define the vector $\vec{E} = \{\epsilon_1, \ldots, \epsilon_N, \dot{\epsilon}_1, \ldots, \dot{\epsilon}_N\}^\dagger$, and with the use of the map $\mathbf{T}$, the time evolution over a breather period of the perturbation will be

$$\vec{E}(t = t_b) = \mathbf{M} \times \vec{E}(t = 0). \tag{1.11}$$

The above equation provides us with a method of calculating numerically the tangent map $\mathbf{M}$. The numerical integration of the linearized equations (1.10) over a breather period, with the appropriate initial conditions, gives one column of the tangent map. In order to find the tangent map we have to integrate the linearized equations $2N$ times, using each time as an initial condition one column of the $2N \times 2N$ unit matrix I_{2N}. For every column of I_{2N} we choose as an initial condition, the numerical integration yields the corresponding column of $\mathbf{M}$.

We can now solve equation (1.9) to find $\vec{\Delta}$,

$$(\mathbf{M} - 1)\vec{\Delta} = -(\mathbf{T}(\vec{X}) - \vec{X}). \tag{1.12}$$

The above equation cannot be solved directly since due to the translational invariance of the system, the tangent map has one eigenvalue equal to 1 and therefore $(\mathbf{M} - 1)$ is not invertible. Instead of finding the inverse matrix it is possible to find a pseudo-inverse using the singular value decomposition method [107]. This method consist on writhing $\mathbf{M}$ as the product of an column orthogonal matrix $\mathbf{U}$, a diagonal matrix $\mathbf{W}$ with positive or zero elements (the singular values), and the transpose of an orthogonal matrix $\mathbf{V}$.

$$(\mathbf{M} - 1) = \mathbf{U} \cdot \mathbf{W} \cdot \mathbf{V}^T. \tag{1.13}$$

The matrices **U** and **V** are each orthonormal in the sense that their columns are orthonormal. This decomposition can always be performed, even for non-square matrices. The inverse of **U** and **V** are equal to their transposes; **W** is diagonal, so its inverse is the diagonal matrix whose elements are the reciprocals of the elements w_j. One of the singular values is equal to zero; thus instead of the reciprocal of this value we put zero. The pseudo-inverse of the matrix is then:

$$(\mathbf{M}-1)^{-1} = \mathbf{V}[diag(1/w_j)]\mathbf{U}^T, \tag{1.14}$$

where we put for all the singular values $w_j = 0$, zero instead of $1/w_j$. Each of the singular values, corresponds to a direction in the $2\times N$ dimensional phase space of the system. Putting in the pseudo-inverse matrix zero is equivalent to eliminating the modification of the initial solution in this direction.

An other efficient and sometimes more accurate method for solving equation (1.12) is to minimize the distance in the phase space, between the initial and the final point. The distance can be expressed by the norm $||\mathbf{T}(\vec{X}) + \mathbf{M}\vec{\Delta} - (\vec{X} + \vec{\Delta})||^2$. The tangent map can be written with four $N \times N$ block matrices **A**,**B**,**C** and **D** as

$$\mathbf{M} = I_{2N} + \begin{pmatrix} \mathbf{A} & \mathbf{B} \\ \mathbf{C} & \mathbf{D} \end{pmatrix}. \tag{1.15}$$

For time reversible solutions, the initial velocity of every oscillator is zero therefore we can chose $\vec{\Delta} = (\vec{\delta}, 0)$, where $\vec{\delta}$ is a vector with N elements. The minimization of the norm gives

$$\vec{\delta} = -(\mathbf{A}^* \cdot \mathbf{A} + \mathbf{C}^* \cdot \mathbf{C})^{-1} \cdot (\mathbf{A}^*, \mathbf{C}^*)(\mathbf{T}(\vec{X}) - \vec{X}) \tag{1.16}$$

where $(\mathbf{A}^*, \mathbf{C}^*)$ is a $N \times 2N$ matrix. The matrix $(\mathbf{A}^* \cdot \mathbf{A} + \mathbf{C}^* \cdot \mathbf{C})$ is then invertible when the continuation of the breather is possible [11]-[15],[19].

In FPU chains there is no corresponding anticontinuous limit. The numerical method described here can be applied with some modifications. A simple way is to introduce artificially an on-site potential $V(u)$. Following

an appropriate path in the parameter parameter space, the breather solution can be continued up to the point where the on-site potential has been removed [8]-[15],[19].

1.3 Linear stability analysis.

Long time simulations of equation (1.2) or (1.4) show that the breather can be sustained in the system without energy loss. An other way of examining the stability of the breather is to perform a small perturbation of the solution and see how it evolves in time. The evolution of sufficiently small perturbations can be described with the linearized equations (1.10). The linear stability analysis is based on the Floquet analysis of periodic orbits (see Appendix A).

Equation (1.11) shows that a small perturbation of the breather, will grow or decay, depending on the eigenvalues of the tangent map $\mathbf{M}$ which will be called the Floquet operator or Floquet matrix. Since the dynamical system is Hamiltonian, the Floquet matrix is symplectic which implies that if λ is an eigenvalue of $\mathbf{M}$, then λ^*, $1/\lambda$ and $1/\lambda^*$ are also eigenvalues of $\mathbf{M}$. This mean that when one eigenvalue is not on the unit circle, in the complex plane, then there exists at least one eigenvalue with modulus larger than 1 ($|\lambda| > 1$) outside the unit circle. When an eigenvalue of the Floquet matrix has modulus larger than 1, then a small perturbation will grow exponentially in time and therefore the breather is linearly unstable.

A discrete breather is linearly stable when all the eigenvalues of the Floquet matrix $\mathbf{M}$ lie on the unit circle in the complex plane. When one or more of the eigenvalues have modulus larger than 1, then the breather is linearly unstable and a small perturbation will grow exponentially in time, in the direction of the corresponding eigenvector.

If we take the derivative over time of equation (1.4) we see that $\epsilon_i = \dot{u}_i$ is a solution of equation (1.10).This solution correspond to a doubly

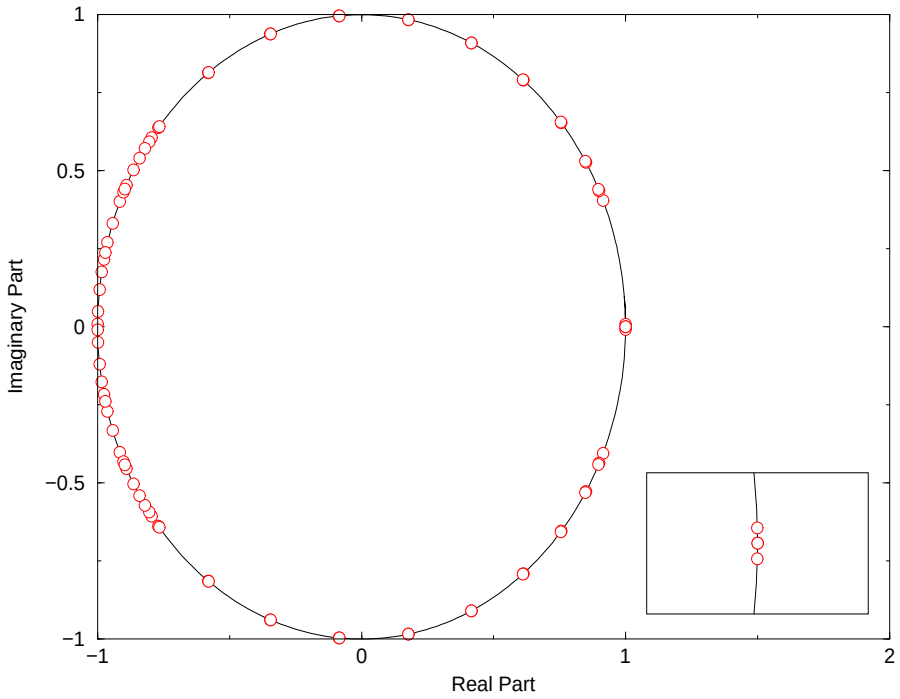

Figure 1.3: The eigenvalues of the Floquet matrix in the complex plane for a breather in the double well Φ^4 potential. In the inset we see a magnification around 1.

degenerate eigenvalue equal to 1. For small values of coupling, the single breather is stable. The eigenvalues of the Floquet matrix except of the pair at 1, are grouped into two symmetric bands which are related to the phonons of the system. The corresponding eigenvectors are extended in all the lattice. As the coupling increases, the eigenvalues move around the unit circle. Depending on the details of the potential, some of the eigenvalues may escape from the phonon band and move toward 1. The corresponding eigenvector for these eigenvalues are in most of the cases localized.

Generally there are three different types of instabilities that can occur in the system as the coupling increases:

- Two symmetric eigenvalues collide on the unit circle at -1 and move on the real axes.
- Two symmetric eigenvalues collide at 1 and move on the real axes. In this case the continuation of the breather may end. The continuation remains possible when the corresponding eigenvector has a different spatial symmetry than the breather.
- Two eigenvalues with different Krein signatures (and their symmetric pair) collide at some point of the unit circle different than ± 1 and get out the unit circle.

The Krein signature for a pair of eigenvalues ($\lambda_\nu = \exp \pm\theta_\nu$) of the Floquet matrix can be defined as

$$\kappa(\theta_\nu) = sign\left(i\sum_{i=1}^{N}(\epsilon_i^\nu \cdot \epsilon_{i+N}^{\nu *} - \epsilon_i^{\nu *} \cdot \epsilon_{i+N}^\nu)\right)$$

where ϵ_i^ν is the complex eigenvector associated with the eigenvalue.

1.4 Mobility of a breather.

We consider a one dimensional lattice of anharmonic oscillators coupled with linear coupling. For this 1D system and for soft on-site potential, it has been observed that when the coupling increases, a pair of eigenvalues of the Floquet matrix escape from the phonon band and moves toward 1 [16]. This pair of eigenvalues collides at 1 and escapes in the real axes. Before the collision (see inset on figure 1.3) the eigenvalues are very close to 1 but they lie on the unit circle, therefore the breather is stable.

The pair of eigenvalues are complex conjugate and therefore their eigenvectors of the Floquet matrix are complex conjugate. The eigenvector corresponding to these two eigenvalues has real part which is localized and antisymmetric around the center of the breather, in the position subspace and zero contribution in the velocity subspace. The imaginary part has zero

contribution in the position subspace while it is localized and antisymmetric around the center of the breather, in the velocity subspace. This eigenvector is called the pinning mode. We can see the imaginary part of the pinning mode for a breather in the double well Φ^4 potential for frequency $\omega_b = 1.32$ and coupling $C = 0.62$ in figure (1.4).

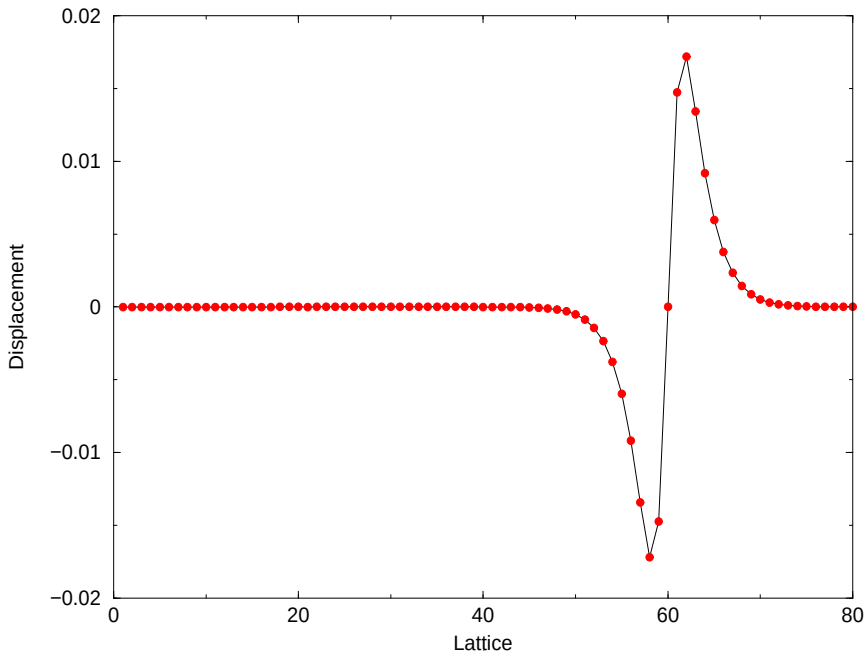

Figure 1.4: The imaginary part of the pinning mode for a breather in the double well Φ^4 potential.

If we excite the static breather with the pinning mode and evolve the system in time, we see that the breather becomes mobile. In figure (1.5) we can see the time evolution of the mobile breather.

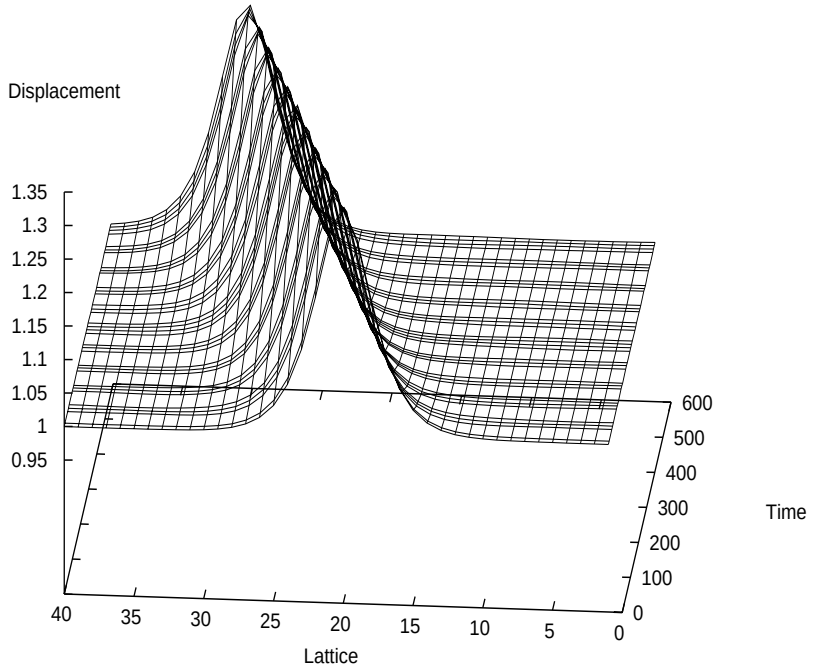

Figure 1.5: The time evolution of a mobile breather in the double well Φ^4 potential. We plot the breather every period.

1.5 Breathers in various one dimensional models.

The breather existence theorem and the numerical method described in the previous sections are applicable for arbitrary lattice dimension. In this section we will consider only one dimensional systems.

The equation of motion for a one dimensional Klein-Gordon lattice of identical oscillators, coupled with linear coupling is (we have set the mass of each oscillator equal to unity):

$$\ddot{u}_i + V'(u_i) - C(u_{i+1} + u_{i-1} - 2u_i) = 0 \tag{1.17}$$

where the on-site potential $V(x)$ can be any nonlinear potential. The po-

tential must have at least one equilibrium point at x_0. For a single oscillator the frequency of small oscillations around the equilibrium point is denoted with ω_0 and it is equal with the square root of the second derivative of the potential at the equilibrium point ($\omega_0^2 = V''(x_0)$).

In the limit of the small amplitude oscillations, we can linearize the previous equation and find the phonons on the system. The phonon frequencies form a band with frequencies between ω_0 and $\sqrt{\omega_0^2 + 4C}$. The dispersion relation is $\omega^2(q) = \omega_0^2 + 4C\sin(q/2)$ where $-\pi \leq q \leq \pi$ is the wave vector and ω is the phonon frequency. There is a gap between 0 and ω_0. The non-resonance condition of the breather frequency with the phonons, forces the breather frequency and all the harmonics to lie outside the phonon band.

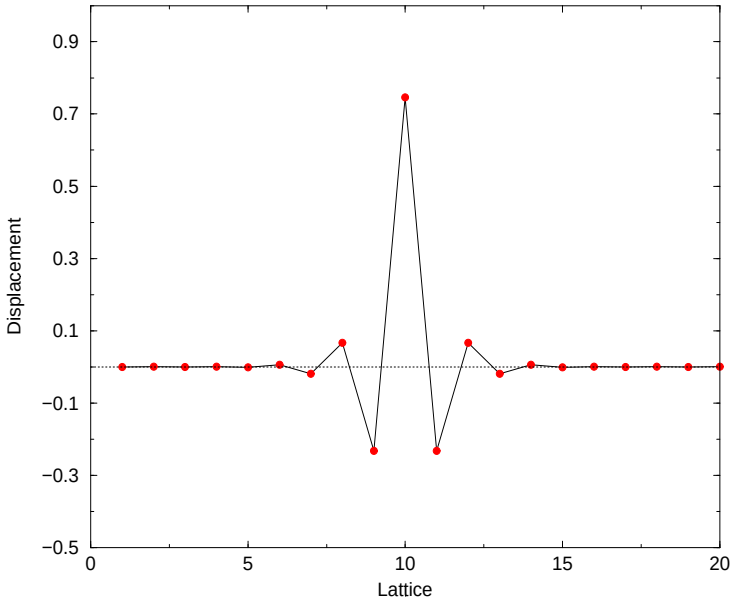

Figure 1.6: Discrete breather in the hard Φ^4 potential.

Depending on the frequency of the oscillation, the potential is classified as soft or hard. In a soft potential, the frequency of the oscillation is always smaller than ω_0 and it decrease when the amplitude of oscillations increase.

In a hard potential, the frequency of oscillations is always larger than ω_0 and it increases as the amplitude of oscillations increase.

For a hard potential, the breather frequency and all the harmonics, in the anticontinuous limit, are always larger than ω_0. For nonzero values of coupling C, in order to avoid resonance with the phonons, the frequency must be larger than the highest phonon frequency ($\omega_b > \sqrt{\omega_0^2 + 4C}$).

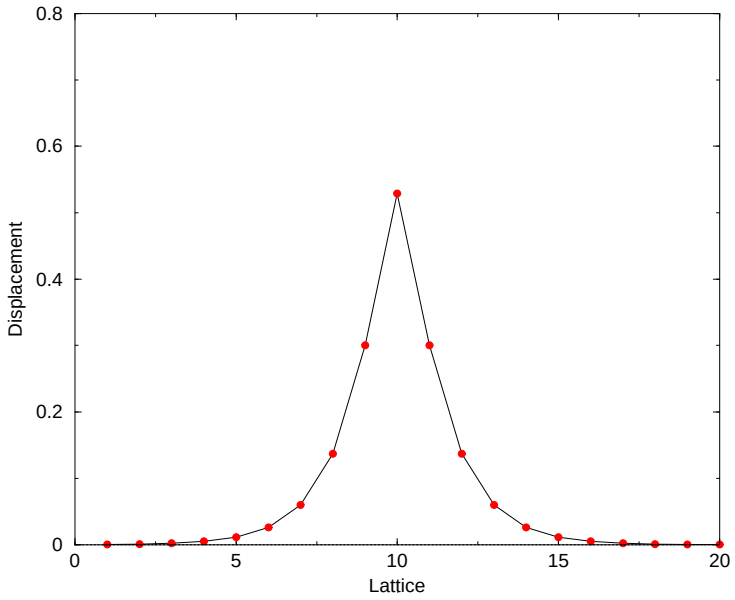

Figure 1.7: Discrete breather in the soft Φ^4 potential.

For a soft potential, the breather frequency, in the anticontinuous limit, is smaller than ω_0. In order to avoid resonances with the higher harmonics, all the harmonics must be different than ω_0 ($p\omega_b \neq \omega_0$ with p integer). For nonzero coupling the breather frequency and all the harmonics must lie outside the phonon band ($p\omega_b < \omega_0$ or $p\omega_b > \sqrt{\omega_0^2 + 4C}$ with p integer).

Some of the anharmonic potential were DB can be found are:

$$V_1(x) = \frac{1}{2}x^2 + \frac{1}{4}x^4 \tag{1.18}$$

$$V_2(x) = \frac{1}{2}x^2 - \frac{1}{3}x^4 \tag{1.19}$$

$$V_3(x) = \frac{1}{4}(1 - x^2)^2 \tag{1.20}$$

$$V_4(x) = 1 - \cos(x) \tag{1.21}$$

The first is the hard Φ^4 and contains a square and a quadratic term. The second is the soft Φ^4 and it has the shape of an inverted double well. These two are symmetric around zero. The third is the soft double well Φ^4; it has two equilibrium points at ± 1. The fourth is the Sine-Gordon potential; it is soft and it has infinite number of equilibrium points.

1.6 Discrete Breathers in FPU chains.

Recently [35] it was proved that discrete breathers can exist in FPU chains as exact solutions of the system. For the proof they use an alternative definition of the anticontinuous limit. They consider a diatomic lattice of particles, coupled with nearest neighbor anharmonic interaction W. The anticontinuous limit considered is obtained when the mass ratio m/M goes to zero, where m is the mass of the light particles while M is the mass of heavy particles.

In this limit $M \to \infty$ the heavy particles remain fixed while the motion of the light particles decouples. Each of the light particles can oscillate with a frequency ω_b. In [35] it was proved that these periodic orbits can be continued for finite values of the mass M. In [36] discrete breathers of the previous model were calculated using a variation of the Newton method described in section (1.2). In some cases, depending on the interaction W, it is possible to continue the periodic orbit until $M = m$, then the breather found corresponds to the breather in the monoatomic FPU lattice.

An alternative way for studying the FPU lattice is by adding in the Hamiltonian of the FPU lattice (1.1) a nonlinear on-site potential multiplied with some parameter λ (1.1) [15],[19]. Then for $\lambda = 0$ we have the

initial FPU Hamiltonian, while for $\lambda \neq 0$ the Hamiltonian describes a Klein-Gordon lattice. With this potential it is now easy to define an anticontinuous limit ($\lambda = 1$ and $C = 0$). Then by following a valid path in the parameter space (λ and C) breathers are found in the anticontinuous limit and can be continued with the Newton method, until $\lambda = 0$.

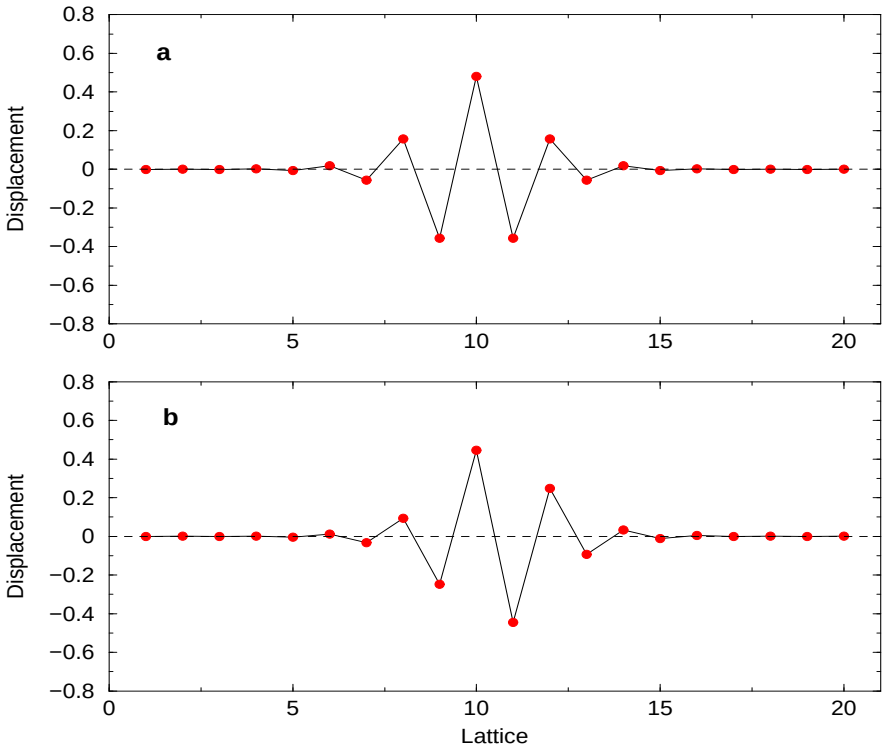

Figure 1.8: **a**) The Sievers-Takeno mode in an FPU lattice with frequency $\omega_b = 2.3$ and coupling $C = 1$. **b**) The Page mode for the same frequency and coupling.

In what follows we use the last method for finding discrete breathers in FPU lattices. For simplicity we chose the parameter $\lambda = 1 - C$ and the on-site potential V to be equal with W. For the hard Φ^4 potential and for a monoatomic lattice ($m_i = 1$), it is possible to continue all the periodic orbits from the anticontinuous limit until $\lambda = 0$. If in the anticontinuous

limit there is only one particle oscillating, while the others are at rest, the breather found is Sievers-Takeno mode [1]. When two neighboring particles are oscillating in anti phase, the breather found is the Page mode [2]. In figure (1.8**a**) we can see the Sievers-Takeno while in figure (1.8**b**) we can see the Page mode for the FPU lattice. The linear stability analysis of the Sievers-Takeno mode and the Page mode shows that the first is unstable because a pair of eigenvalues lie outside the unit circle in the complex plan. The Page mode is stable (figure 1.9).

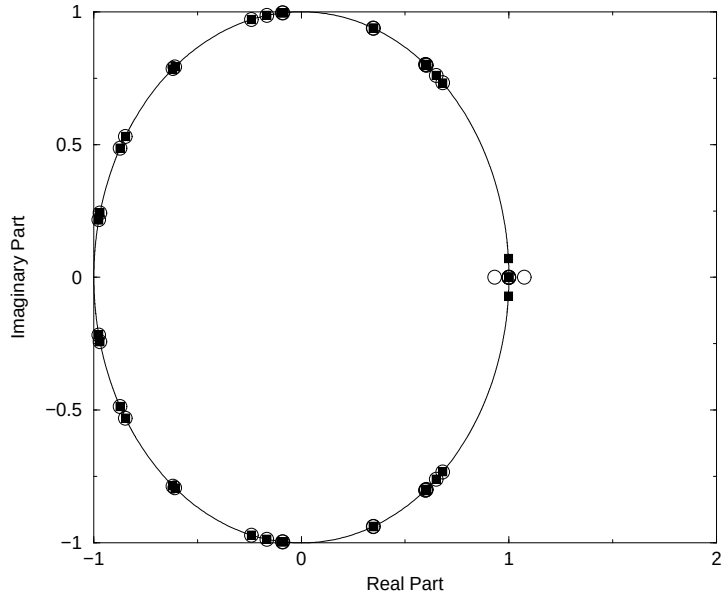

Figure 1.9: The linear stability analysis for FPU breather. Circles denote the eigenvalues of the Floquet matrix for the Sievers-Takeno mode while squares the eigenvalues of the Floquet matrix for the Page mode. The first is unstable while the second is stable.The frequency and the coupling are $\omega_b = 2.3$ and $C = 1$.

1.7 Experimental observation of discrete breathers.

Discrete breathers can also exist in non Hamiltonian systems. In [19], [39],[40] a model was proposed for breathers in arrays of Josephson junctions. Discrete breathers were predicted theoretically for this model and recently there were two experiments where arrays of Josephson junctions where constructed and discrete breathers where observed in these lattices [46]-[49].

Discrete breathers have also been observed experimentally in the vibrational states in crystals of highly nonlinear materials [50]. The experiments were performed in a quasi-one-dimensional system, the halide-bridged transition metal complex $\{[Pt(en)_2][Pt(en)_2Cl_2](ClO_4)_4\}$ where (en) = ethylenediamine. The strong coupling between the electronic motion and the lattice makes this material highly nonlinear. The experimental technique used to excite highly energetic vibrational motions was Raman spectroscopy. In the overtone resonant Raman spectra some strongly increasing anharmonic redshifts in the fundamental peaks where observed. These redshifts are associated to the existence of localized modes (DB) in the system created as a result of the nonlinearity.

1.7.1 Discrete breathers in Josephson arrays.

Discrete breathers have been observed experimentally in coupled Josephson junctions [47],[48]. A Josephson junction is formed between two superconducting island separated by a thin insulating barrier. Each island is characterized by a macroscopic wave function $\Psi \sim e^{i\theta}$. The dynamics of a single junction is described by the phase difference $\phi = \theta_2 - \theta_1$ between the two superconducting island of the junction. The current through a single junction is described with the Josephson relation

$$i = \ddot{\phi} + \Gamma\dot{\phi} + \sin\phi \tag{1.22}$$

where Γ represents the dumping. The response of the junction to a current is measured by the voltage of the junction which is given by the equation $u = (\Phi_0/2\pi)d\phi/dt$. In the first experiment they consider an anisotropic ladder array [47] (see figure 1.10**a**). In the ladder there are horizontal junctions (described with the phase differences ϕ_i^u for the upper horizontal junctions and with $\tilde{\phi}_i^u$ for the lower junctions) and vertical junctions (described with the phase differences ϕ_i^v). The two type of junctions have different critical current, I_{ch} is the critical current for the horizontal junctions while I_{cv} for the vertical and $h = I_{ch}/I_{cv}$ is the anisotropy parameter. The Josephson junction ladder is biased with an external dc current I transpose to the horizontal junctions. In the second experiment [48] they construct an annular anisotropic ladder which can be consider similar with the previous, with periodic boundaries (see figure 1.10**b**).

The equations that describe the system can be written in the form

$$\ddot{\phi}_i^v + \Gamma\dot{\phi}_i^v + \sin\phi_i^v = \gamma - \frac{1}{\beta_L}(-\triangle\phi_i^v + \bigtriangledown\tilde{\phi}_{i-1}^h - \bigtriangledown\phi_{i-1}^h), \tag{1.23}$$

$$\ddot{\phi}_i^h + \Gamma\dot{\phi}_i^h + \sin\phi_i^h = -\frac{1}{h\beta_L}(\phi_i^h - \tilde{\phi}_i^h + \bigtriangledown\phi_i^v), \tag{1.24}$$

$$\ddot{\tilde{\phi}}_i^h + \Gamma\dot{\tilde{\phi}}_i^h + \sin\tilde{\phi}_i^h = \frac{1}{h\beta_L}(\phi_i^h - \tilde{\phi}_i^h + \bigtriangledown\phi_i^v), \tag{1.25}$$

where $\bigtriangledown\phi_i = \phi_{i+1} - \phi_i$, $\triangle\phi_i = \phi_{i+1} + \phi_{i-1} - 2\phi_i$ and β_L is a parameter which depends on the geometry and the critical current of the vertical junctions.

The breathers that where observed in these two experiments are roto-breathers in the sense that one or more of the vertical junctions are whirling wile all the others are oscillating with amplitudes that decay exponentially from the center.

For the construction of these localized states, a local current I_{local} is applied into one of the vertical junctions. This local current excites one or more of the vertical junctions. The excitation remains when the local current is removed creating the breather. The number of the vertical junctions that are whirling can be seen in a current-voltage $I - V$ diagram as a decrease

of the voltage. In this $I - V$ diagram one can see the discrete breathers on the system and from the decrease of the voltage to calculate the number of vertical junction that are excited. An other method used for the observation of these breathers is the low temperature scanning laser microscopy. A focused low-powered laser is used to scan the ladders surface. The laser heats locally the sample in an area of a few micrometers creating a voltage variation. Then the voltage variation is measured as a function of the beam coordinate. In [48] there are several pictures showing the discrete breathers measured using this method.

1.7.2 Discrete breathers in a low dimensional material.

Recently it was reported that discrete breathers where observed experimentally in the vibrational states of a quasi-one-dimensional, highly nonlinear and discrete material, the halide-bridged transition metal complex $\{[Pt(en)_2][Pt(en)_2Cl_2](ClO_4)_4\}$ where (en) = ethylenediamine [50] (for simplicity called $PtCl$). The source of the nonlinearity in this material is the strong coupling between the lattice and the electronic motion. Therefore Raman spectroscopy can be used for the investigation of localized modes due to nonlinearity. The material is a homogeneous quasi-one-dimensional crystal formed of $Pt(en)_2$ units. Each unit is associated with two ClO_4. Raman Resonance has been used in the past to study the ground state as well as the photoexcited states (see references in [50]).

The Raman spectra of this material was obtained using an Ar^+ laser illumination at 514 nm and a single crystal of $PtCl$ at 12 K. The fundamental Raman spectra exhibits fine structure with up to six well-resolved modes. In the overtone spectra the fine structure of the fundamental evolves to a three peak pattern which indicates the localization of the energy into a single $PtCl_2$ unit. The fundamental and the overtone spectra for the pure ^{35}Cl as well as the ^{37}Cl isotopic sample is shown in [50]. In this spectra can be seen that the dominant peak in each overtone exhibits a strong

anharmonic redshift. This behavior on the overtone spectra indicates that all the vibrational energy is localized in one $PtCl_2$ unit. The localization is possible only if the nonlinearity is sufficiently strong, otherwise the quantum tunneling will not allow localized bound states to exists.

1.7.3 Discrete breathers in spin wave modes in antiferromagnets.

Recently it was proposed that discrete breathers can appear in an easy-axis antiferromagnetic chain [51] when the system is driven by a circularly polarized ac cw field. The Hamiltonian of the system is

$$H = 2J \sum_n \vec{S}_n \cdot \vec{S}_{n+1} - D \sum_n (S_n^z)^2, \tag{1.26}$$

with exchange constant J and anisotropy constant D positive.

The molecular dynamics simulations have shown that localized modes spontaneously appear on this model for driving frequencies in the gap below the antiferromagnetic resonance for any positive value of D. These modes are created due to modulational instabilities of the uniform spin wave mode. The parameters used for the molecular dynamics simulations are chosen to match those of FeF_2 easy-axis antiferromagnet, the $(C_2H_5NH_3)_2CuCl_4$ quasi-one-dimensional antiferromagnet and an anisotropic one dimensional antiferromagnet. In all cases the localized modes appear spontaneously in the simulations.

These localized modes were observed experimentally [52] in the $(C_2H_5NH_3)_2CuCl_4$ antiferromagnet (usually called $C(2)CuCl_4$). For the experiment a $C(2)CuCl_4$ single crystal with typical dimensions $3, 3, 0.5\ mm^3$ was used. The sample was first exposed to a driving pulse with driving frequency 1.46 GHz and for different power, for 400 μs. The absorption spectra of the sample was measured 20 μs after the driving pulse.

The absorption spectra can be seen in FIG. 2 in [52]. In this figure is observed that for small driving power the antiferromagnetic resonance

peak breaks into a broad band. The existence of intrinsic localized modes is associated with this breakup of the antiferromagnetic resonance.

1.7.4 Discrete breathers in waveguide arrays.

An other system where discrete breathers have been observed is an array of coupled waveguides [53]. The array consists of a large number of identical coupled waveguides. The system can be described with the discrete nonlinear Scrödinger equation (DNLS)

$$i\frac{dE_n}{dz} + \beta E_n + C(E_{n+1} + E_{n-1}) + \gamma |E_n|^2 E_n = 0 \qquad (1.27)$$

where E_n is the electric field in the nth waveguide, C is the coupling constant, β is the linear propagation constant and γ is the nonlinear parameter depending on physical properties of a single waveguide. In this equation the time is replaced with the distance in the z direction.

For the observation of discrete breathers an optical parametric oscillator (OPO) pumped by a laser was used. The light from the OPO was polarized and reshaped before it was focused with a lens on one side of the array. At the other side of the array the outgoing light was imaged with an infrared camera. Half of the outgoing light was collected in a detector in order to measure the output power.

When the input power was low the output had a linear behavior. The light was spread into two lobes traveling away from the center of the array, with many secondary central peaks. As the power of the incoming light was increased, the outgoing light started to form a central intense lobe. At even higher power, a discrete breather was formed. The images of the outgoing light for the three cases as they were imaged with the infrared camera as well as the power distribution as a function of the waveguide number, of the outgoing light, can be seen in [53].

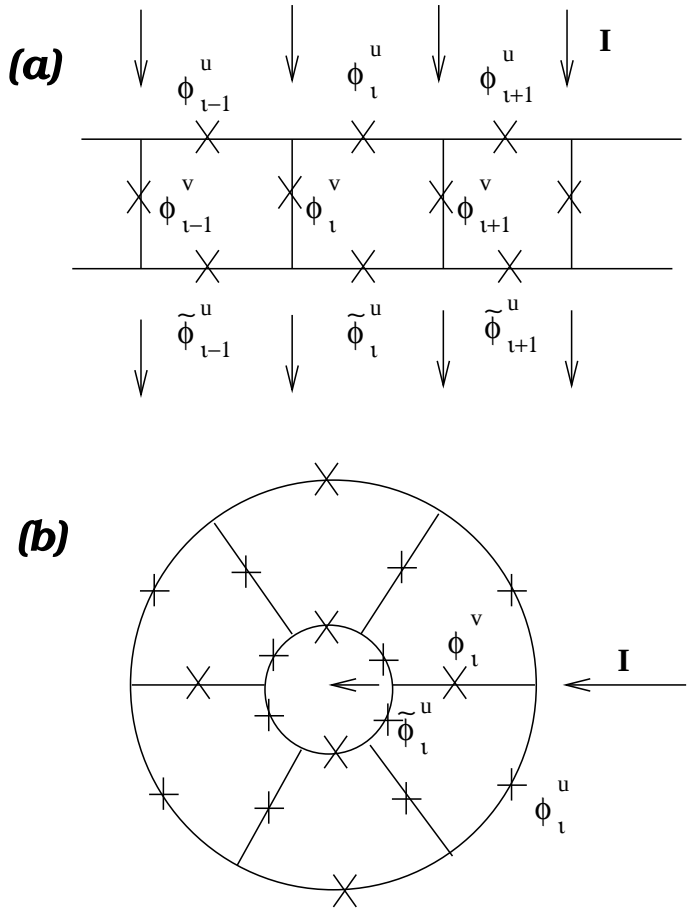

Figure 1.10: **a**: The Josephson junction ladder. Josephson junctions are marked as $\times$. **b**: The Josephson junction annual ladder.

Chapter 2

Discrete breathers as impurity modes: a simple model.

In the present chapter we present a simple Klein-Gordon model where discrete breathers (DB) exist. The system we are studying is a one dimensional lattice of coupled harmonic oscillators with linear coupling, where we have inserted an extra nonlinear term in the on-site potential at the central oscillator. Using the standard Newton method we show that breathers exist in this simple system. We also find using the rotating wave approximation, an analytical expression for the solution. We then compare these simple breathers to the exponentially localized mode of a linear system with a mass impurity and we find that some of their properties are very similar.

In figure 2.1**a** we can see a lattice of coupled harmonic oscillators. At the central site ($i = 0$) we add a nonlinear term at the on-site potential. The nonlinear term in the on-site potential of the central oscillator is essential in order to fulfill the necessary conditions for the existence of DB's. In this case the system supports breather solutions, centered at the nonlinear site, that are exponentially localized with a frequency outside of the phonon band and similar to a system with nonlinear potential in all sites [5]-[9].

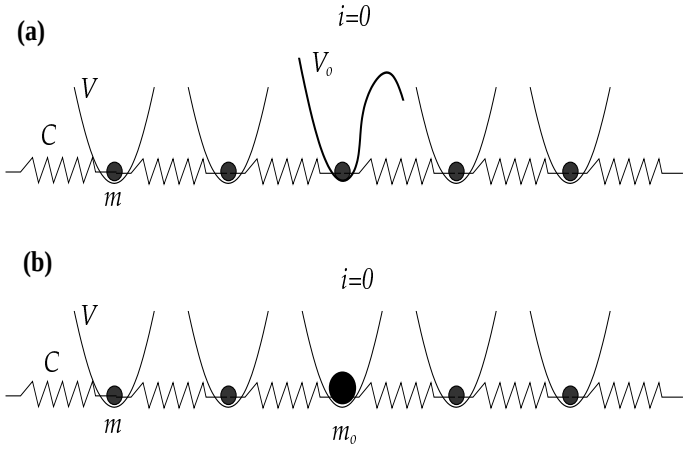

Figure 2.1: A lattice of coupled harmonic oscillators. **a)** A nonlinear term has been added in the on-site potential (V_0) of the central oscillator ($i = 0$). **b)** A mass impurity (m_0) has been placed at the central site ($i = 0$) of the lattice.

The Hamiltonian of the system is the one given in (1.3) and the and the corresponding equations of motion are given in (1.17). We consider the mass of every oscillator to be equal to unity ($m_i = 1$), and the local potential $V(x)$ harmonic for every oscillator except for that site where the breather is centered. We take three cases of different potentials:

$$V_1(x_i) = \frac{1}{2}x_i^2 + \delta_{i,0}\frac{1}{4}x_i^4 \tag{2.1}$$

$$V_2(x_i) = \frac{1}{2}x_i^2 - \delta_{i,0}\frac{1}{4}x_i^4 \tag{2.2}$$

$$V_3(x_i) = \frac{1}{2}x_i^2 + \delta_{i,0}\frac{1}{2}(x_i^3 + \frac{1}{4}x_i^4) \tag{2.3}$$

where $\delta_{i,0}$ is the Kronecker Delta. All three potentials have an equilibrium point at $x = 0$ and the frequency of small oscillations around the equilibrium point is $\omega_0 = 1$. The potential V_1 is hard in the sense that the frequency increases when the amplitude of the oscillation increases and the corresponding breathers must have frequency ω_b higher than the phonon

frequency ($\omega_b^2 > \omega_0^2 + 4C$) while V_2 and V_3 are soft potentials and the frequency of oscillations decreases when the amplitude increases, thus $\omega_b < \omega_0$. The main difference between the second and the third potential is that the second is symmetric around the equilibrium point at zero while the third is not. We will see the effect of the symmetry of the potential later when we try to apply the rotating wave approximation and compare the breather solution with the linear impurity mode.

For the calculation of the linear impurity mode we consider only the linear part of the potential. We also set one of the masses to be different than unity $m_0 = 1 + dm$ (figure 2.1**b**). For the numerical calculation of the breather in the system and the linear impurity mode we use a small system with periodic boundary conditions.

A single site nonlinearity and the means through which it affects self-trapping has been investigated in the context of the discrete nonlinear Schrödinger equation [88]-[89]. In the present work we show that a single nonlinear site is sufficient to support exponentially localized and periodic solutions (discrete breathers) in the system. Using the standard Newton method in section 2.1 we find numerically the exact breather solution. We also perform the Floquet analysis in order to investigate the linear stability. At the end of section 2.1 we compare the solution with the well known discrete breathers in a non-linear Klein-Gordon chain. In section 2.2 we use the rotating wave approximation to find an analytical expression for the solution and we compare it with the exact numerical solution. In section 2.3 we compare the nonlinear impurity with the well known mass impurity mode in a linear system.

2.1 Numerical Calculation of Breathers.

For the numerical investigation we consider breathers centered on the nonlinear site. In the anticontinuous limit $C = 0$ the breather solution exists

and is trivial to find; the particle at the nonlinear site oscillates with frequency ω_b chosen to be different from ω_0. The oscillation frequency depends on the amplitude of the oscillation. This trivial breather solution can be continued to nonzero values of C. In order to continue the solution we increase the coupling with small steps and we use the standard Newton method to find the new solution [9]-[18]. Using this method we are able to continue the breather solution for large values of C until the frequency or one of its harmonics enters the phonon band.

In figure 2.2 we portray the breather solution for the potentials shown in equations (2.1)-(2.2) and for several values of the frequency and the coupling. We observe that the solution is always exponentially localized around the nonlinear site. For the hard potential (figure 2.2a and 2.2b) the neighboring sites are oscillating with opposite phase while for the soft potential (figure 2.2c-2.2f) the neighboring sites are oscillating in phase. The potential of equation (2.2) is symmetric while the potential of equation (2.3) is not. This affects the breather solution in the following way: in the first case the oscillation of every particle is symmetric around zero while the second is not. In figure 2.2e and 2.2f we plot both the maximum and the minimum amplitude of the oscillation for the asymmetric breather.

In order to investigate the stability of the solution we use the Floquet analysis for the system. In figure 2.3 we observe that all the eigenvalues of the Floquet matrix of the system lie on the unit circle and therefore the solution is linearly stable. We also performed long time simulation in the system in order to confirm the stability of the solution. In figure 2.3a we plot the eigenvalues of the Floquet matrix of the system for the hard potential in the complex plane. In figure 2.3b and 2.3c we see the eigenvalues of the Floquet matrix for the case of the soft potential of equation (2.2) and (2.3) respectively, in the complex plane. All the eigenvalues lie on the unit circle and the breathers are linearly stable.

We have seen that one nonlinear site is sufficient for breather existence

and the solutions are stable. That result shows that only the central site of the breather has strong nonlinear behavior while the rest can be considered like linear oscillators. We may think of the central site to oscillate in the nonlinear regime with frequency different from that of linear phonons, while the neighbors to this central site are forced to oscillate with the same frequency due to the coupling. This localized energy cannot travel in the system since the oscillators are out of resonance. For that reason the excitation remains exponentially localized around the central nonlinear site.

Using the same method we can find the breather solution which corresponds to the same value of coupling and frequency in a system with nonlinearity in every site and we compare with the previous case. We see in figure 2.2 with dashed line and with points, the breather solution for the three different potentials.

As we can see in figures 2.2a and 2.2b, there are no significant differences between these two cases for a hard potential. In these plots we can compare the breathers for two different values of the coupling and we can see that they are identical.

For a soft potential like V_2 and V_3 and for small coupling the two breathers are very close to each other (figure 2.2c and 2.2e). For larger values of the coupling we observe in figure 2.2d and 2.2f that the breather with single site nonlinearity remains exponentially localized while in the fully nonlinear system more than one site have strong nonlinear behavior in the center but they preserve the exponential behavior in the tails. When the coupling increases the central site of the breather in the system with nonlinearity in every site changes very little while in the case of only one nonlinear potential its amplitude is increased (figure 2.2c and 2.2d). This shows an important difference between the hard and soft anharmonicity. For the soft potential not only the central site but also the neighboring sites experience the an-harmonic part for large coupling. But the main properties of the breather remain the same viz. exponentially localized oscillation

with frequency outside of the phonon band. When the neighboring sites are harmonic, the central site has to oscillate with larger amplitude in order to force the neighbors to follow it.

2.2 Rotating Wave approximation.

From the numerical solution it is clear that breathers decay exponentially in space. Therefore it is possible to use the following ansatz as an approximate solution [18],[23]

$$x_i = \alpha_0 \alpha^{|i|} (-1)^i \cos(\omega_b t) \tag{2.4}$$

$$x_i = \alpha_0 \alpha^{|i|} \cos(\omega_b t) \tag{2.5}$$

for the hard and the soft potential respectively. If we substitute into the equation of motion (1.17) for $m_i = 1$ we derive two equations, one for the central site ($i = 0$) and one for the remaining lattice. For the hard potential of equation (2.1) we obtain finally after performing the rotating wave approximation (RWA) the following equations:

$$\frac{3}{4}\alpha_0^2 = \omega_b^2 - 1 - 2C(\alpha + 1) \tag{2.6}$$

$$C\alpha^2 + (2C + 1 - \omega_b^2)\alpha + C = 0 \tag{2.7}$$

In order to derive these two equations we use the equality $\cos^3(A) = \frac{3}{4}\cos(A) + \frac{1}{4}\cos(3A)$ and neglect the higher order terms. From equation (2.7) we see that the frequency of the breather can be treated as a parameter. The exponential localization parameter α depends only on the coupling and the breather frequency. Necessary condition for a solution to exist is the frequency to be out of the phonon band ($\omega_b^2 < 1$ or $\omega_b^2 > 1 + 4C$). For a hard potential the breather frequency is above the phonon band. The solution is

$$\alpha = \frac{-(2C + 1 - \omega_b^2) - \sqrt{\omega_b^4 - (4C + 2)\omega_b^2 + 4C + 1}}{2C} \tag{2.8}$$

and from equation (2.6) we have

$$\alpha_0 = \pm\sqrt{\frac{4}{3}(\omega_b^2 - 1 - 2C - 2C\alpha)} \tag{2.9}$$

in figure 2.4a it is shown α as a function of the frequency ω_b^2 and in figure 2.4b it is shown the amplitude of the central site α_0.

For the soft potential of equation (2.2) if we substitute into the equation of motion (1.17) we have

$$\frac{3}{4}\alpha_0^2 = 1 - \omega_b^2 - 2C(\alpha - 1) \tag{2.10}$$

$$C\alpha^2 + (\omega_b^2 - 2C - 1)\alpha + C = 0 \tag{2.11}$$

and the solution is

$$\alpha = \frac{-(\omega_b^2 - 2C - 1) - \sqrt{\omega_b^4 - (4C+2)\omega_b^2 + 4C + 1}}{2C} \tag{2.12}$$

$$\alpha_0 = \pm\sqrt{\frac{4}{3}(1 - \omega_b^2 + 2C - 2C\alpha)} \tag{2.13}$$

We can see in figure 2.4c and 2.4d the dependence of α and α_0 as a function of the frequency.

From figure 2.4 it is clear that for a symmetric potential the rotating wave approximation gives solution close to the exact numerical solution for large enough coupling. For a soft potential we see from the same figure that for small frequencies, when the second harmonic of the breather frequency approaches the phonon band, the exact numerical solution differs from the approximate one. In this case higher harmonic corrections should be considered. For a non-symmetric potential the ansatz is not a good approximation because the oscillations of the particles are not symmetric around zero.

2.3 Dynamical impurities.

For a system of linear coupled identical oscillators is known that when one of the masses is replaced with a larger or a smaller one, then one of the

eigenfrequencies of the system escapes from the phonon band, and for that eigenstate the corresponding eigenvector is exponentially localized around that mass [90]. A large mass impurity creates a localized mode with corresponding frequency smaller than the phonon frequency while a small mass impurity creates a mode with frequency larger than phonons. The first link to breathers appears here, a hard potential can be related to a small mass impurity while the soft potential can be related to a large mass impurity. In both systems the solution is exponentially localized with frequency outside of the phonon band.

In order to compare the two cases (mass impurities and breathers) we use equation (1.17) with $m_i = 1$ for breathers with one of the potentials of equations (2.1),(2.2) and (2.3), while for the mass impurity we use only the linear part of the potential and we set in one site the mass to be equal to $m_0 = 1 + dm$ where dm is a small quantity positive or negative. For breathers we use the standard Newton method while for the linear impurity we use the exact solution which can been found analytically using the Green function and numerically diagonalizing the matrix of the system. For each potential we first choose the coupling and the frequency, then create the breather with the given frequency and look for the mass that corresponds to a linear impurity mode with the same frequency. We then compare the two solutions, the breather and the impurity mode. We mention here that the impurity mode is a solution of the linear system, thus for the comparison, we choose to normalize this mode so that to have the same amplitude with the breather at the central site.

We can see in figure 2.5a and 2.5b the linear impurity mode and the breather with the same frequency for the first potential V_1, for two different values of the coupling. As we can see they are essentially identical, there is no difference in the limit allowed by the numerical errors. The same can be observed in figure 2.5c and 2.5d for the second potential V_2. In figure 2.5e and 2.5f we plot both the maximum and the minimum displacement of

the breather, because V_3 is non symmetric, which means that the breather oscillation will not be symmetric too. In this case we can observe that there are some differences between the breather and the impurity mode but these differences can be explained by the non symmetric oscillation of the breather and the fact that the impurity mode is a solution of the linear system, ie. it will be necessarily symmetric. We thus can see that the only case where the breather profile is different from the impurity mode is when the potential is not symmetric; in all the other cases they are identical.

The linear impurity mode can be found analytically using the ansatz from equations (2.4) and (2.5) for smaller and larger mass respectively. If we substitute in the equation of motion we derive the following equations: for a smaller mass ($-1 < dm < 0$):

$$-\omega^2(1+dm)+1+2C(\alpha+1)=0 \tag{2.14}$$

$$C\alpha^2+(1+2C-\omega^2)\alpha+C=0 \tag{2.15}$$

for a larger mass ($dm > 0$):

$$-\omega^2(1+dm)+1-2C(\alpha-1)=0 \tag{2.16}$$

$$C\alpha^2+(\omega^2-1-2C)\alpha+C=0 \tag{2.17}$$

If we compare equation (2.7) with (2.15) and equation (2.11) with equation (2.17) we observe that they are identical. The exponential localization parameter α in every case depends only on the frequency for a fixed value of coupling. The specific frequency can be chosen by modifying the mass impurity in equations (2.14) and (2.16).

From the analysis above we can conclude that breathers are dynamical impurities in the system induced by the nonlinearity. The use of the rotating wave approximation demonstrates that the mechanism responsible for the exponential localization of breathers is the same with that of mass impurities. When one lattice site is initially displaced in the nonlinear regime of

the potential, then this site plays the role of an impurity since all the others are still oscillating in the linear regime and this impurity creates the exponentially localized solution of the system. One of the differences between linear and nonlinear impurities is that equations (2.6),(2.7),(2.10) and (2.11) are approximate and are not valid when one of the higher harmonics of the breather frequency enters in the phonon band. The breather solution exists only when all harmonics of the frequency are outside of the phonon band while a linear impurity mode exists for every frequency as long as an appropriate mass (dm) is chosen. The mass impurity mode has a fixed frequency for a given impurity mass while the amplitude of oscillations and the total energy can vary. A breather can have a wide range of frequencies and there is a relation between the frequency and the total energy or the maximum amplitude of the oscillation. The impurity mode is linear with only one frequency while the breather is highly nonlinear and all the harmonics of the frequency are excited.

In a system of coupled harmonic oscillators we can find breather solutions when we add a single an-harmonic nonlinear potential term. This solution is stable and has similar properties with the well known breathers that can be found if we add anharmonicity in every oscillator. Using the rotating wave approximation we can obtain an analytical expression for the breather solution. This solution is a very good approximation when the higher harmonics of the main frequency are not close to the phonon band. If we compare our solution with a mass impurity mode we can see that nonlinearity plays similar role in a system as a mass impurity and the mechanism responsible for the exponential localization of the solution is in both cases similar.

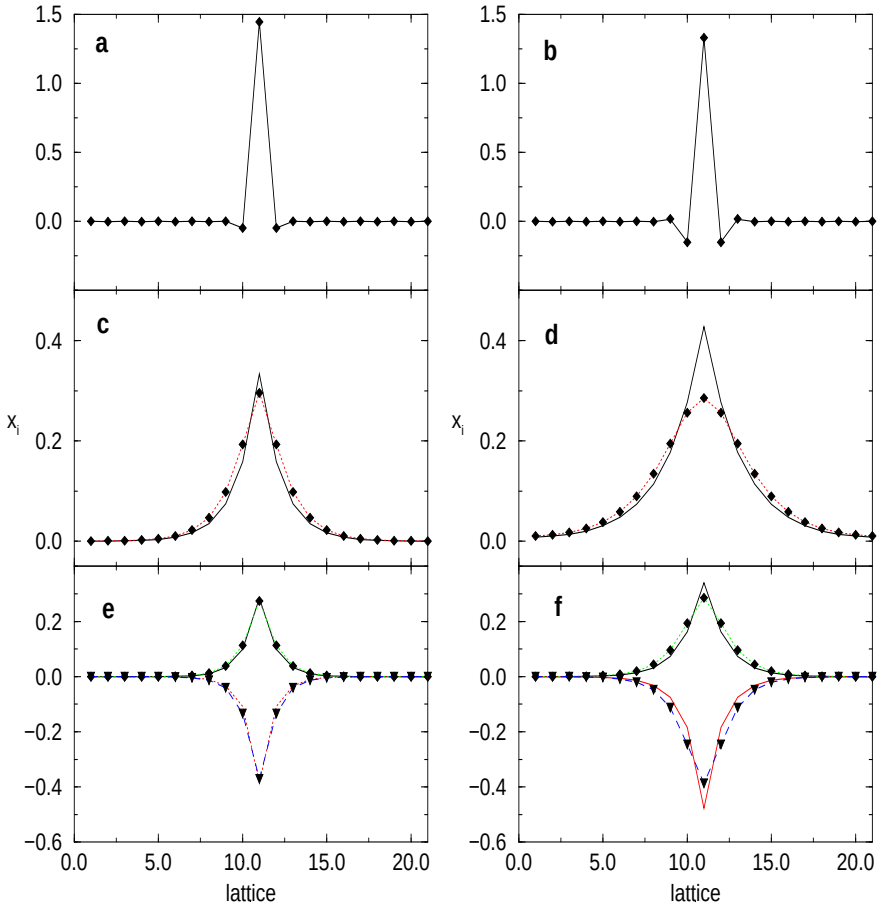

Figure 2.2: Solid line depicts the breather in a system with only one nonlinear site while with dotted line and boxes a breather in a fully nonlinear lattice. **a)** Potential V_1, $C = 0.051$ and $\omega_b = 1.625$. **b)** Potential V_1, $C = 0.151$ and $\omega_b = 1.625$. **c)** Potential V_2, $C = 0.051$ and $\omega_b = 0.9848$. **d)** Potential V_2, $C = 0.151$ and $\omega_b = 0.9848$. **e)** Potential V_3, $C = 0.051$ and $\omega_b = 0.9608$. **f)** Potential V_3, $C = 0.101$ and $\omega_b = 0.9608$. In figures **e** and **f** the minimum displacement of both breathers (dashed line and long dashed line with triangles respectively) is shown additionally.

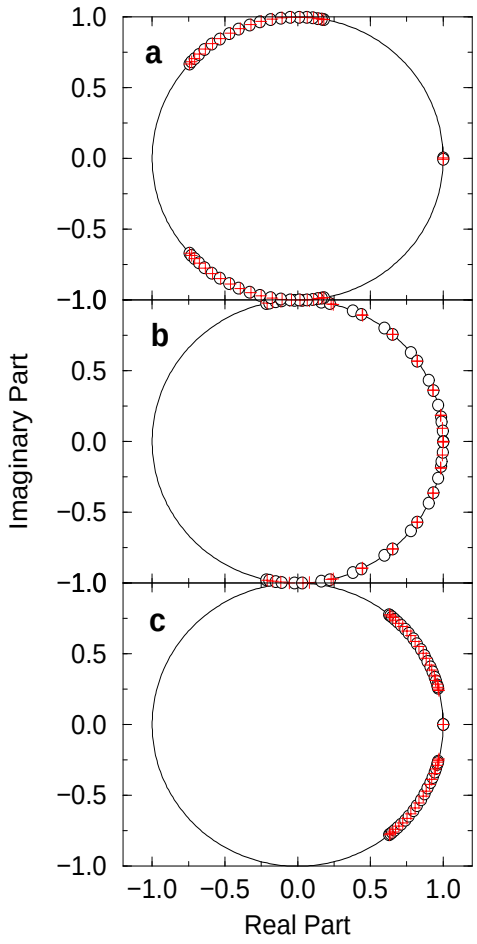

Figure 2.3: Solid line is the unit circle, with circles denote the eigenvalues of the Floquet matrix for the system with only one nonlinear site and with crosses are shown the eigenvalues of the Floquet matrix of the fully nonlinear system. **a)** Potential V_1, $C = 0.051$ and $\omega_b = 1.625$. **b)** Potential V_2, $C = 0.051$ and $\omega_b = 0.9848$. **c)** Potential V_3, $C = 0.051$ and $\omega_b = 0.9608$. **f)** Potential V_3, $C = 0.101$ and $\omega_b = 0.9608$.

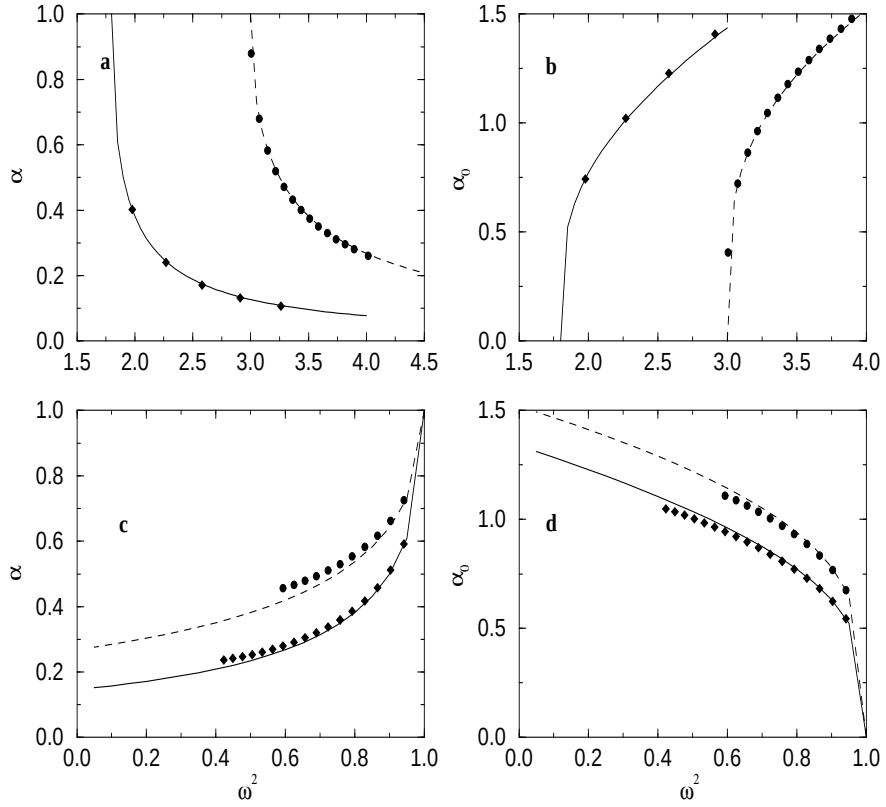

Figure 2.4: With a continuous line we plot the RWA solution while with points the exact numerical solution. (a) The exponential localization parameter α in the hard potential as a function of ω^2. The solid line corresponds to coupling C=0.2 and the dashed line to C=0.5. (b) The amplitude of the central site in the hard potential as a function of ω^2. (c) The exponential localization parameter α in the soft potential as a function of ω^2. (d) The amplitude of the central site in the soft potential as a function of ω^2.

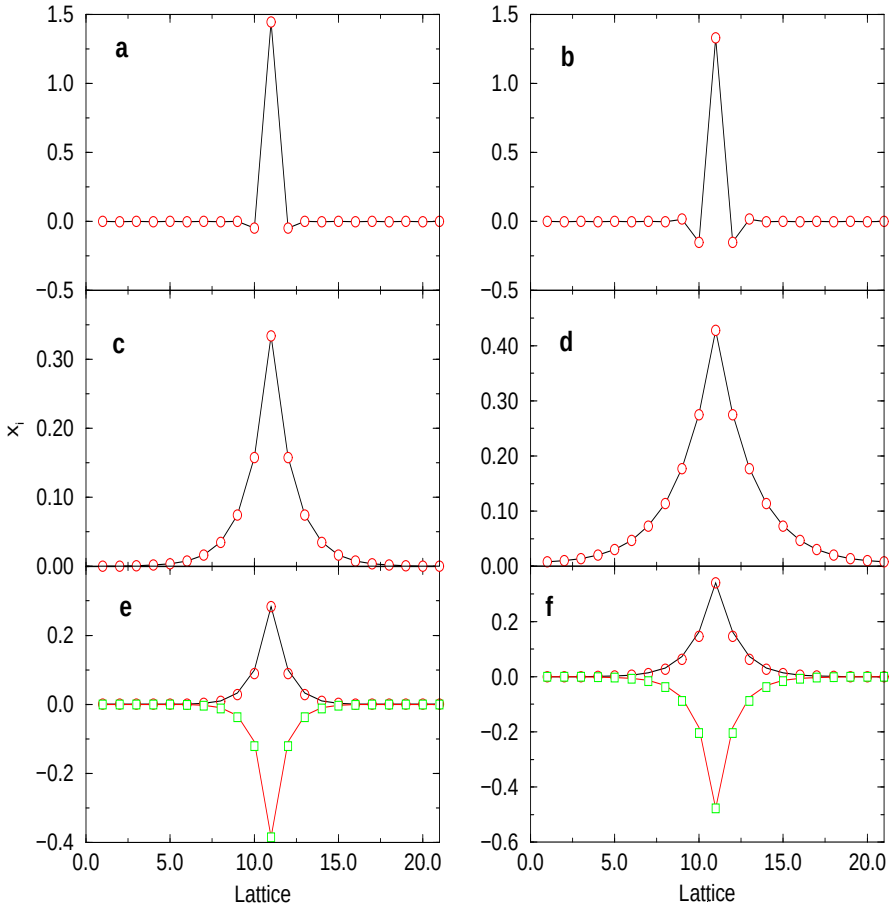

Figure 2.5: Solid line plots the breather in a system with only one nonlinear site while with circles is shown the impurity mode with the same frequency. **a)** Potential V_1, $C = 0.051$, $\omega_b = 1.625$ and $m_0 = 0.4182$. **b)** Potential V_1, $C = 0.151$, $\omega_b = 1.625$ and $m_0 = 0.5056$. **c)** Potential V_2, $C = 0.051$, $\omega_b = 0.9848$ and $m_0 = 1.086$. **d)** Potential V_2, $C = 0.151$, $\omega_b = 0.9848$ and $m_0 = 1.1422$. **e)** Potential V_3, $C = 0.051$, $\omega_b = 0.9608$ and $m_0 = 1.1589$. **f)** Potential V_3, $C = 0.101$, $\omega_b = 0.9608$ and $m_0 = 1.2078$. In figures **e** and **f** the minimum displacement of both breather and impurity mode (dashed line and boxes respectively) is additionally shown.

Chapter 3

Breather modification due to second neighbor interactions.

In the previous two chapters we saw that discrete breathers exist in systems of nonlinear oscillators coupled to each other via short range nearest neighbor interaction. Presently we would like to investigate what happens when we include interactions not only between nearest neighbors but with second neighbors as well. From the Klein-Gordon Hamiltonian (1.3) we can derive the equation of motion if we add an extra term for the second neighbor interaction.

$$H = \sum_i \frac{1}{2}\dot{u}_i^2 + V(u_i) + \frac{C_1}{2}(u_i - u_{i+1})^2 + \frac{C_2}{2}(u_i - u_{i+2})^2 \qquad (3.1)$$

We consider one dimensional chain of oscillators with mass equal to unity and harmonic interaction:

$$\ddot{u}_i = -V'(u_i) + C_1(u_{i+1} + u_{i-1} - 2u_i) + C_2(u_{i+2} + u_{i-2} - 2u_i) \qquad (3.2)$$

where C_1 is the nearest neighbor coupling and C_2 is the coupling extending to second neighbors.

If we linearize equation (3.2) we can calculate the dispersion relation for the system.

$$\omega^2 = \omega_0^2 + 4C_1 \sin^2(\frac{q}{2}) + 4C_2 \sin^2(q) \qquad (3.3)$$

where ω is the frequency and q is the wave vector of the phonons. In figure (3.1) we plot the dispersion relation for several values of the second neighbor coupling C_2.

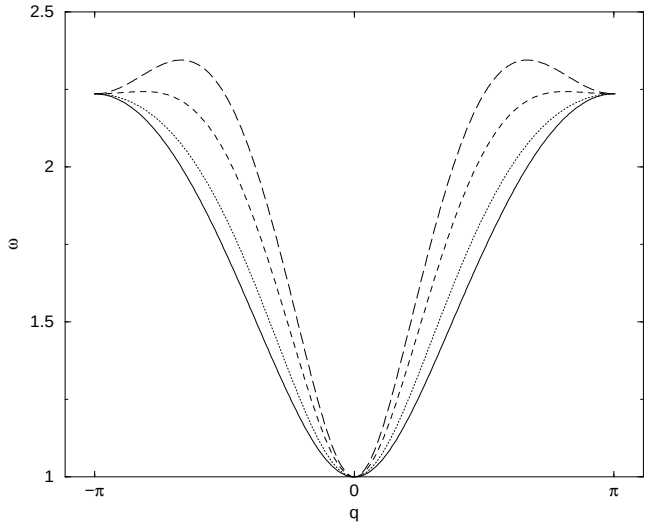

Figure 3.1: The dispersion relation for second neighbors interaction. With continuous line we denote the dispersion relation with $C_2 = 0$, while with dotted line $C_2 = 0.1$, dashed line $C_2 = 0.3$ and long dashed line $C_2 = 0.5$. We take $\omega_0 = 1$.

3.1 Rotating Wave Approximation.

Let us consider that the on-site potential V is harmonic for every oscillator except the one at $i = 0$ as in the previous chapter. We are going to consider the same ansatz as in section (2.2). For the soft potential (2.2) we consider the ansatz (2.5) and for the hard potential (2.1) the ansatz (2.4).

Upon substitution in equation (3.2) we derive the equations for the soft potential:

$$\frac{3}{4}\alpha_0^2 = 1 - \omega_b^2 - 2C_1(\alpha - 1) - 2C_2(\alpha^2 - 1) \tag{3.4}$$

$$P_1(\alpha) \equiv C_2\alpha^4 + C_1\alpha^3 + (\omega_b^2 - 1 - 2C_1 - 2C_2)\alpha^2 + C_1\alpha + C_2 = 0 \tag{3.5}$$

Equation (3.4) can give α_0 as a function of the frequency, the coupling and the localization parameter. The second equation (3.5) can be solved numerically and give the localization parameter α. In the limit $C_2 = 0$ the equation (3.5) takes the form $[C_1\alpha^2 + (\omega_b^2 - 1 - 2C_1)\alpha + C_1]\alpha = 0$ which has three solutions. The relation between the brackets is the same as (2.11) and the solution is given by (2.12) with the substitution $C = C_1$. If we plot the polynomial on the left side of equation (3.5) as a function of α (figure 3.2) we see that there are two solutions between -1 and 1 which can be found numerically through the Newton-Raphson method.

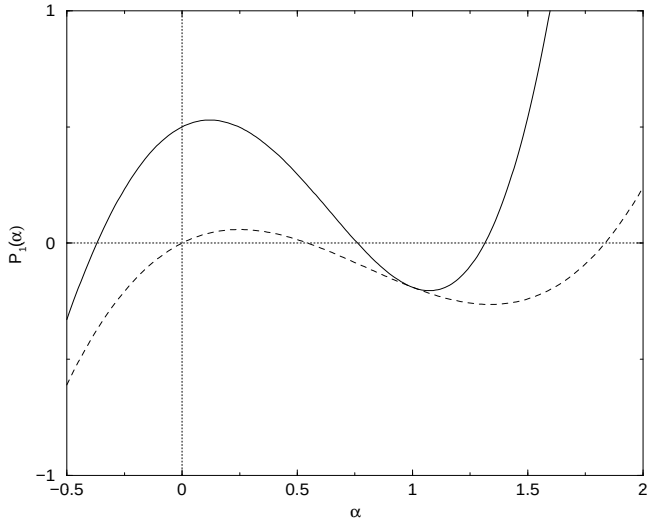

Figure 3.2: The polynomial of equation (3.5) as a function of α for $C_1 = 0.5$ and $\omega_b = 0.9$. Continuous line corresponds to $C_2 = 0.5$, dashed line corresponds to $C_2 = 0$.

Comparing the intersection points in figure (3.2) we see that the interaction between second neighbors makes the breather wider (larger value of α). We also see that there is a second solution for α negative which corresponds to a solution with $a_0 > 1$. Since the potential (2.2) has two local maxima at ± 1, this value of α and α_0 does not correspond to a physically acceptable

solution.

Similarly for the hard potential if we substitute the ansatz (2.4) in equation (3.2) we get:

$$\frac{3}{4}\alpha_0^2 = \omega_b^2 - 1 - 2C_1(\alpha + 1) + 2C_2(\alpha^2 - 1) \tag{3.6}$$

$$P_2(\alpha) \equiv -C_2\alpha^4 + C_1\alpha^3 + (1 - \omega_b^2 + 2C_1 + 2C_2)\alpha^2 + C_1\alpha - C_2 = 0 \tag{3.7}$$

In the limit $C_2 = 0$ equation (3.7) becomes $C_1\alpha^2 + (1 - \omega_b^2 + 2C_1)\alpha + C_1)\alpha = 0$ which can be solved exactly (see equations 2.7 and 2.8). If we plot the left side of equation (3.7) as a function of α we observe that there are real solutions between -1 and 1 only for small values of C_2, for large C_2 there are no intersection points with the α-axes (figure 3.3).

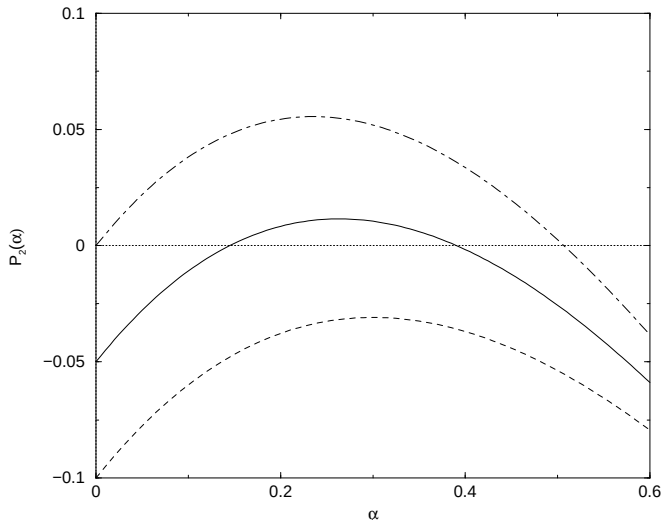

Figure 3.3: The polynomial of equation (3.7) as a function of α for $C_1 = 0.5$ and $\omega_b = 1.8$. Continuous line corresponds to $C_2 = 0.05$, dashed line corresponds to $C_2 = 0.1$ and dot-dashed line corresponds to $C_2 = 0$.

3.2 Numerical calculations and stability.

In order to confirm the results arising from the RWA, we will find the numerically exact DB using the Newton method described in section (1.2).

In figure 3.4 we see the DB calculated for the double well potential (1.20) and in figure 3.5 the DB calculated for the soft Φ^4 (1.19). For a given frequency and a given value of the nearest neighbors coupling (C_1), when the second neighbor interaction increases, the DB becomes wider and occupies more lattice sites as it can be seen in these figures were we plot the solution for $C_2 = 0$ and some non-zero value. This broadening of the DB was predicted by the RWA as we saw in the previous section and more precisely in equation (3.5) and figure 3.2.

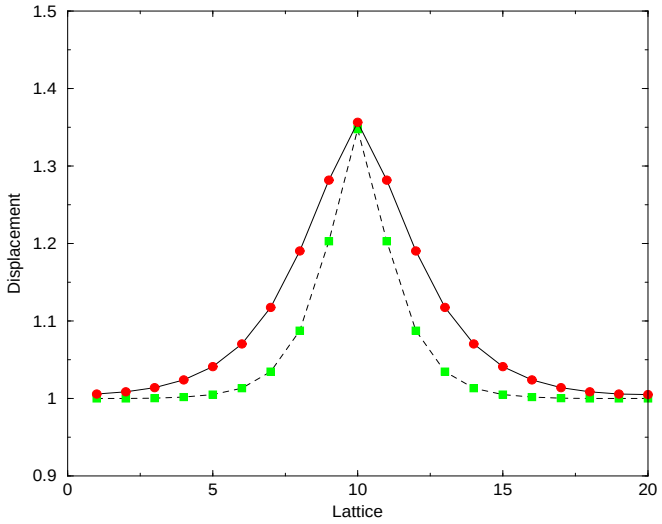

Figure 3.4: The DB in the double well potential for $C_1 = 0.231$ and $C_2 = 0.115$ (continuous line and circles) and $C_2 = 0$ (dashed line and boxes), the frequency is $\omega_b = 1.32$.

The linear stability analysis of the solution shows no significant changes in the stability of the discrete breathers due to second neighbors interaction. When the DB is linearly stable for $C_2 = 0$ in the sense that all the

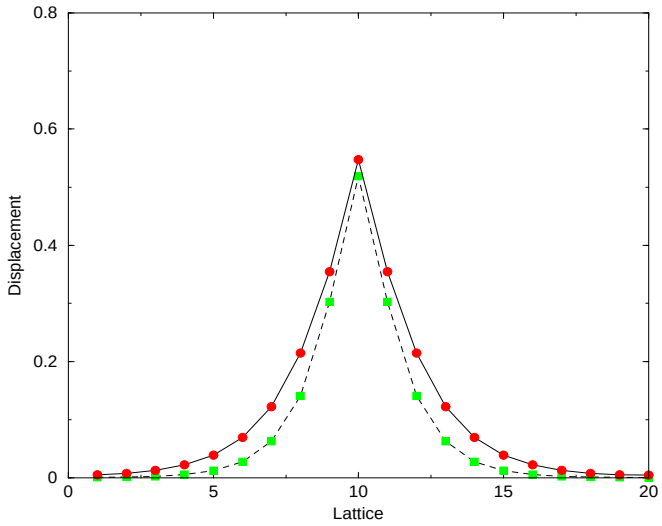

Figure 3.5: The breather in the soft Φ^4 potential for $C_1 = 0.131$ and $C_2 = 0.032$ (continuous line and circles) and $C_2 = 0$ (dashed line and boxes), the frequency is $\omega_b = 0.952$.

eigenvalues of the Floquet matrix lie on the unit circle, then it will remain stable also for non-zero values of C_2. There is one case were the effect of the second neighbor interaction can be dangerous for the DB due to resonances with phonons. For large values of the coupling C_2 the dispersion relation becomes wider as it can be seen from equation (3.3) and figure 3.3. If the DB frequency or one of its higher harmonics is close to the phonon band, then due to the broadening of the band there are pairs of eigenvalues colliding at 1 (in the unit circle in the complex plane) as C_2 increases. After the collision, it is not possible to continue the solution for larger values of C_2.

As we mentioned in the apendix A, linear stability does not mean real stability, therefore the linearly stable DB can be destroyed through a large perturbation. In the case of second neighbor interaction, the solution becomes more robust and can remain intact under the influence of much larger perturbations compared to DB's in systems with only nearest neighbors in-

teraction. This means that although in both cases the DB is linearly stable, when there is interaction between second neighbors the DB is more stable.

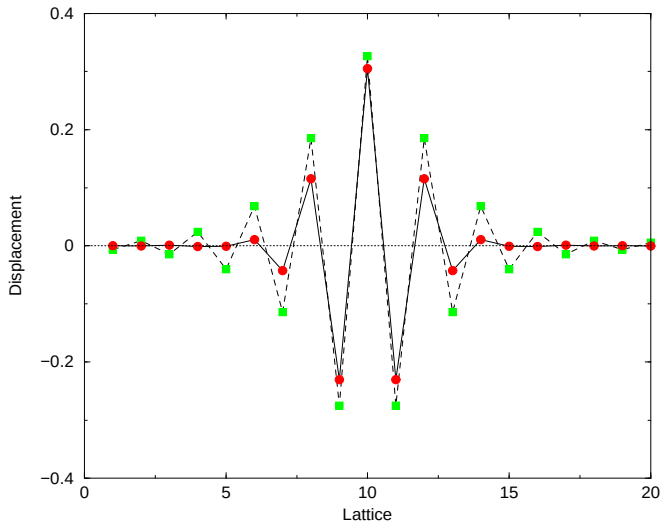

Figure 3.6: The breather in the hard Φ^4 potential for $C_1 = 0.131$ and $C_2 = 0.032$ (continuous line and circles) and $C_2 = 0$ (dashed line and boxes), the frequency is $\omega_b = 1.25$.

In figure 3.6 we see the DB in the hard Φ^4 potential (1.18). As it can be seen from equation (3.7) and figure 3.3, when the coupling between second neighbors increases, the width of the breather decreases. This can also be seen in figure 3.6 where we plot the DB for $C_2 = 0$ and for $C_2 = 0.032$ for the same frequency and for the same C_1. The DB found with the use of the Newton method starting from the anticontinuous limit corresponds to the second intersection point in figure 3.3. The first intersection point in figure 3.3 does not correspond to an existing DB. Using as an initial guess for the Newton method the solution given from the ansatz of equation (2.4), α and α_0 the values corresponding to the first intersection point, it converges to the DB solution found from the anticontinuous limit which corresponds to the second intersection point.

Chapter 4

Breathers in higher dimensional lattices.

In this chapter we are going to investigate the existence, stability and mobility of discrete breathers in higher dimensional lattices. The existence theorem is valid for lattices of any dimension [8], [11]. The energy properties of discrete breathers in a d-dimensional lattice (where d is 1,2 or 3), were investigated in [43], [44],[45]. In these works the authors considered a d-dimensional super-cubic lattice with N oscillators on each direction. They found that the breather energy in a system of coupled oscillators with acoustic phonons and for small amplitude oscillations is proportional to the number of oscillators to a power depending on the dimension, viz. $E_b \sim N^{1-2/d}$. According to this expression, in an infinite lattice, the breather energy diverges at $d = 3$, it stays finite (nonzero) for $d = 2$ and it tends to zero for $d = 1$.

We first introduce two different quasi-one dimensional models, investigate DB existence and demonstrate DB mobility under certain conditions. Subsequently we study a two dimensional lattice of oscillators and investigate the existence and the mobility of DB's.

4.1 Breathers in quasi-1D model.

The first quasi-one dimensional model we are going to study arises from a one dimensional one if we consider interaction among second neighbors with strength equal to the one of the nearest neighbors interaction. One way to imagine the topology of the lattice is to think of two parallel one dimensional lattices of oscillators where the second lattice is shifted to the left by half lattice constant. Each oscillator is coupled with its nearest neighbors with coupling C; the motion of the oscillators is along the chain only ie. it is one dimensional. In figure 4.1 we can see a schematic representation of the lattice and the interactions.

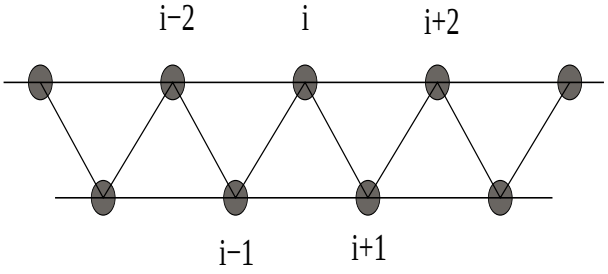

Figure 4.1: A schematic representation of the quasi-1D model.

As we can see from figure 4.1, an oscillator at lattice site i interacts with the oscillators at sites $i-2$, $i-1$, $i+1$ and $i+2$. The Hamiltonian and the equation of motion for this system are respectively:

$$H = \sum_i \frac{1}{2}\dot{u}_i^2 + V(u_i) + C \sum_{\substack{j=i-2 \\ j\neq i}}^{i+2} \frac{1}{2}(u_i - u_j)^2, \tag{4.1}$$

$$\ddot{u}_i = -V'(u_i) + C(u_{i+1} + u_{i-1} - 2u_i) + C(u_{i+2} + u_{i-2} - 2u_i), \tag{4.2}$$

where the second summation in the Hamiltonian is over nearest and second neighbors and C is the coupling. We consider the case of the double well potential $V = \frac{1}{2}(1-x^2)^2$.

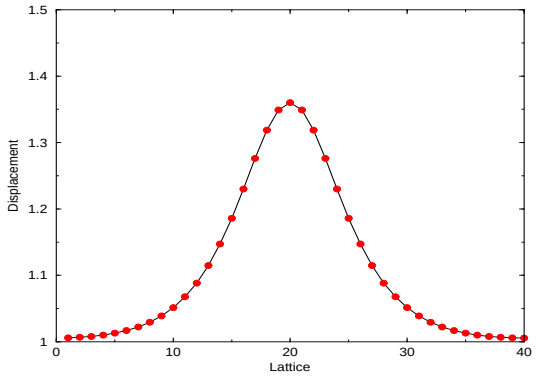

Figure 4.2: The DB for the quasi-1D lattice. $C = 0.6$ and $\omega_b = 1.3$.

In figure 4.2 we plot the DB calculated with the Newton method for this system. The stability analysis shows that the single breather is stable for small values of the coupling $C < 0.15$ and for $C > 0.18$. For C between 0.15 and 0.18 a pair of eigenvalues lies outside the unit circle creating an instability. As the coupling increases from zero, a pair of eigenvalues escapes from the phonon band and moves toward to 1. The corresponding eigenvector has different symmetry than the breather and when the eigenvalues collide at 1, they escape to the real axes. As the coupling increases, the pair of eigenvalues returns to 1 and starts moving again on the unit circle, this time away from 1. At this point a second pair of eigenvalues escapes from the phonon band and moves towards 1. For $C = 0.185$ these two pairs collide at some point on the unit circle. The second pair of eigenvalues coresponds to the the pining mode for the system. After the collision, the eigenvalues associated with the pining mode move towards 1 while the other pair moves back to the phonon band. These collisions can be seen in figure 4.5 where we plot the argument and the modulo of the eigenvalues as a function of C.

Using the Newton method we are able to construct multi-breathers starting from the anticontinuous limit with more than one oscillator excited. We

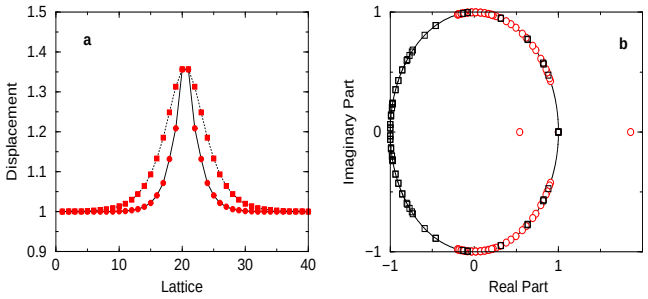

Figure 4.3: **a**) The "1,1" multibreather. Solid line and circles corresponds to $C = 0.13$ and $\omega_b = 1.31$ while dotted line and squares corresponds to $C = 0.33$ and $\omega_b = 1.31$. **b**) The stability analysis of the "1,1" multibreather. Circles corresponds to $C = 0.13$ and squares to $C = 0.33$. The multibreather for small coupling is unstable with a pair of eigenvalues outside the unit circle, in the real axis.

use the notation of section 1.1 to identify the multi-breathers, with "$1,1$" we mark the multi-breather where two neighboring sites are oscillating in phase at the anticontinuous limit (figure 4.3a) while with "$1,-1$" we mark the multi-breather where two neighboring sites are oscillating in anti-phase at the anticontinuous limit (figure 4.4a).

The "$1,1$" multi-breather is unstable for small values of the coupling. There exists a pair of eigenvalues outside the unit circle on the real axis, around 1. As the coupling increases from zero, they move away from one, and as it continues to increase, they start approaching. For $C > 0.3$ this pair of eigenvalues reaches the unit circle and the breather becomes stable (figure 4.3b). This pair of eigenvalues is associated with the pining mode; the difference is that there is no contribution to the velocities, the corresponding eigenvector has non-zero elements only in the position regime and therefore it cannot move the breather.

The second multi-breather ("$1,-1$") is stable for small values of the coupling ($C < 0.01$). For $C = 0$ there exist two pairs of eigenvalues at one and as the coupling increases one of these two pairs moves toward the

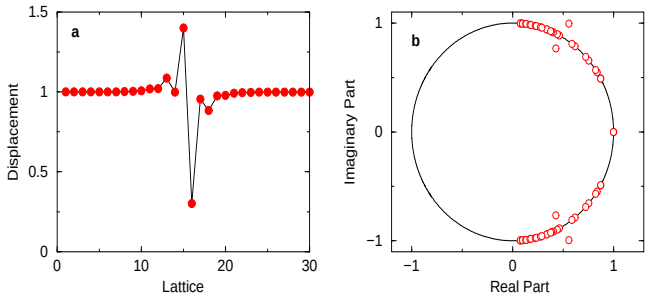

Figure 4.4: **a**) The "1,-1" multibreather for $C = 0.101$ and $\omega_b = 1.31$. **b**) The stability analysis of the "1,-1" multibreather. The multibreather is unstable with two pairs of eigenvalues outside the unit circle.

phonon band. When this pair collides with the phonon band 4 eigenvalues escape outside the unit circle (figure 4.4b). At $C = 0.21$ these eigenvalues reenter the unit circle but another pair of eigenvalues escape from the phonon band and collide at 1; the corresponding eigenvector has the same symmetry like the breather and therefore the continuation of the solution becomes impossible for $C > 0.21$.

4.1.1 Ladder.

The second quasi-one dimensional model we are going to study has the shape of a ladder. The ladder consists of two parallel sub-lattices of oscillators and each oscillator is coupled with its nearest neighbors in the same sub-lattice and with its neighbor on the other sub-lattice; motion takes place along the ladder long axis only. A schematic representation of the lattice is plotted in figure 4.6.

The Hamiltonian and the equations of motion for the ladder are:

$$\begin{aligned} H &= \sum_i \Big[\tfrac{1}{2}\dot{u}_i^2 + \tfrac{1}{2}\dot{v}_i^2 + V(u_i) + V(v_i) + \tfrac{C}{2}(u_{i+1} - u_i)^2 \\ &\quad + \tfrac{C}{2}(v_{i+1} - v_i)^2 + \tfrac{C}{2}(v_i - u_i)^2\Big] \end{aligned} \tag{4.3}$$

$$\ddot{u}_i = -V'(u_i) + C(u_{i+1} + u_{i-1} - 2u_i) + C(v_i - u_i) \tag{4.4}$$

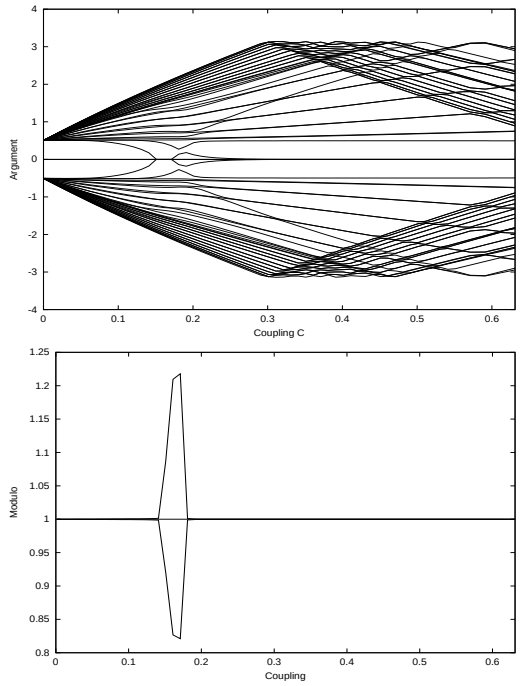

Figure 4.5: The eigenvalues of the Floquet matrix as a function of the coupling C. In the first figure the argument is plotted while in the second the modulo of the eigenvalues. There is an instability for $0.15 < C < 0.18$ due to a collision at 1 of a pair of eigenvalues. We can see in the first figure, a pair of eigenvalues that escape from the phonon band and collide at 1 for $C = 0.15$. At $C = 0.185$ there is a second collision with an other pair of eigenvalues.

$$\ddot{v}_i = -V'(v_i) + C(v_{i+1} + v_{i-1} - 2v_i) + C(u_i - v_i) \tag{4.5}$$

$\{u_i\}$ describes the oscillations on the first sub-lattice and $\{v_i\}$ describes the oscillations on the second sub-lattice, C is the coupling and $V = \frac{1}{2}(1-x^2)^2$.

Breathers can be calculated in this system with the use of the Newton method. In figure 4.7 we plot the single breather with only one site excited at the anticontinuous limit. In figure 4.8 we plot a multi-breather with two sites excited in phase at the anticontinuous limit. In figure 4.9 we plot the energy of the single breather with continuous line, and that of the multi-

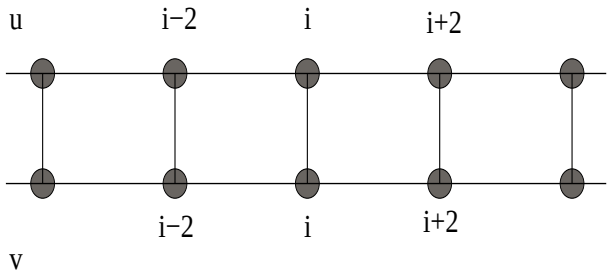

Figure 4.6: A schematic representation of the ladder.

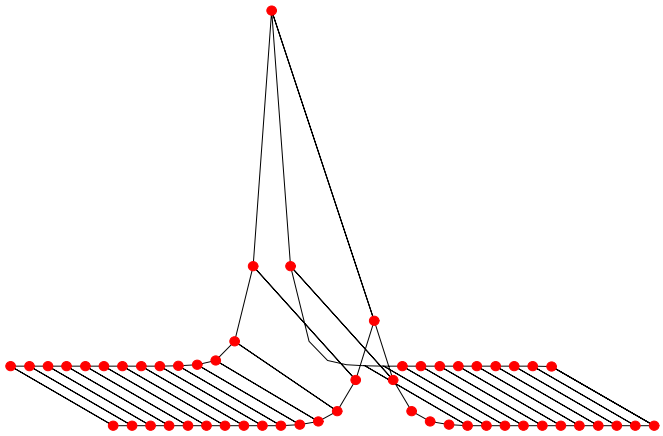

Figure 4.7: A single breather on the ladder. $C = 0.1$ and $\omega_b = 1.3$.

breather with dashed line as a function of the coupling C for $\omega_b = 1.3$. For $C < 0.25$ there are two curves. At $C = 0.25$ the two breathers have the same energy due to a pitchfork bifurcation that occurs. For $C > 0.25$ there exist only the multi-breather.

For $C < 0.25$ the single breather is stable while the multi-breather is unstable. In figure 4.10 we plot the argument and the modulo of the Floquet eigenvalues for the multi-breather as a function of the coupling. For $C < 0.25$ there is a pair of eigenvalues outside the unit circle, on the real axis. As C reaches the bifurcation value $C = 0.25$, the eigenvalues enter the unit circle

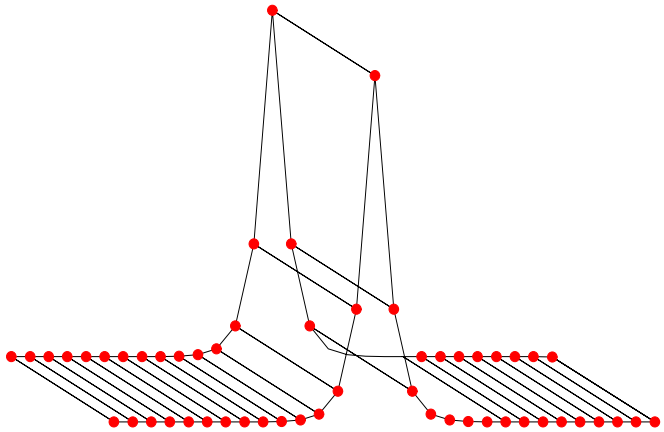

Figure 4.8: The multi-breather with 2 sites in the same unit cell excited. $C = 0.1$ and $\omega_b = 1.3$.

and the multi-breather becomes stable. After they enter the unit circle they start moving towards the phonon band. For large values of coupling, another pair of eigenvalues escapes from the phonon band and moves towards 1. These eigenvalues correspond to the pining mode of the system. The pining mode consists of two parts, one for every sub-lattice. Every part is antisymmetric around the center of the breather. Using the pining mode we are able to excite the multibreather and make it move in a direction parallel to the ladder.

4.2 Breathers in two dimensions.

We now consider a two dimensional square lattice. Every lattice site is occupied by a single oscillator. Each oscillator is coupled with its nearest neighbors with linear coupling. A schematic representation of the lattice is plotted in figure 4.11 The Hamiltonian and the equations of motion of the system are:

$$H = \sum_{i,j} \frac{1}{2}\dot{u}_{i,j}^2 + V(u_{i,j}) + \frac{C}{2}\left((u_{i,j} - u_{i+1,j})^2 + (u_{i,j} - u_{i,j+1})^2\right) \qquad (4.6)$$

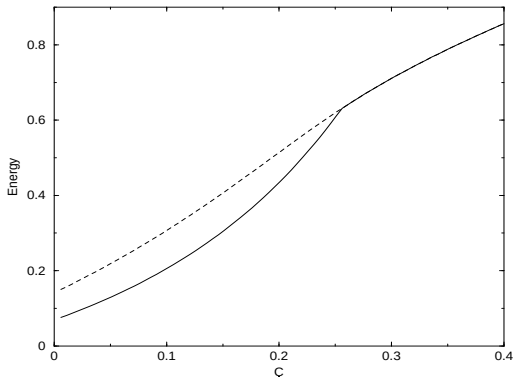

Figure 4.9: The Pitchfork bifurcation in the ladder.

$$\ddot{u}_{i,j} = -V'(u_{i,j}) + C(u_{i+1,j} + u_{i-1,j} - 2u_{i,j}) + C(u_{i,j+1} + u_{i,j-1} - 2u_{i,j}) \quad (4.7)$$

where C is the coupling and V is the on-site potential. The summation in the Hamiltonian is over i and j, i corresponds to the x-direction of the lattice while j to the y-direction. For the on-site potential we consider the case of the soft double well potential of equation (1.20).

In figure 4.12 we plot the single breather for the soft double well potential. For small values of the coupling the single breather is stable. As the coupling increases, a pair of eigenvalues escape from the phonon band and collide at 1. After the collision they escape on the real axes and the breather becomes unstable. As the coupling increases more, these eigenvalues return at 1 and reenter the unit circle. At this point two pairs of eigenvalues escape from the phonon band and move towards 1; the corresponding eigenvectors for these two pairs are the pining modes of the system. These two pining modes are antisymmetric around the center of the breather in directions which are rotated 45^o from the main directions of the lattice (see figure 4.13).

If we excite the single breather using one of the pining mode, the breather becomes mobile and start to move in the direction of the pining mode. In figure 4.14 we plot the breather of figure 4.12 when we excite it with one

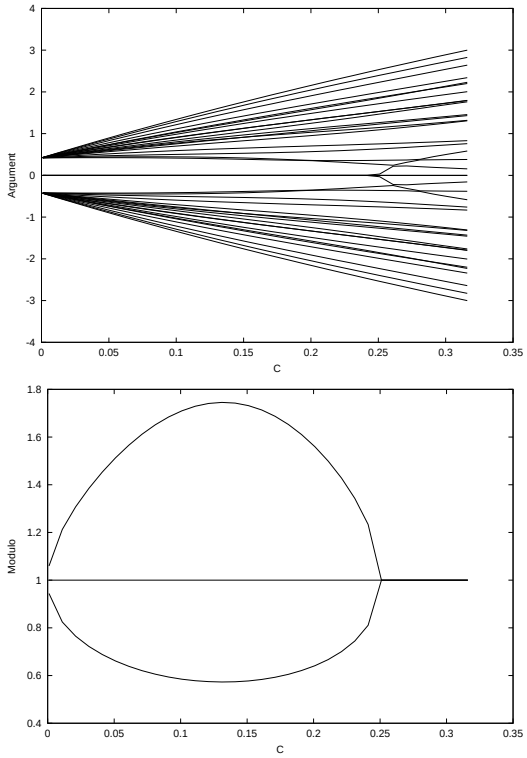

Figure 4.10: The eigenvalues of the Floquet matrix as a function of the coupling C for the multi-breather on the ladder. In the first figure we plot the argument while in the second we plot the modulo of the eigenvalues. The multi-breather is unstable for $C < 0.25$ and stable for larger values.

of the pining modes after $t = 400$ time units. As we can see the breather has been moved several lattice sites due to the excitation. If we excite the breather using the linear combination of the two pining modes, then the breather start to move in one of the main directions of the lattice (figure 4.15).

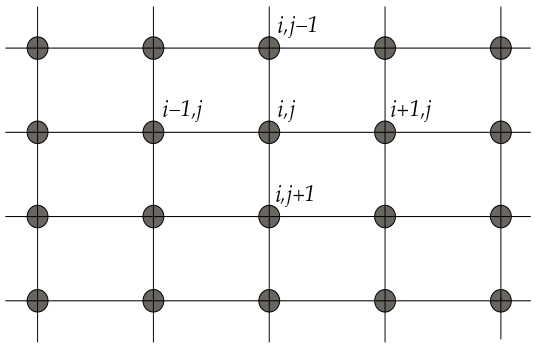

Figure 4.11: A schematic representation of the two-dimensional lattice.

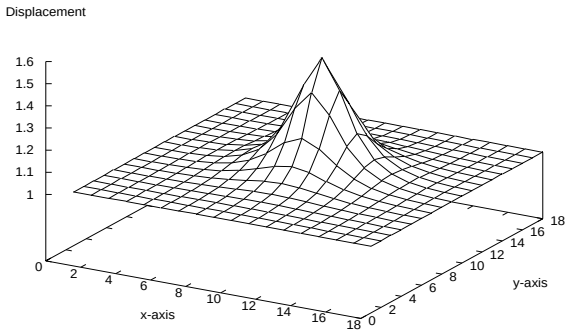

Figure 4.12: The single breather in the two-dimensional lattice for the soft double well potential. $C = 0.452$ and $\omega_b = 1.3$.

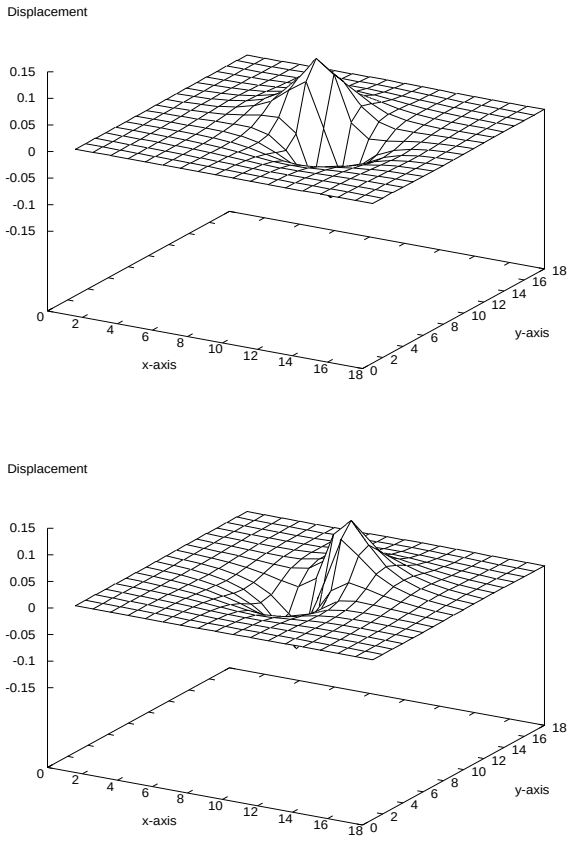

Figure 4.13: The pining modes of the single breather in the two-dimensional lattice for the soft double well potential.

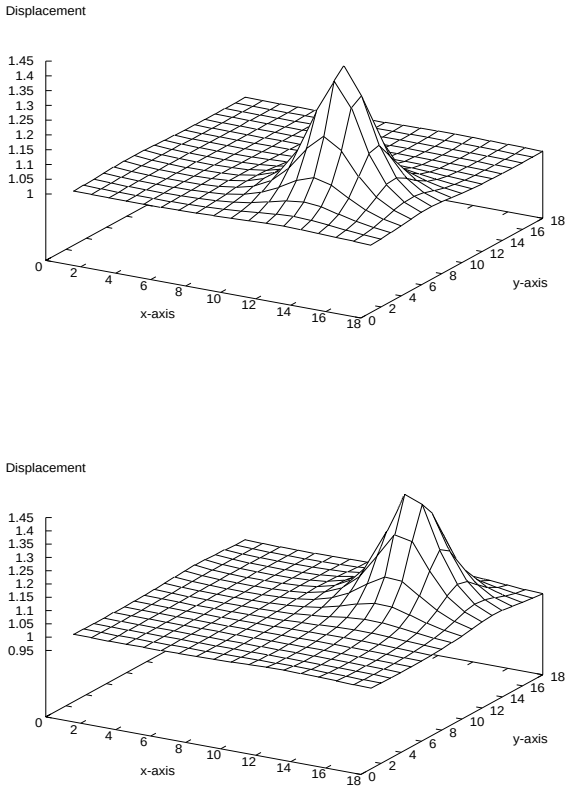

Figure 4.14: The mobile breather of figure 4.12 after t=400 time units. The first is excited with the first pining mode of figure 4.13 while the second is excited with the second pining mode.

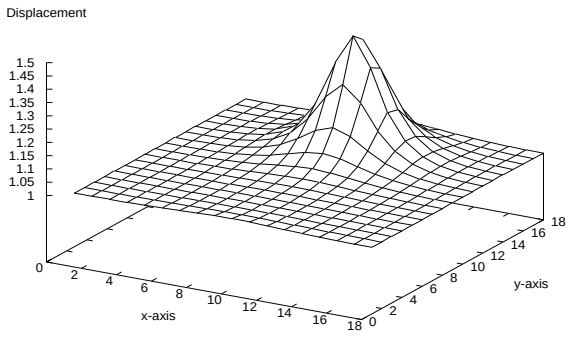

Figure 4.15: The mobile breather of figure 4.12 after t=400 time units. The breather is excited with a linear combination of the pining modes of figure 4.13 and is moving in the y-direction.

Chapter 5

Breathers in Hydrogen-bonded networks.

Hydrogen bonded (HB) systems, such as ice, carbohydrates, solid alcohol and others exhibit some properties that can be explained in terms of a highly nonlinear behavior of the system. The electrical conductivity in these systems occurs due to proton transport in the form of topological solitons [59]-[63]. The hydrogen bonds are of the type (...X-H...X-H...X-H...X-H...) where X is some heavy negative ion and H is the proton. Each proton is connected with the ions with a covalent bond (-) and a hydrogen bond (...) (see figure 5.1). The protons in the HB can be found in equilibrium positions separated by a potential barrier. This potential is due to the interaction of the protons with the ions. The height of the potential barrier that separates the two equilibria depends strongly on the distance between adjacent X ions.

If we consider that the heavy ions (X) are static, the proton motion can be described with the classical Hamiltonian in a standard dimensionless form:

$$H \;=\; \sum_n [\frac{1}{2}\dot{u}_n^2 \;+\; \frac{1}{2}C(u_{n+1}-u_n)^2 \;+\; V(u_n)], \qquad (5.1)$$

where $u_n = u_n(t)$ is the displacement of the nth proton of the chain from its equilibrium position, C is the strength of the nearest-neighbor oscillator coupling and V is an on-site potential normalized by $V''(0) = 1$.

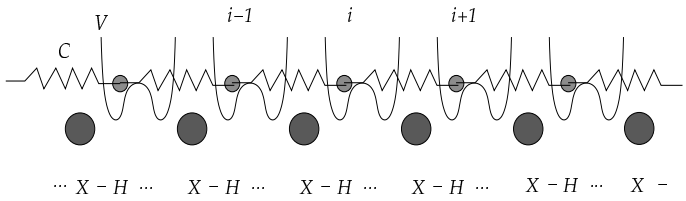

Figure 5.1: The hydrogen-bonded network. Large circles correspond to heavy ions (X) and small circles to protons (H). The heavy ions are considered to be static.

It has be shown that this model exhibits nonlinear waves like breathers [8]-[16] and topological solitons (kinks) [60]-[62],[116],[117]. We are going to study the interaction between these two different types of nonlinear waves [21]. In this work we will be reporting results primarily for sine and double-well nonlinear on-site potentials. In order to address the particle-like properties of discrete but relatively wide sine-Gordon breathers we use the well known exact continuous breather solution [65]. To find the center of mass dynamics of the breather solution we introduce the dynamical variables $X_B(t), \dot{X_B}(t)$, representing, respectively, the position and velocity of the breather center of mass. We use the approach of ref. [64] and work in the continuous limit ($n = x$). Contrary to previous work [66]-[68], we introduce only *one* collective coordinate, namely the position of the breather center. Therefore, on the basis of the standing breather solution, we write the following approximate *moving* breather ansatz:

$$\begin{aligned} u_B(x,t) &= 4\arctan[\tan\mu \ \sin(\cos\mu \ t) \\ &\times \ \text{sech}\left(\sin(\frac{\mu}{c_0})(x - X_B)\right)] \end{aligned} \tag{5.2}$$

where $0 < \mu < \pi/2$, and $c_0 \equiv \sqrt{C}$ is the dimensionless characteristic velocity. It appears that the critical width λ_c for the existence of this (standing) breather solution is $\lambda_c = c_0$.

As with the breather solution, we also introduce the kink solution with a set of collective coordinates, respectively $X_K(t), \dot{X_K}(t)$. The moving kink

ansatz is

$$u_K(x,t) = 4\arctan\exp\left[\pm(x - X_K)/c_0\right] . \tag{5.3}$$

Upon substitution in the continuous system Hamiltonian, summing these solutions ($u = u_B + u_K$) and elimination of all but the center of mass dynamical variables of the breather and kink, we obtain the averaged effective breather-kink energy, that, for small velocities, reads

$$E = E_B + \frac{1}{2}M_B\dot{X}_B^2 + E_K + \frac{1}{2}M_K\dot{X}_K^2 + U(R), \tag{5.4}$$

with the effective interaction potential

$$\begin{aligned} U(R) &= -8\tan^2\mu\int_{-\infty}^{\infty} dx\ \mathrm{sech}^2\frac{x-R}{c_0} \\ &\times\ \mathrm{sech}^2(\frac{\sin\mu}{c_0}x)[1+\tan^2\mu\ \mathrm{sech}^2(\frac{\sin\mu}{c_0}x)]^{-3/2}, \end{aligned} \tag{5.5}$$

where $R = X_B - X_K$. In these equations the expected stationary breather and kink energies and masses are given by

$$E_B = 16c_0\sin\mu, \quad M_B = (16/c_0)\cos\mu\ (\tan\mu - \mu) \tag{5.6}$$

$$E_K = 8c_0, \qquad M_K = 8/c_0\ . \tag{5.7}$$

For $\mu \to \pi/2$ we have $M_B = 2M_K$, while in the other extreme $\mu \to 0$ we have $M_B \to 0$.

For the kink and breather collective coordinates we calculated also the field momentum P given by

$$P = -\int_{-\infty}^{\infty} dx\ \overline{u_t u_x} = M_B\dot{X}_B + M_K\dot{X}_K \tag{5.8}$$

where the overbar denotes the time-averaged quantity over one breather period.

These equations approximate the complicated problem of a breather interacting with a sine-Gordon kink as a problem of two classical particles of masses M_B and M_K respectively with internal energies E_B and E_K interacting through the complex potential $U(R)$, where R is the relative distance

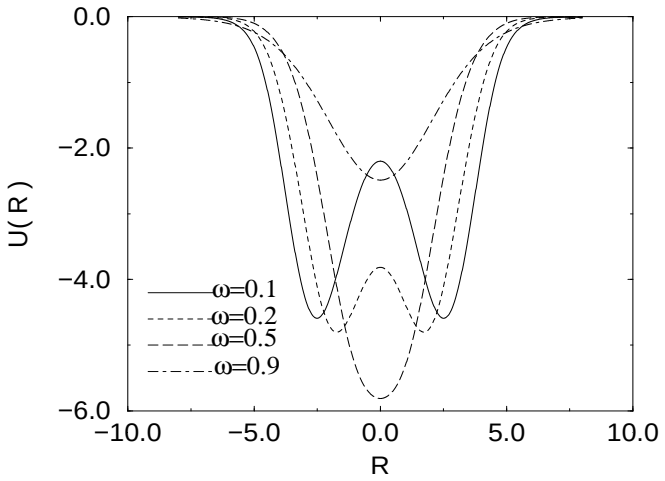

Figure 5.2: Kink-breather attractive potential for breather frequencies ω_b=0.1, 0.2, 0.5, and 0.9. In the regime $\omega_b \leq \omega_0/3$ the potential has the form of a double well.

between the particles. In figure 5.2 we plot the breather-kink interaction potential for various breather frequencies. We observe that the potential has a double well structure for smaller breather frequencies but switches to a single well at higher frequencies. The double well structure signifies that there is an equilibrium distance from the kink at which the system of breather-kink can be at rest, or that the breather can execute bounded oscillations around this minimum. This result, does not seem to be specific to the sine-Gordon system. For instance, for the case of a ϕ^4 lattice with the on-site potential $V(u) = (1 - u^2)^2/8$, a similar approach can be used, although the analytical calculations are considerably more difficult since the ϕ^4-breather is not symmetric. To find, in the continuum approximation, a small-amplitude breather solution to this model, we can also use the multiple-scale asymptotic expansion (for details see, e.g., refs. [71]) in the small parameter $\epsilon = \sqrt{1 - \Omega^2}$, where Ω is the breather frequency. Sub-

stituting the expansion

$$u_n(t) = \pm 1 + \frac{1}{2}\epsilon[A_n e^{i\Omega t} + \epsilon D_n e^{2i\Omega t} + \text{c.c.}] + \epsilon^2 C_n + \ldots \tag{5.9}$$

(where the upper (lower) sign stands for oscillations in the right (left) well of the double-well on-site potential) into the discrete equation of motion and equating coefficients at the same powers of the parameter ϵ, one finds the equation

$$\begin{aligned} & \kappa\epsilon^{-2}(A_{n+1} - 2A_n + A_{n-1}) - A_n \\ \mp \quad & 3A_n C_n \mp \frac{3}{2}A_n D_n - \frac{3}{8}A_n^3 = 0 \end{aligned} \tag{5.10}$$

and the relations $C_n = \mp 3A_n^2/4$ and $D_n = \pm A_n^2/4$. Using the solution in the continuum limit of these equations, one can write the corresponding (standing) breather solution:

$$\begin{aligned} u_B(x,t) &= \pm 1 + \frac{2c_0}{\sqrt{3}\lambda}\text{sech}\frac{x}{\lambda}\cos(\Omega t) \\ &\mp \left(\frac{c_0}{\lambda}\right)^2 \text{sech}^2\frac{x}{\lambda}\left[1 - \frac{1}{3}\cos(2\Omega t)\right] , \end{aligned} \tag{5.11}$$

where $\lambda = c_0/\epsilon$ is the correlation length of oscillations and the breather frequency Ω is given by $\Omega^2 = 1 - (c_0/\lambda)^2$. In the continuum limit, $\lambda \gg 1$.

Consider now the (anti)kink motion in the ϕ^4 model with sufficiently small velocities and denote the (anti)kink position by $X_K(t)$. Then for sufficiently small velocities the (anti)kink solution of Eq. (5.1) in the continuum limit can approximately be represented by

$$u_K(x,t) = \pm \tanh[(x - X_K)/2c_0], \tag{5.12}$$

where the upper (lower) sign corresponds to the kink (anti-kink). We are interested in the breather-(anti)kink interaction. Note that the ansatz for this interaction cannot be assumed in the *additive* form because of topological arguments. Using equations (5.11) and (5.12), the additive form should

be modified to

$$\begin{aligned} u(x,t) &= \frac{2c_0}{\sqrt{3}\lambda}\mathrm{sech}\frac{x-X_B}{\lambda}\cos(\Omega t) \\ &\pm \left\{1-\left(\frac{c_0}{\lambda}\right)^2\mathrm{sech}^2\frac{x-X_B}{\lambda}\left[1-\frac{1}{3}\cos(2\Omega t)\right]\right\} \\ &\times \tanh\frac{x-X_K}{2c_0}, \end{aligned} \tag{5.13}$$

where the upper (lower) sign corresponds to the interaction of a breather with a kink (anti-kink).

The total energy can be represented to lowest order in λ by the same sum of equation (5.4), but with

$$\begin{aligned} U(R) &= \left(\frac{c_0}{\lambda}\right)^2\int_{-\infty}^{\infty}dx\ \mathrm{sech}^2\frac{x-R}{\lambda}\mathrm{sech}^2\frac{x}{2c_0} \\ &\times \left(\frac{c_0}{\lambda}\tanh\frac{x-R}{\lambda}\tanh\frac{x}{2c_0}-\frac{1}{4}\mathrm{sech}^2\frac{x}{2c_0}-\frac{1}{2}\right)\ . \end{aligned} \tag{5.14}$$

This effective potential has the form of a single well, centered at $R = 0$. Here in the lowest orders of ϵ, the breather and kink energies and masses are given by

$$E_B = 4c_0^2/3\lambda, \quad M_B = 4c_0^2/9\lambda^3, \tag{5.15}$$

$$E_K = 2c_0/3, \quad M_K = 2/3c_0\ . \tag{5.16}$$

Except for the well-known kink relation $E_K = M_K c_0^2$, we note a similar breather relation with low amplitudes. Indeed, for small amplitudes the correlation length of the SG breather $\lambda = c_0/\sin\mu \simeq c_0/\mu$. Using the last relation, one finds for both models the following equation: $E_B = 3M_B\lambda^2$.

There is clear numerical evidence presented in figure 5.3 showing the breather trapped in the vicinity of the kink and executing small oscillations around the minimum of an effective potential. These minima can bee seen in figure 5.2 in the Sine-Gordon model, but only for very small frequencies, where the breather is unstable. Numerical evaluation of the expression of equation (5.14) for the same parameters set as in figure 5.3 results in a single

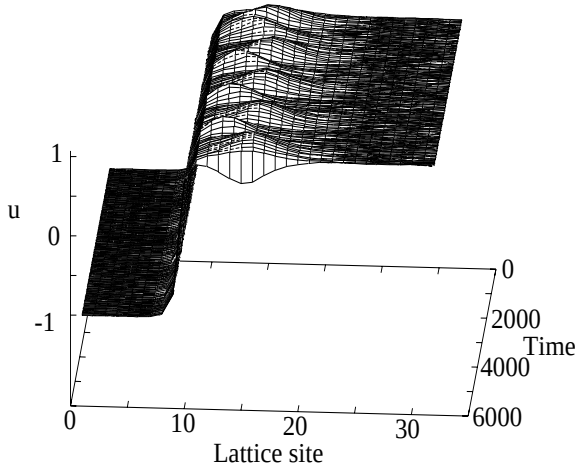

Figure 5.3: Trapping of an initially static breather in the vicinity of a ϕ^4 kink. Parameters are $\omega_0^2 = 2$,$\omega_b = 1.37819$ and coupling $C = 0.301$.

attractive well centered around $R = 0$. This indicates that for the case of the asymmetric ϕ^4 breather additional collective coordinates are necessary for explicit prediction of the double well feature of the kink-breather attractive potential that is seen numerically in figure 5.3. By plotting the average over a period, of the potential energy of the system we see that when the breather comes close to the kink, it sees a potential barrier and it is forced to return.

The trapping of a breather in the vicinity of a kink is not the only possible breather-kink dynamical configuration. For an initially static breather-kink system, depending on the parameter regime and additional perturbations due to proximity to the discreteness regime, we may have a detrapped situation. In figure 5.4. we present numerical simulations for the sine-Gordon system with an initially static breather-kink configuration. When the breather is placed close to the kink, it is repelled (figure 5.4a), while when placed further is attracted to the kink (figure 5.4b). In the last case, shown in the figure, we note that the breather is actually destroyed with a

subsequent generation of linearized modes.

Let us finally consider the case of moving breathers impinging on the kink. To generate moving breathers we use the method of ref. [16]. We recall that the moving breather, in addition to an inertial mass also carries internal energy E_B. This energy, in principle can be deposited in any lattice location whenever the breather "reacts" with another species, such as for instance a kink. This situation is seen in figure 5.5 where a kinetic breather reacts with the kink, releasing all internal and kinetic energy to the kink which then begins moving. In this case, breather energy is transformed into kink kinetic energy. In figure 5.6, on the other hand, we observe a breather-kink elastic collision, where the breather is simply reflected from the kink with very little distortion. Finally, in figure 5.7 we observe a third kink-breather reaction pathway though which the breather energy is released to the vicinity of the kink with subsequent generation of linearized modes. In this case, the breather is destroyed without passing its internal energy to the kink in the form of kinetic energy.

From the previous analysis we observe that the breather-kink interaction is a complex one, leading to a variety of outcomes. From the energy transfer point of view, a breather is an efficient agent that acts as a particle with its internal structure characterized by a given amount of internal energy. It is also characterized by certain reactivity features that enable it to transfer and deposit this energy in lattice regions with kinks. The kink-breather reaction is complex, characterized by a trapping potential that depends on the breather frequency and the breather initial momentum and possibly the relative phase. For breathers with low frequencies we find that a length scale is created within which a breather-kink bound state can be formed. Moving breathers on the other hand can react with kinks transforming all their energy into kink kinetic energy, or having an elastic collision with the kink. Finally, complete breather annihilation is also possible with subsequent generation of linearized extended modes.

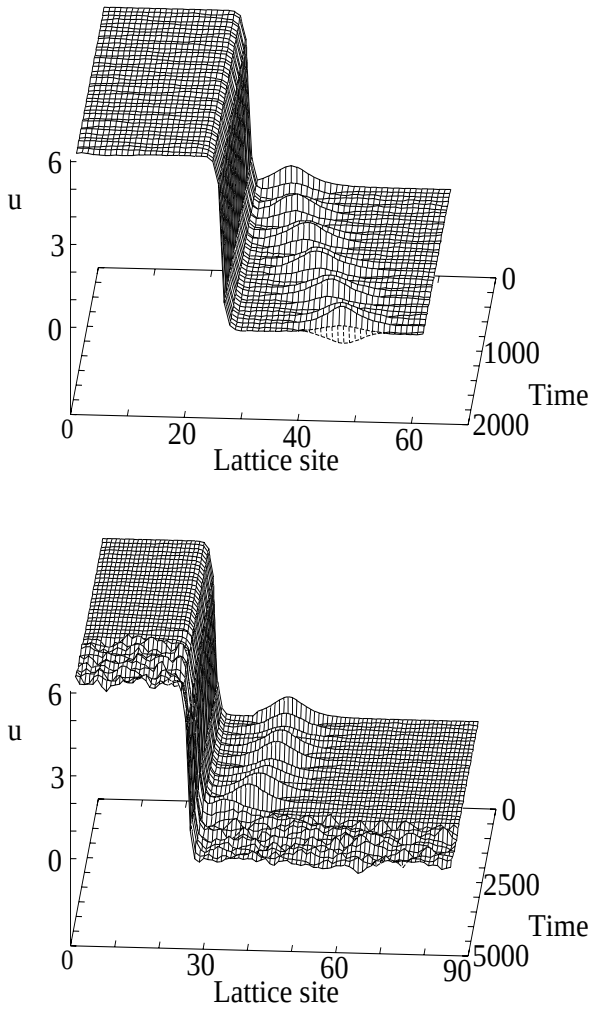

Figure 5.4: **(a)** Breather repulsion when placed close to the center of the kink with zero initial velocity. ($\omega_0 = 1.0, \omega_b = 0.9844, C = 0.251$). **(b)** Breather absorption by the kink, while breather internal energy is transformed into phonons. ($\omega_0^2 = 2, \omega_b = 1.3921, C = 0.691$).

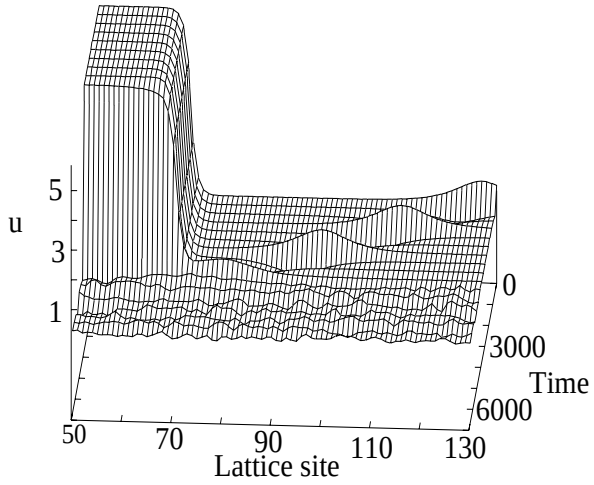

Figure 5.5: The breather is absorbed by the kink while its internal energy is transformed into kinetic energy for the latter. We also see that some phonons are excited. The value of the parameters are, $\omega_0 = 1$, $\omega_b = 0.9844$, coupling $C = 0.649$, perturbation strength $l = 0.161043$

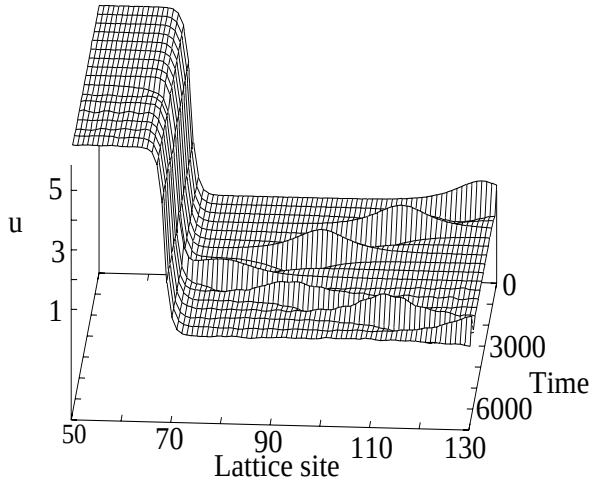

Figure 5.6: In this case we increase the perturbation strength and see that the breather is reflected from the kink. The parameters are the same as in figure 5.4 except of $l = .161172$

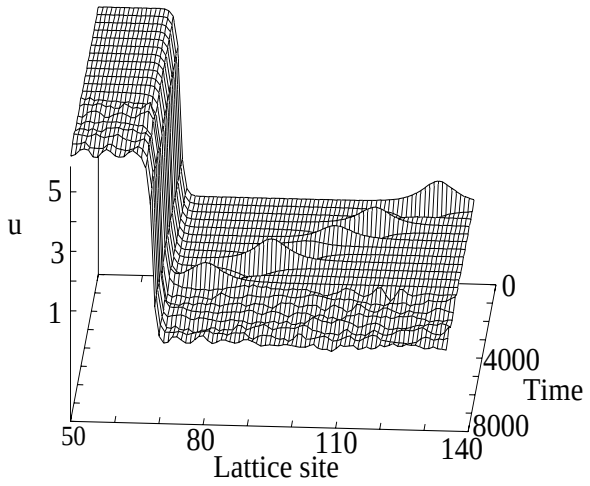

Figure 5.7: In this figure we see that the breather is absorbed by the kink, and the internal energy of the kink is transformed into outgoing phonons. Parameters are $\omega_0^2 = 2$, $\omega_b = 1.3921$, coupling $C = 0.691$ and $l = 0.166813$.

Chapter 6

Discrete Breathers in strong hydrogen bonds.

In this chapter we consider a diatomic chain of heavy ions coupled through strong, unimodal hydrogen bonds, that are much stronger than other system interactions. Each proton of the hydrogen bond experiences a single-minimum potential resulting from its interaction with nearest-neighbor heavy ions; this potential contains soft or hard anharmonicity. This diatomic chain of nonlinearly coupled masses admits discrete breather solutions in the gap of the phonon spectrum. Simple analytical arguments accompanied by explicit solutions demonstrate the existence of gap breathers with both types of symmetry, viz. the odd-parity or even parity pattern. Depending on the type of the anharmonicity the breather can be centered at a hydrogen-bonded proton for a soft interaction or at a heavy ion for a hard interaction. These analytical results are verified numerically through the use of the numerically exact procedure from the anti-continuous limit.

6.1 Introduction.

The basic idea in the nonlinear model for proton dynamics in a HB chain stems from the fact that the proton potential in each H-bond of the chain can be constructed as the sum of two two-body ion-proton potentials, e.g., the

Morse potentials [73]. If this (asymmetric) two-body potential is sufficiently strong compared with other interactions (eg., between heavy ions or with an external on-site coupling), the resulting potential for the HB proton has only one minimum and the H-bond in this case is referred to as the strong H-bond [74]. Otherwise, this potential has two degenerate minima separated by a barrier [73],[76],[64] and long wavelength breather solutions have been studied earlier[70]. Schematically, a chain with strong hydrogen bonding can be represented by the diatomic sequence $\cdots$ –X–H–X–H–X–H–X– $\cdots$, where X denotes a heavy ion and H a proton.

In general, a 1D anharmonic diatomic lattice that has a gap in its phonon band, admits standing (anharmonic gap modes) and moving (gap solitons) solutions which were studied using different approximate techniques [77]-[80]. There is also a proff that discrete breathers are excact solution in some casses [35], [36]. In particular, the diatomic chain with realistic (soft and asymmetric) two-body nearest-neighbor potentials was studied recently both analytically and numerically [35],[36],[81]. In all previous studies, the method used for finding the gap breathers was unable to give more information regarding the origin of these solutions and their stability. The main aim of present work is to find in chains with strong hydrogen bonding exact solutions for discrete gap breathers and to investigate their stability, using the anticontinuous limit approach [15]. This numerical work is accompanied by analytical arguments based on the similarity [22] between the mass-impurity mode [83] and intrinsic localized modes.

6.2 The diatomic FPU model.

The system we are studying is a diatomic Fermi-Pasta-Ulam (FPU) chain. In each unit cell there is a heavy atom (eg. oxygen with mass $M = 16$) and a light atom (eg. hydrogen with mass $m = 1$). Each atom is considered to interact only with its nearest neighbors with an an-harmonic potential

W. We consider two qualitatively different potentials W, one being soft while the other hard. The displacement of the heavy atoms is Q_n while the displacement of the light atoms is q_n. The Hamiltonian of the system is:

$$H = \sum_n \left[\frac{1}{2} M \dot{Q_n}^2 + \frac{1}{2} m \dot{q_n}^2 + W(Q_n - q_n) + W(q_n - Q_{n+1}) \right] \tag{6.1}$$

where the summation is over all the unit cells of the lattice. The equations of motion are,

$$M \ddot{Q}_n = W'(q_n - Q_n) - W'(Q_n - q_{n-1}) \tag{6.2}$$

$$m \ddot{q}_n = W'(Q_{n+1} - q_n) - W'(q_n - Q_n). \tag{6.3}$$

For the potential W we will use one of the following two functions:

$$W(x) = \frac{1}{2} x^2 - \frac{1}{4} x^4 \tag{6.4}$$

$$W(x) = \frac{1}{2} x^2 + \frac{1}{4} x^4 \tag{6.5}$$

For the numerical calculation of the breathers it is essential to introduce in our system an anticontinuous limit. To achieve this we add an on site nonlinear potential in every particle multiplied with some parameter η while the nonlinear dispersion potential is multiplied with parameter λ. The anticontinuous limit is then for $\eta = 1$ and $\lambda = 0$ while the original system we want to study corresponds to $\eta = 0$ and $\lambda = 1$. The continuation from the trivial solution found in the anticontinuous limit can be through any path in the parameter space which connects these two points. For simplicity we choose $\eta = 1 - \lambda$ and the on site potential be equal to potential W. The new modified equations are

$$M \ddot{Q}_n = -(1 - \lambda) W'(Q_n) + \lambda (W'(q_n - Q_n) - W'(Q_n - q_{n-1})) \tag{6.6}$$

$$m \ddot{q}_n = -(1 - \lambda) W'(q_n) + \lambda (W'(Q_{n+1} - q_n) - W'(q_n - Q_n)) \tag{6.7}$$

6.3 Phonons and Dispersion relation.

Since we deal with a diatomic chain, it is well known that if we linearize the equations of motion, we can find the phonon dispersion relations of the system. The phonon spectrum consists of two bands, the acoustic one corresponding to frequencies between 0 and ω_1 as well as the optical one, corresponding to to frequencies between ω_2 and ω_3. The dispersion relation and the characteristic frequencies can be calculated analytically [106].

A necessary condition for the breather to exist is to avoid resonances with phonons, meaning that the DB frequency and all its harmonics must lie outside the phonon band. The continuation of the breather from the anticontinuous limit can be performed only if in every continuation step the frequency fulfills the previous restriction.

To find a valid continuation path it is necessary to know, for each λ, the dispersion relation. The corresponding linearized equations of equations 6.6 and 6.7 are

$$M\ddot{Q}_n = -(1-\lambda)Q_n + \lambda(q_n - 2Q_n + q_{n-1}) \tag{6.8}$$

$$m\ddot{q}_n = -(1-\lambda)q_n + \lambda(Q_{n+1} - 2q_n + Q_n) \tag{6.9}$$

and if we substitute $Q_n = A\exp(ikn - i\omega t)$ and $q_n = B\exp(ikn - i\omega t)$ where k is the wave-vector and ω is the phonon frequency, we can find the dispersion relation. The frequencies of the acoustic band as a function of λ are

$$\omega_a = \sqrt{\frac{(M+m)(\lambda+1) - \sqrt{\Delta}}{2Mm}} \tag{6.10}$$

and for the optical band

$$\omega_o = \sqrt{\frac{(M+m)(\lambda+1) + \sqrt{\Delta}}{2Mm}} \tag{6.11}$$

where $\Delta = (m-M)^2(\lambda+1)^2 + 4mM\lambda^2(2+2\cos(k))$. In figure 6.1 we show with continuous lines the higher and the lower frequency of the acoustic and the optical band. In order to avoid resonance with the second harmonic, the

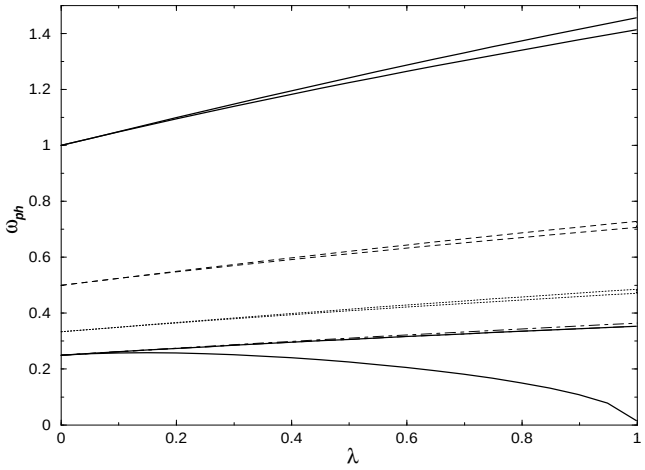

Figure 6.1: The dispersion relation for the diatomic FPU lattice with masses M/m=16/1 as a function of λ. With continuous line we plot the optical and the acoustical band. With dashed line we plot the optical band divided by 2, which corresponds to the breather frequencies for which the second harmonic enters in the optical band. With dotted line we plot the optical band divided by 3, which corresponds to the breather frequencies for which the third harmonic enters the optical band. With dotted-dashed line we see the optical band divided by 4, which corresponds to the breather frequencies for which the fourth harmonic enters the optical band. Due to the specific value of the M/m ratio, the lower dotted-dashed line collides with the upper boundary of the acoustic band.

breather frequency must lie outside the region which is denoted with dashed lines and corresponds to the higher and the lower frequencies of the optical band divided by 2. Similarly for the third harmonic, the frequency must lie outside the region denoted with dotted lines and corresponds to the higher and the lower frequencies of the optical band divided by 3 and the doted-dashed line the same frequencies divided by four (for the fourth harmonic). Due to the mass ratio $M/m = 16/1$ the fourth harmonic resonance region overlaps with the acoustic band creating a thin zone just above it which

is forbidden for the frequency. For every step in the continuation path, it is essential for the frequency to lie outside the phonon band. Thus the frequency can lie within the gap between the optical and the acoustic band as long as the harmonics do not resonate with the phonons, or above the optical band.

6.4 Local anharmonicity and Rotating Wave Approximation.

One of the properties of a breather solution is that it is exponentially localized thus only the central particles are oscillating with large amplitude while the rest of the system can be consider to be harmonic. A first approximation in order to calculate the breather is to neglect the anharmonic term from the interaction potential except for the interaction of the central cite of the breather with its neighbors.

For a soft interaction potential W (given in equation 6.4), the breather will be centered in a light particle. We can consider the center of the breather to be on cite q_0. The equations of motion for central cite, the nearest neighbors and the lattice will be respectively

$$m\ddot{q}_0 = -(1-\lambda)W'(q_0) + \lambda(W'(Q_1 - q_0) - W'(q_0 - Q_0)) \tag{6.12}$$

$$M\ddot{Q}_1 = -(1-\lambda)Q_1 + \lambda((q_1 - Q_1) - W'(Q_1 - q_0)) \tag{6.13}$$

$$m\ddot{q}_n = -(1-\lambda)q_n + \lambda((Q_{n+1} - q_n) - (q_n - Q_n)) \tag{6.14}$$

$$M\ddot{Q}_n = -(1-\lambda)Q_n + \lambda((q_n - Q_n) - (Q_n - q_{n-1})) \tag{6.15}$$

The first approximation for the breather solution can be found if we apply the rotating wave approximation in the above equations. Since we are interested for the breather solution in the FPU chain, we set $\lambda = 1$. One basic property of the breathers is that they are spatially localized. We thus consider an ansatz that assumes the system is divided into two sub-lattices, one for the heavy particles and one for the light particles. In each sub-lattice,

we consider that the amplitude of the oscillation is decaying exponentially from the center of the breather and the nearest neighbors in the same sublattice they have opposite signs (they oscillate in anti-phase). All the above assumptions are expressed in the following equations:

$$q_0 = E_0 \cos(\omega t) \tag{6.16}$$

$$Q_n = (-1)^n A_0 p^{|n|-1} \cos(\omega t) \quad for \quad n > 0, \tag{6.17}$$

$$Q_n = (-1)^{n-1} A_0 p^{|n|} \cos(\omega t) \quad for \quad n \leq 0, \tag{6.18}$$

$$q_n = (-1)^n B_0 p^{|n|-1} \cos(\omega t) \quad for \quad n \neq 0, \tag{6.19}$$

If we substitute this ansatz in equations (6.12)-(6.15) and neglect the higher order terms, we can derive the following algebraic equations.

$$(m\omega^2 - 2)E_0 - 2A_0 + \frac{3}{2}(A_0 + E_0)^3 = 0, \tag{6.20}$$

$$(M\omega^2 - 2)A_0 - E_0 + B_0 + \frac{3}{4}(A_0 + E_0)^3 = 0, \tag{6.21}$$

$$(m\omega^2 - 2)B_0 + (1 - p)A_0 = 0, \tag{6.22}$$

$$(M\omega^2 - 2)A_0 p + (p - 1)B_0 = 0. \tag{6.23}$$

In order to derive these equations we have used the approximation $\cos^3(x) \simeq \frac{3}{4}\cos(x)$. These equations can be solved numerically with the Newton-Raphson method and the solution for the case where $M = 16$, $m = 1$ and for several values of the frequency can be seen in figure 6.2.

The same analysis can be performed for the case of a hard potential W (given in equation 6.5). The breather now must be centered on a heavy particle (Q_0). If we consider again that the interaction is harmonic for the lattice except for the interaction with the central site, we derive the following equations:

$$M\ddot{Q}_0 = -(1 - \lambda)W'(Q_0) + \lambda(W'(q_0 - Q_0) - W'(Q_0 - q_{-1})) \tag{6.24}$$

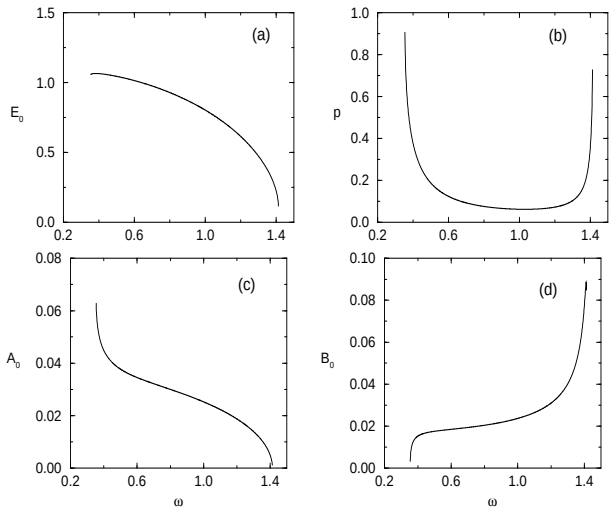

Figure 6.2: The rotating wave approximation for the soft potential. We observe the dependence of the parameters of equations (6.20)-(6.23) as a function of frequency.

$$m\ddot{q}_0 = -(1-\lambda)q_0 + \lambda((Q_1 - q_0) - W'(q_0 - Q_0)) \tag{6.25}$$

$$m\ddot{q}_n = -(1-\lambda)q_n + \lambda((Q_{n+1} - q_n) - (q_n - Q_n)) \tag{6.26}$$

$$M\ddot{Q}_n = -(1-\lambda)Q_n + \lambda((q_n - Q_n) - (Q_n - q_{n-1})) \tag{6.27}$$

As in the case of a soft potential we consider the ansatz

$$Q_0 = E_0 \cos(\omega t) \tag{6.28}$$

$$Q_n = (-1)^n A_0 p^{|n|-1} \cos(\omega t) \quad for \quad n \neq 0, \tag{6.29}$$

$$q_n = (-1)^n B_0 p^{|n|} \cos(\omega t) \quad for \quad n \geq 0, \tag{6.30}$$

$$q_n = (-1)^{n-1} B_0 p^{|n|-1} \cos(\omega t) \quad for \quad n < 0, \tag{6.31}$$

If we set $\lambda = 1$ and substitute into equations (6.24)-(6.27) we derive the following algebraic equations:

$$(M\omega^2 - 2)E_0 + 2B_0 + \frac{3}{2}(B_0 - E_0)^3 = 0, \tag{6.32}$$

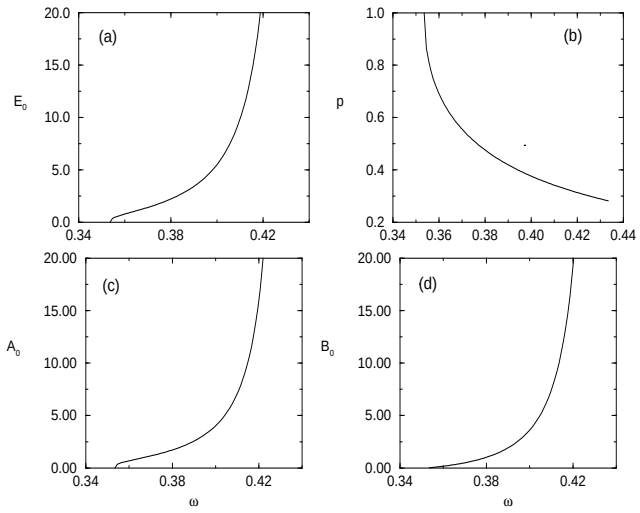

Figure 6.3: The rotating wave approximation for the hard potential. The values of E_0, A_0 and B_0 grow very fast as the frequency increase. For larger values of the frequency, there are only complex solutions of the corresponding equations.

$$(m\omega^2 - 2)B_0 - A_0 + E_0 - \frac{3}{4}(B_0 - E_0)^3 = 0, \tag{6.33}$$

$$(M\omega^2 - 2)A_0 + (p-1)B_0 = 0, \tag{6.34}$$

$$(m\omega^2 - 2)B_0 p + (1-p)A_0 = 0. \tag{6.35}$$

In order to derive these equations we have used the approximation $\cos^3(x) \simeq \frac{3}{4}\cos(x)$. These equations can be solved numerically with the Newton-Raphson method and the solution for the case where $M = 16$, $m = 1$ and for several values of the frequency can be seen in figure 6.3.

In addition to using an approximate approach based on the RWA one can also use the numerically exact method based on the idea of the anticontinuous limit and calculate for both hard and soft anharmonicity the exact numerical solution for the equations (6.12)-(6.15) or (6.24)-(6.27) respectively. The continuation from the anticontinuous limit ($\lambda = 0$) is performed in a path (in the $\lambda - \omega$ space) which avoids all the resonances of the breather

frequency or the harmonics with the phonon band. For each step we increase λ by a small quantity $\Delta\lambda$ and then we calculate the phonon frequencies from equations (6.10) and (6.11). If there is a resonance we modify the breather frequency by a small quantity in order to avoid the resonance. We then calculate the exact numerical breather using the standard Newton method, for these specific values of λ and ω. In the next step we increase λ and we proceed.

In this simple model the only existing breather is the odd parity or Sievers-Takeno mode[1]. The even parity or Page mode [2] cannot be found due to the fact that it involves more than one anharmonic oscillator and thus it cannot exist in the single anharmonic oscillator model. We will find the even parity mode and study its stability in the next section where we will treat the original system with nonlinear interactions for every particle.

For the soft interaction potential the breather solution can be found for every allowed frequency within the gap. The breather is always centered on a light particle. The stability analysis shows that when the breather frequency or one of the harmonics is just below the optical band, the breather is stable while when one of the higher harmonics approaches the optical band from above the breather is unstable.

For the hard interaction potential the breather solution can be found only for frequencies close to the acoustic band and it is centered on a heavy particle. The stability analysis shows that when one of the harmonics is just above the optical band the breather is stable while when one of the harmonics is just below the optical band the breather becomes unstable.

6.5 Even and Odd parity modes

Let us now use the anticontinuous limit and the Newton method to investigate the existence and the stability of the Sievers-Takeno (ST) mode or odd parity mode and the Page (P) mode or even parity mode. We will use the

equation 6.6 and 6.7. We choose some initial condition at the anticontinuous limit ($\lambda = 0$) and with the Newton method we continue this solution until $\lambda = 1$. The continuation must be in a path (in the $\lambda - \omega$ space) which avoids all the resonances of the frequency or the harmonics with the phonons.

For the soft interaction potential of equation (6.4) both (ST) and (P) modes can be found. For the ST mode, the initial condition at the anti-continuous limit is chosen so that all the particles are at rest except one of the light particles oscillating with some frequency within the gap. For the (P) mode the initial condition is chosen so that all the particles are at rest except for two neighboring light particles (in the light particle sublattice) chosen to oscillate at some frequency within the gap, with opposite phase. The (P) mode is a multibreather with a heavy particle at rest in the center and its nearest neighboring light particles oscillating in antiphase.

Using the Newton method both (ST) mode and (P) mode can be found for all the valid frequencies. In figure 6.4a we can see the (ST) mode for two different frequencies, one just below the optical band and one with second harmonic just above the optical band. In figure 6.4b we can see the (P) mode for the same frequencies.

If we perform the Floquet stability analysis for the (ST) mode we can see that this mode is stable when the frequency is just below the optical band and unstable when the harmonics aproach the optical band from above. One pair of eigenvalues moves toward 1 on the unit circle as the frequency decreases and for some specific value they collide at 1 and escape on the real axes making the (ST) mode unstable. For the mass ratio $M/m = 16/1$ there exist a critical frequency where the breather change its stability which is $\omega_c = 0.9627$. This frequency is close to the minimum of the $p(\omega)$ curve and therefore the change in the stability can be related with the change on the slope of this curve.

The (P) mode is unstable for all the frequencies with more than one Floquet eigenvalues to lie outside the unit circle. In figure 6.4c we plot the

(ST) mode Floquet eigenvalues and in figure 6.4d we plot the (P) mode Floquet eigenvalues.

The (ST) mode and the (P) mode can be found for the hard potential (6.5), using the Newton method and the anticontinuous limit. For this potential the (ST) mode is centered in a heavy particle. The initial condition places all particles at rest and one heavy particle oscillating with some frequency within the gap. For the (P) mode the initial condition places all particles at rest except for two neighbors in the heavy sublattice which are oscillating at some frequency within the gap, in antiphase. In figure 6.5a we can see the (ST) mode for two frequencies. The first frequency is just above the acoustic band while the second frequency has its third harmonic just below the optical band. In figure 6.5b we see the (P) mode for the same frequencies.

The stability analysis shows that for this specific mass ratio M/m the (ST) mode is unstable for every frequency within the gap. Due to the fact that the mass ratio has an integer square root equal to 4, when the frequency is in a thin region just above the acoustic band, the fourth harmonic resonates with the optical band. To avoid this resonance we studied the case where the mass ratio is of the order $M/m = 2.5/1$. For this case, when the breather frequency is in the gap, all its harmonics are higher than the optical band and therefore we avoid the resonances. The stability analysis for this mass ratio shows that the (ST) breather is stable only when its frequency is close to the acoustic band. For larger frequencies the breather is unstable. The critical frequency, where the instability occurs is at 0.9492 while the upper edge of the acoustic band corresponds to frequency 0.8944 and the difference is 0.0548. For this specific mass ratio the stability analysis shows that there exist a critical frequency within the gap at $\omega = 1.1$. For all frequencies larger than the critical value, the (P) mode is unstable while for all the lower frequencies the (P) mode is stable. The stability analysis for the (ST) mode and for mass ratio $M/m = 16/1$ is shown in figure figure

6.5c.

For every mass ratio we can find that the (P) mode is stable when the frequency is just above the acoustic band or one of its harmonics is just above the optical band and unstable when the frequency or one of its harmonics is just below the optical band. The stability analysis for the (P) mode is shown in figure 6.5d.

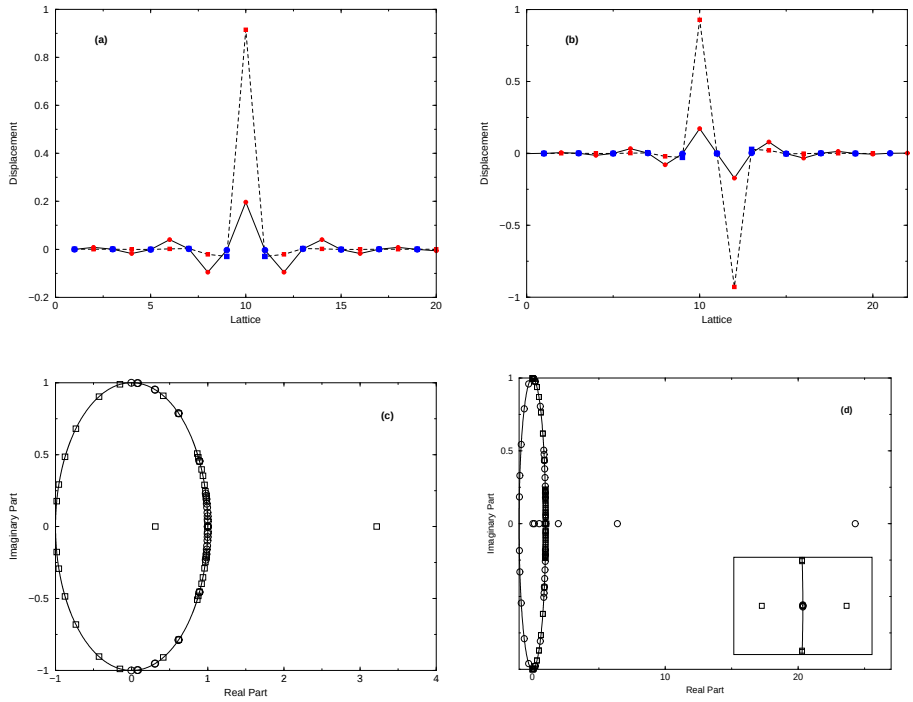

Figure 6.4: The Sievers-Takeno and the Page mode for a soft interaction. The mass ratio is $M/m = 16/1$. **a)** With continuous line and circles the ST mode for frequency $\omega = 1.4$ and with dashed line and squares the ST mode with frequency $\omega = 0.74$. **b)** With continuous line and circles the P mode for frequency $\omega = 1.4$ and with dashed line and squares the P mode mode with frequency $\omega = 0.74$. **c)** The stability analysis for the ST mode of figure 6.4a. Circles correspond to $\omega = 1.4$ and squares to $\omega = 0.74$. **d)** The stability analysis for the P mode of figure 6.4b. Circles correspond to $\omega = 1.4$ and squares to $\omega = 0.74$. In the inset, a magnification around 1 shows the instability of the first P mode.

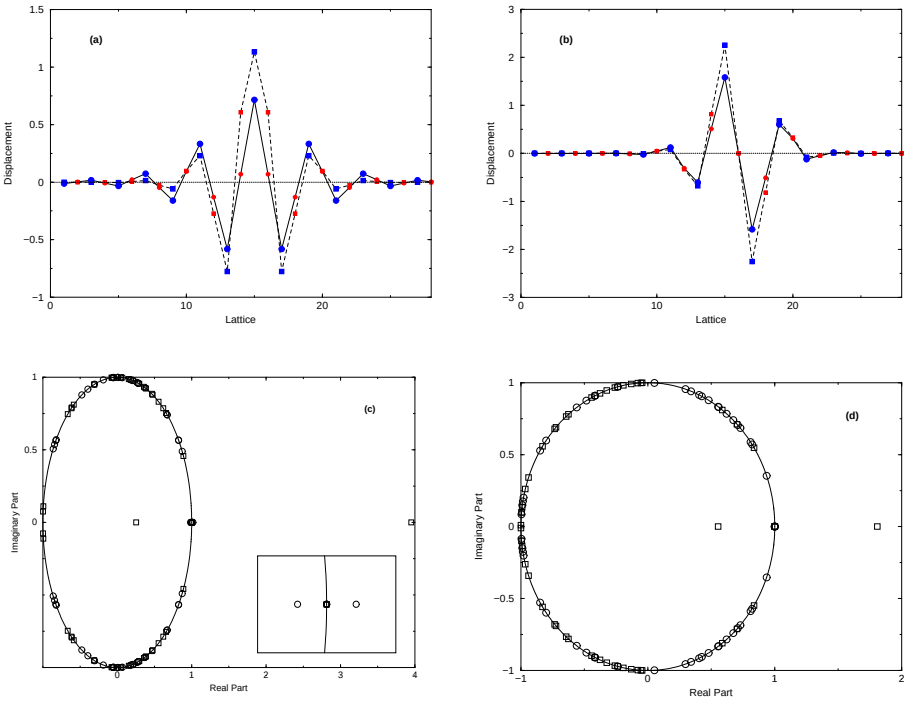

Figure 6.5: The Sievers-Takeno and the Page mode for a hard interaction. The mass ratio is $M/m = 16/1$. **a)** With continuous line and circles the ST mode for frequency $\omega = 0.384$ and with dashed line and squares the ST mode with frequency $\omega = 0.451$. **b)** With continuous line and circles the P mode for frequency $\omega = 0.505$ and with dashed line and squares the P mode mode with frequency $\omega = 0.627$. **c)** The stability analysis for the ST mode of figure 6.5a. Circles correspond to $\omega = 0.384$ and squares to $\omega = 0.451$. In the inset a magnification around 1 shows the instability of the first ST mode. **d)** The stability analysis for the P mode of figure 6.5b. Circles correspond to $\omega = 0.505$ and squares to $\omega = 0.627$.

Chapter 7

Interaction of breathers with mass impurities.

In the present chapter we investigate the existence and the mobility of DB's in one dimensional Klein-Gordon system with a mass impurity. Recently [41],[42] they found that DB's exist in a disorder system. It was also found that DB's with frequency within the phonon band can exist in a disorder system. In this case the intra-band breathers, ie. the breathers with frequency within the phonon band, can be delocalized. In this chapter we investigate a simpler system with only one mass impurity.

The equations of motion for the system are

$$m_i\ddot{x}_i + V'(x_i) - C(x_{i+1} + x_{i-1} - 2x_i) = 0 \tag{7.1}$$

where we consider that all the masses $m_i = 1$ except one site where we put the impurity $m_0 = 1 + dm$. dm can be positive when the impurity has mass larger than 1, or negative when the impurity has mass between 0 and 1. For the numerical investigation we are going to use the double well potential form of equation (1.20).

The mass impurity in the system generates an exponentially localized mode with frequency outside the phonon band. In the limit of small amplitude oscillations the frequency and the shape of this localized mode can be

found using the linearized equations either using the Green's function of the lattice [90] or using the ansatz (2.4) or (2.5) as it was described in section 2.3. The ansatz (2.4) corresponds to a small mass impurity (negative dm) while the ansatz (2.5) corresponds to a large mass impurity ($dm > 0$).

7.1 Energy Bifurcation

It is known that when there is no mass impurity ($dm = 0$) we can linearize the system and find the extended phonon solutions and the phonon band. It is also known that when a single impurity is introduced into the system, an exponentially localized solution appears with frequency outside of the phonon band. In our case, due to the fact that there is an on-site potential and because dm is positive, the impurity frequency ω_i is below the phonon band. The impurity frequency depends on the impurity mass and the coupling C.

From the existence theorem [8] we know that the breather frequencies (ω_b) and all the harmonics must be outside of the phonon band. For soft on-site potential this means that ω_b must be lower than the frequency of the phonons. One question that arises relates to the location of the impurity frequency (ω_i). This problem was first investigated in ref.[41]-[42] for a disordered system with a hard on-site potential.

Using numerical investigations, we have seen that single breathers and multi-breathers exist in the system when their frequency is lower than the impurity frequency. We also performed the Floquet analysis for stability and found that the single breather is stable up to the point where the energy curve changes upwards (figure 7.1) and the multi breather is stable or unstable similar to the case where there is no impurity (ref.[9]-[15]).

In order to investigate the case when the breather frequency is close or higher than the impurity frequency, we use the Newton method and calculate the single breather with the central site k close to the impurity and

frequency ω_b lower than the impurity frequency ω_i. We also calculate the multi-breathers with two sites excited, the central site of the single breather k and the impurity i, with the same frequency ω_b. We use the following name convention for the breathers: we call "1,0" the single breather, "1,1" the multi-breather with the two excited sites in phase and "1,-1" the multi-breather with the two excited sites in anti-phase.

Using the Newton method keep the value of the coupling fixed, we increase the breather frequency in small steps and we examine the existence and the stability of the three breathers. The continuation is in general possible, up to a critical frequency $\omega_c < \omega_i$. The single breather and the "1,-1" multi-breathers are linearly stable while the "1,1" multi-breather is unstable. It is useful to define the energy of the breather E_b as the total energy of the lattice. For time reversible solutions all the velocities at $t = 0$ are zero therefore the breather energy is

$$E_b = \sum_i \left(V(x_i) + \frac{C}{2}(x_{i+1} - x_i)^2 \right) \tag{7.2}$$

When we plot the energy of the breather as a function of the frequency we observe that the energy of the single breather and the energy of the "1,1" multi-breather, collide at some frequency ω_c and the continuation of these solutions is no more possible for $\omega > \omega_c$, the "1,-1" multi-breather can be continued with no problem for frequencies very close to the phonon band. We can see the energy as a function of the frequency and the energy bifurcation in figure 7.1, while in figure 7.2 the single breather and the multi-breather profile for $\omega_b \simeq \omega_c$.

If we plot the breather profile as the frequency of the breather ω_b approaches the critical frequency ω_c we see that the single breather and the "1,1" multi-breather collide. The "1,-1" multi-breather can be continued until its frequency collides with the phonon band. We plot the profile of that multi-breather for several frequencies in figure 7.3. The bifurcation frequency is always smaller than the impurity frequency and it depends on

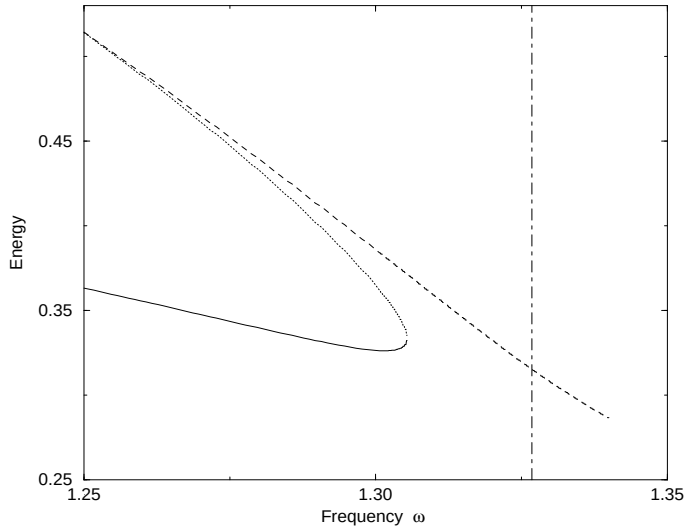

Figure 7.1: The energy as a function of the frequency of the single breather (continuous line) the "1,1" multi-breather (dotted line) and the "1,-1" multi-breather (dashed line). The vertical long dashed line corresponds to the impurity frequency. The coupling is $C = 0.231$ and the mass impurity is $m_i = 1.3$.

the coupling, the impurity mass and the distance of the impurity from the center of the breather. We can see in table 7.1i the dependence of ω_c on distance and in table 7.1ii the dependence on the impurity mass.

Looking the Floquet eigenvalues and eigenvectors, we see that a second pair of eigenvalues escapes from the phonon band and collides at 1, as the breather frequency gets closer to the bifurcation. The eigenvector that corresponds to that frequency is exponentially localized and centered on the impurity site.

7.2 Breather Scattering from impurity.

It has been shown that a breather can be mobile in a perfect one dimensional lattice (ref.[16]). When there is a mass impurity on the lattice, behavior of a mobile breather differs. Depending on the impurity and the velocity of the

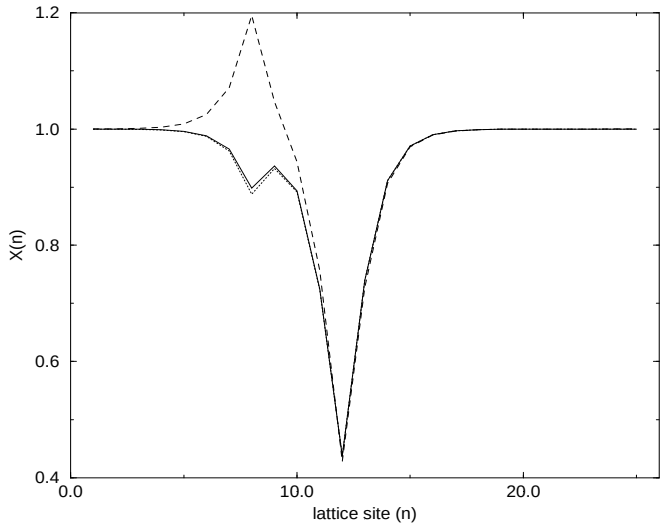

Figure 7.2: The single breather (continuous line) the "1,1" multi-breather (dotted line) and the "1,-1" multi-breather (dashed line). The coupling is $C = 0.231$ and the mass impurity is $m_i = 1.3$.

breather we observe different types of behavior when the mobile breather approaches the impurity. For the numerical investigation we excite a single breather or a multi-breather using the pinning mode method [16]. We chose several initial velocities and mass impurities. We performed the simulations in a large system that at the edges includes absorbing boundaries in order to avoid interaction with reflected phonons.

When the mass impurity is small (the difference of the impurity mass with the other particles is of the order of 0.02 or smaller) the breather can cross the impurity and continue to move in the same direction. The velocity of the breather after the collision is smaller. Depending on the initial velocity of the breather before the collision, some phonons are excited as a result of the collision.

When the impurity mass increases the behavior of the breather after the collision differs. The breather can be trapped at the impurity. Part of

Distance	ω_c
2	1.226
3	1.281
4	1.305
5	1.316
6	1.321
7	1.324
8	1.325

mass	ω_i	ω_c
1.2	1.366	1.337
1.3	1.326	1.305
1.4	1.286	1.268
1.5	1.247	1.233

Table 7.1: i) The relation of the bifurcation frequency with the distance of the impurity site from the center of the breather. In the first column we see the distance in lattice sites, while in the second column we see the bifurcation frequency as calculated numerically with accuracy 10^{-3}. The mass is $m_i = 1.3$ and the coupling $C = 0.231$.
ii) The relation of the bifurcation frequency with the impurity mass. In the first column we see the impurity mass, in the second column we see the impurity frequency ω_i and in the third column we can see the bifurcation frequency ω_c. The coupling is $C = 0.231$ and the distance of the impurity from the center of the breather is $d = 4$.

its energy is released in the lattice in the form of phonons (figure 7.4). In that case there is no reflection or refraction of the breather and most of the energy remains at the impurity site. The phonon energy after the collision is larger for larger initial velocities of the breather.

For even larger impurities the mobile breather is no longer an exact solution of the system because its frequency is between the bifurcation frequency and the phonon band. In this case, if we choose the breather center to be far from the impurity, then we can find the single breather and its pinning mode as approximate solutions of the system. In that case we see that when the impurity mass is very large (of the order of 1.2), the breather splits in two parts. The first part remains pinned in the impurity while the second part is reflected (figure 7.5). In this case the system seems to try to relax in the "1,-1" multi-breather solution, which is exact solution, with the impurity site pinned and the other site moving. The amount of energy that remains in the impurity site is proportional to the velocity of the breather prior the

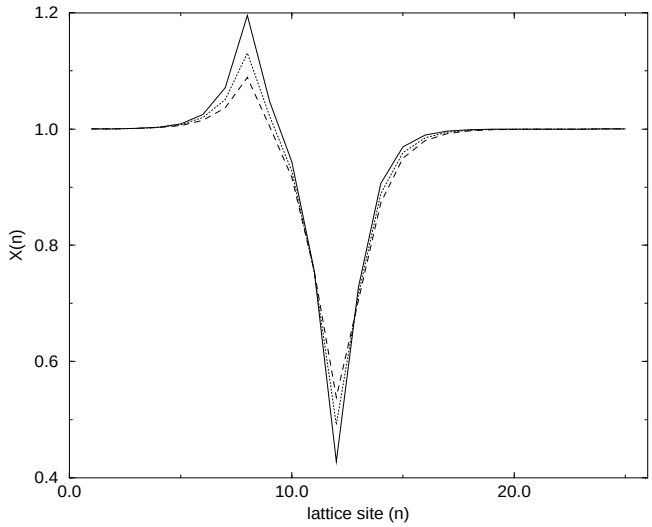

Figure 7.3: The "1,-1" multi-breather. Continuous line corresponds to breather frequency below the bifurcation $\omega_b = 1.4$, dotted line corresponds to frequency equal to the bifurcation $\omega_b = 1.32$ and dashed line corresponds to frequency larger than the bifurcation $\omega_b = 1.35$. The coupling is $C = 0.231$ and the mass impurity is $m_i = 1.3$.

collision. If we increase the impurity mass even more, we can see that in all cases the breather is reflected from the impurity and there is no energy left in the impurity site.

Different behavior is observed when we excite the "1,-1" multi-breather in the system. For this multi-breather there exists a pinning mode which does not affect the part of the multi-breather pinned on the impurity site. Using this pinning mode, we can make mobile the first site of the multi-breather while the part on the impurity remains static. We then see that the excited part is moving towards the impurity. Depending on the velocity we can observe several phenomena. When the velocity is small, we can see that the moving part slows down as it approaches the impurity, stops relatively far from it where there is not much overlap between the two parts (figure 7.6) and then it is reflected. When we increase the velocity we observe that

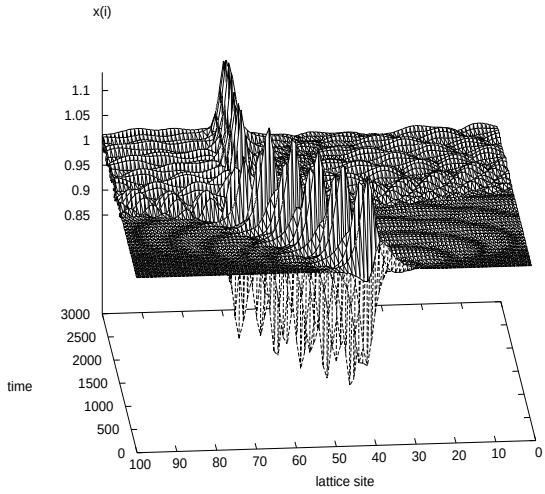

Figure 7.4: A mobile breather can be trapped from a mass impurity after the collision. $\omega_b = 1.35$ the coupling is $C = 0.231$ and the mass impurity is $m_i = 1.15$.

the overlap of the two parts of the breather before the reflection becomes larger.

When the velocity increases even further we observe a resonance and the two parts collide into one single breather with the simultaneous emission of phonons. Depending on the velocity, the single breather can stay in the impurity site (figure 7.7) or jump to the neighboring sites (figure 7.8). There have been observed many resonances of this kind separated from windows where we can see only reflection.

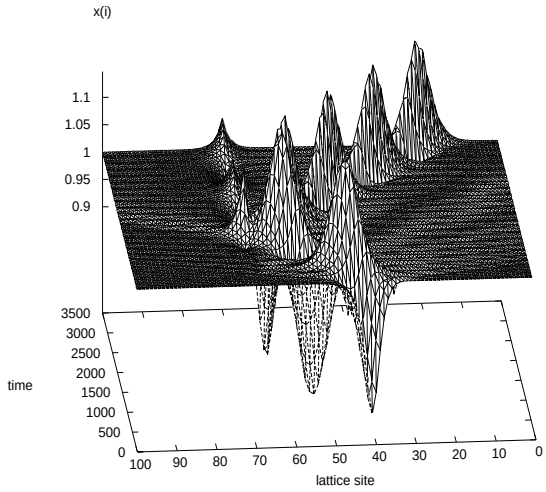

Figure 7.5: The mobile breather splits into two parts after the collision. The first part remain pinned on the impurity site wile the other is reflected. $\omega_b = 1.35$ the coupling is $C = 0.231$ and the mass impurity is $m_i = 1.25$.

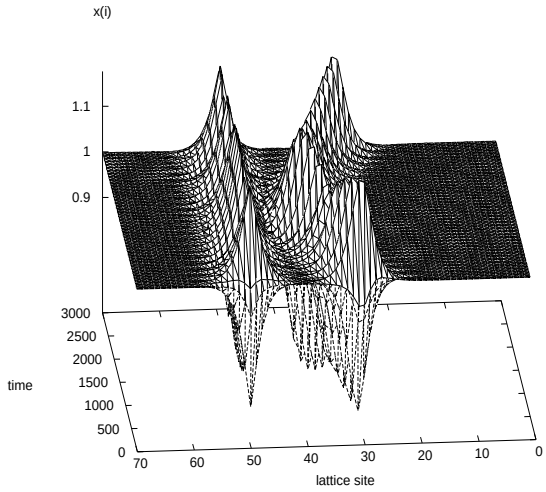

Figure 7.6: The "1,-1" multi-breather with one site moving towards the other. After the collision, the mobile part of the multi-breather is reflected. $\omega_b = 1.35$ the coupling is $C = 0.231$ and the mass impurity is $m_i = 1.25$.

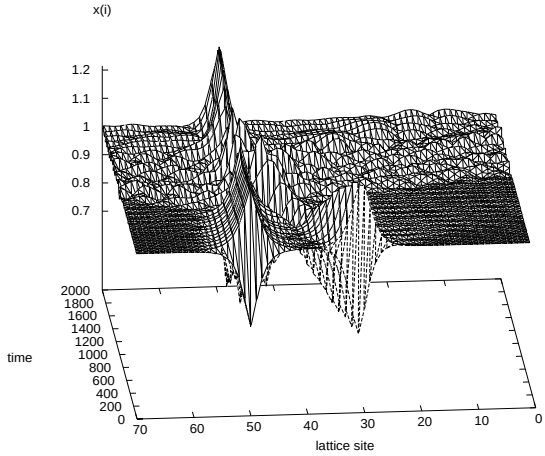

Figure 7.7: The "1,-1" multi-breather with one site moving towards the other. After the collision, the mobile part is absorbed from the impurity site and there are excited phonons. $\omega_b = 1.35$ the coupling is $C = 0.231$ and the mass impurity is $m_i = 1.25$.

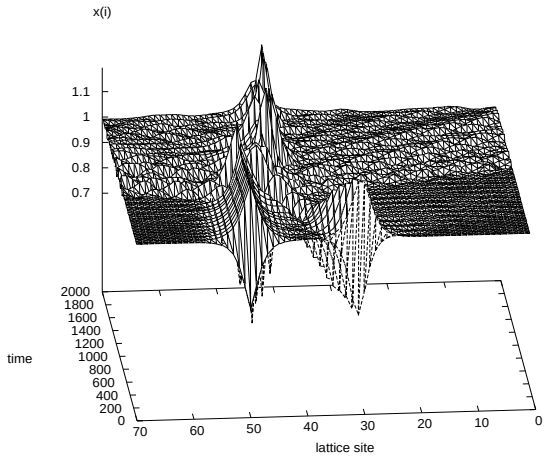

Figure 7.8: The "1,-1" multi-breather with one site moving towards the other. After the collision, all the energy is transfered into a single mobile breather moving away from the impurity. $\omega_b = 1.35$ the coupling is $C = 0.231$ and the mass impurity is $m_i = 1.25$.

Chapter 8

Conclusions and discussion.

We have study the intrinsically localized excitations or discrete breathers (DBs), in systems of coupled oscillating particles. The systems we considered can be separated into two types, lattices of coupled non-linear oscillators (Klein-Gordon) and lattices of particles coupled with non-linear interaction (FPU). For the investigation we have mainly use a numerical method based on the MacKay-Aubry existence theorem. We have also used in some cases, analytical methods like the rotating wave approximation and the continuous medium analytical solution for comparison with the numerical results.

The existence theorem in combination with the experimental observation and the numerical results obtained in a large variety of systems allow as to conclude that discrete breathers exist in every discrete and nonlinear system. Their existence arise from the interplay of nonlinearity and the discreteness. Their stability and the exponential localization are closely related. Typically, discrete breathers vanish when their frequency or one of its harmonics is in resonance with the linear phonons but there are examples where they have been found to exist in cases when the frequency is in resonance with one or more normal modes of the system. However in this exceptional cases, the breathers that survive are in general multibreathers. Typically the stability change from stable to unstable or vice versa when there is a change on the slope of the α versus ω curve where α is a parameter related with

the localization and ω is the frequency.

The exponential localization allow as to simplify the system and assume that only one (or in the case of multibreathers more) particle sense the nonlinear part of the interaction while the rest, since they are oscillating with small amplitude, they can be considered linear. This simplification allow as to retrieve some approximate equations that relate the localization with the frequency. This results are in good agreement with the numerical solutions as long as the harmonics of the breather frequency are not very close to the phonon band.

As we have find, they exist not only in one dimensional lattices but also in quasi one dimensional and two dimensional lattices. Their properties though are related with the dimensions of the lattice. In quasi one dimensional lattices they appear bifurcations between different breather solutions, similar with the bifurcations that appear in one dimensional lattices due to the existence of impurities. It has also been found that they can be mobile in higher than one dimensional lattices. The details of the mobility are depending on the geometry of the lattice. In the quasi one dimensional lattice the pinning mode, which is related with the mobility, appear after a pitchfork bifurcation in which the single breather vanish and the stable solution becomes the double breather. In the two dimensional lattice, there are two different pinning modes which are orthogonal to each other. For coupling larger than a critical value, it has been found that using a linear combination of the two different pinning modes, the breather can move along the main directions of the lattice or along the diagonals.

The study of the mobility and the interactions of breathers with the lattice (impurities) or with other excitations (kinks) leads as into the conclusion that mobile breathers behave like particles with internal structure. An internal energy can be associated into them as well as an kinetic energy and an effective mass. During the interactions with the impurities or with the kinks, in some cases they behave like particles and they sustain all their

energy after the interaction and in other cases they release part (or all) of their internal energy which can be transformed into radiation or kinetic energy (when it interacts with a kink). It has been found that there exist an effective attraction between a breather and a kink. This attraction, when the velocity of the breather is small, leads into trapping of the breather in the vicinity of the kink. A similar attraction is observed between a breather and an impurity mode. It has been observed that the mobile breather can be trapped from the impurity.

As it has been shown earlier, discrete breathers are formed spontaneously when energy is injected into a system. This spontaneous creation has the result that the relaxation of the energy in the system is delayed. The simultaneous existence however of breathers and impurities can trap the energy and therefore prevent the achievement of thermal equilibrium.

An other possible case where the discrete breathers might be important is in the biological macromolecules. It is known that in many biological processes, an excitation is created in one point through an interaction with the environment and this excitation is transfered through long macromolecules into another point where the energy is used for chemical reactions. Discrete breathers could be involved in this process as carriers of the energy from one point into the other. For example I would like to mention the double helix of the DNA. It is known that the double chain, during the process multiplication, open into two single chains and it creates two copies of itself. However it is not yet known how the opening of the chain begins. One possible answer to this question it could be that discrete breathers are involved during this process. As we have seen, they can be trapped from impurities. We have also seen that they can bee mobile in double chain systems. One could imagine therefore that discrete breathers are traveling along the DNA double helix and they are trapped at some point because of the existence of an impurity at this point. The accumulation of energy at this point could brake the intra-chain bond initiating this way the splitting process.

Appendix A

Hill's equation.

The equation of motion for a single particle in a potential $V(u)$ is

$$\ddot{u} + V'(u) = 0, \tag{A.1}$$

This equation exhibits periodic orbits around the equilibrium point of the potential. The frequency of the oscillations depends on the initial conditions and the details of the potential. We assume that $u_b(t)$ is a periodic solution with period ω_b. A question of interest is if this orbit is stable or unstable. One way to check the stability is by adding small perturbations around the orbit and see how they evolve in time:

$$u(t) \rightarrow u(t) + \epsilon(t)$$

If we substitute this expression on equation (A.1) and remove higher order terms we get the linearized equation of the system:

$$\ddot{\epsilon} + V''(u_b)\epsilon = 0 \tag{A.2}$$

where the second derivative of the potential $V''(u_b)$ is a periodic function of time with period equal with the period of the periodic orbit ($T_b = 2\pi/\omega_b$).

The stability of the periodic orbit u_b depends on the solutions of equation (A.2). When the solutions of this equation are bounded the periodic orbit is linearly stable while when the solutions are unbounded and they grow in

time exponentially fast, then the periodic orbit is unstable. Note that linear stability is not "real" stability and one has to consider other methods like the Liapunov stability ([110]) for more precise results, but the linearly stable orbits persist for long time and therefore can be considered stable. An other point is that in some cases the solution of equation (A.2) can grow as a polynomial of t. Although this solution is also unbounded, we nevertheless consider it linearly stable.

Equation (A.2) in the most general form is known as the Hill's equation:

$$\ddot{\epsilon} + f(t)\epsilon = E\epsilon, \tag{A.3}$$

where $f(t)$ is a periodic function in time with period T_b and E is a constant. If we consider the transformation $t \rightarrow x$ then equation (A.3) is the well known Schrödinger equation for a periodic potential. Depending on the form of the periodic function $f(t)$ the Hill's equation can be found in the literature with different names. One of the most common is the Mathieu's equation or parametric oscillator, when $f(t) = \cos(t)$ [110],[112].

A.1 Floquet theorem for Hill's equation.

In this section we will determine some general properties of the solutions of Hill's equation. The analysis is based on the Floquet theory for linear ordinary differential equations with periodic coefficients. Let x_1 and x_2 be two linearly independent solutions of equation (A.3). We can choose these two solutions to fulfill the initial conditions,

$$\begin{array}{ll} x_1(0) = 1 & x_2(0) = 0 \\ \dot{x}_1(0) = 0 & \dot{x}_2(0) = 1 \end{array} \tag{A.4}$$

The Wronskian of the system is constant and equal to

$$W = x_1 \cdot \dot{x}_2 - x_2 \cdot \dot{x}_1 = 1. \tag{A.5}$$

Since $f(t)$ is periodic it can be proved through the use of the transformation $z = t + T_b$ that $x_1(t + T_b)$ and $x_2(t + T_b)$ are also solutions of the

Hill's equation; therefore can be written as a linear combination of $x_1(t)$ and $x_2(t)$:

$$x_1(t+T_b) = \mu_{11}x_1(t) + \mu_{12}x_2(t) \tag{A.6}$$

$$x_2(t+T_b) = \mu_{21}x_1(t) + \mu_{22}x_2(t) \tag{A.7}$$

where μ_{ij} are constants. If we take the derivative of the previous equations we have

$$\dot{x}_1(t+T_b) = \mu_{11}\dot{x}_1(t) + \mu_{12}\dot{x}_2(t) \tag{A.8}$$

$$\dot{x}_2(t+T_b) = \mu_{21}\dot{x}_1(t) + \mu_{22}\dot{x}_2(t) \tag{A.9}$$

From the initial conditions we have,

$$\begin{array}{ll} \mu_{11} = x_1(T_b), & \mu_{12} = \dot{x}_1(T_b), \\ \mu_{21} = x_2(T_b), & \mu_{22} = \dot{x}_2(T_b). \end{array} \tag{A.10}$$

We can write equations (A.8) and (A.9) in the matrix notation as

$$\vec{x}(t+T_b) = \mathbf{M}\cdot\vec{x}(t) \tag{A.11}$$

where

$$\mathbf{M} = \begin{pmatrix} \mu_{11} & \mu_{12} \\ \mu_{21} & \mu_{22} \end{pmatrix}, \qquad \vec{x} = \begin{pmatrix} x_1 \\ x_2 \end{pmatrix} \tag{A.12}$$

Next we can use the linear transformation

$$\vec{y} = \mathbf{P}\cdot\vec{x} \tag{A.13}$$

$$\vec{x} = \mathbf{P}^{-1}\cdot\vec{y} \tag{A.14}$$

where $\mathbf{P}$ is a 2×2 constant nonsingular matrix and $\vec{y} = [y_1, y_2]^{\dagger}$. Substituting into (A.11) gives

$$\vec{y}(t+T_b) = \mathbf{P}\cdot\mathbf{M}\cdot\mathbf{P}^{-1}\cdot\vec{y}(t) \tag{A.15}$$

We choose $\mathbf{P}$ so that $\mathbf{B} = \mathbf{P}\cdot\mathbf{M}\cdot\mathbf{P}^{-1}$ is in one of the *Jordan canonical form*. This form depends on the eigenvalues and the eigenvectors of $\mathbf{M}$. The eigenvalues of $\mathbf{M}$ or $\mathbf{B}$ are given by

$$\begin{vmatrix} \mu_{11}-\lambda & \mu_{12} \\ \mu_{21} & \mu_{22}-\lambda \end{vmatrix} = 0 \tag{A.16}$$

which gives the equation

$$\lambda^2 - 2\gamma\lambda + 1 = 0, \tag{A.17}$$

where we have use the fact that the Wronskian of the system is constant and equal to 1, and $\gamma = (\mu_{11} + \mu_{22})/2 = (x_1(T_b) + \dot{x}_2(T_b))/2$. For $\gamma \neq \pm 1$ there are 2 distinct eigenvalues

$$\lambda_{1,2} = \gamma \pm \sqrt{\gamma^2 - 1} \tag{A.18}$$

and $\mathbf{B}$ has the diagonal form

$$\mathbf{B} = \begin{pmatrix} \lambda_1 & 0 \\ 0 & \lambda_2 \end{pmatrix} \tag{A.19}$$

For $\gamma = \pm 1$ then there is only one eigenvalue $\lambda = \gamma = \pm 1$, and $\mathbf{B}$ has either the form

$$\mathbf{B} = \begin{pmatrix} \pm 1 & 0 \\ 0 & \pm 1 \end{pmatrix} \tag{A.20}$$

or the form

$$\mathbf{B} = \begin{pmatrix} \pm 1 & 0 \\ 1 & \pm 1 \end{pmatrix} \tag{A.21}$$

If $\mathbf{B}$ has one of the form (A.19) or (A.20) then equation (A.15) can be rewritten

$$\begin{aligned} y_1(t + T_b) &= \lambda_1 y_1(t) \\ y_2(t + T_b) &= \lambda_2 y_2(t) \end{aligned} \tag{A.22}$$

If we multiply with $\exp(-\theta_{1,2}(t + T_b))$ we can express the solutions in the normal form

$$\begin{aligned} y_1(t) &= \exp(\theta_1 t)\phi_1(t) \\ y_2(t) &= \exp(\theta_2 t)\phi_2(t) \end{aligned} \tag{A.23}$$

where $\phi_{1,2}(t)$ are periodic functions with period T_b and $\theta_{1,2}$ are the characteristic exponents defined from the equation $\lambda_{1,2}\exp(-\theta_{1,2}T_b) = 1$.

When $\mathbf{B}$ has the form (A.21) then equation (A.15) can be rewritten

$$\begin{aligned} y_1(t + T_b) &= \lambda y_1(t) \\ y_2(t + T_b) &= \lambda y_2(t) + y_1(t) \end{aligned} \tag{A.24}$$

If we multiply with $\exp(-\theta(t+T_b))$ we can express the solutions in the normal form

$$\begin{aligned} y_1(t) &= \exp(\theta t)\phi_1(t) \\ y_2(t) &= \exp(\theta t)\phi_2(t) + t\phi_1(t) \end{aligned} \tag{A.25}$$

where $\phi_{1,2}(t)$ are periodic functions with period T_b and θ is the characteristic exponent defined from the equation $\lambda \exp(-\theta T_b) = 1$. Since the product of the eigenvalues is equal to 1 ($\lambda_1 \cdot \lambda_2 = 1$), the solution of the Hill's equation remains bounded only when $|\lambda_{1,2}| = 1$. This means that the periodic solution u_b is stable when the eigenvalues of $\mathbf{M}$ lie on the unit circle in the complex plane. In the case when $\lambda = \pm 1$ and $\mathbf{B}$ has the form (A.21), then one of the solutions is bounded while the other increases in time. Since the solution increases in a polynomial rate as a function of time, we will consider in this case the periodic solution u_b to be stable.

The same analysis can be performed for the system of J coupled oscillators. For a one dimensional system, the equations of motion are

$$\ddot{u}_i + V'(u_i) - C(u_{i+1} + u_{i-1} - 2u_i) = 0 \tag{A.26}$$

These equations can exhibit periodic orbits with period T_b. To investigate the stability, we linearize the equation around the periodic orbit $\{u_i\}$. The linearized equations of motion are:

$$\ddot{\epsilon}_i + V''(u_i)\epsilon_i - C(\epsilon_{i+1} + \epsilon_{i-1} - 2\epsilon_i) = 0 \tag{A.27}$$

The linearized equation of motion can be written in the matrix notation:

$$\dot{\vec{\epsilon}} = \mathbf{P}(t) \cdot \vec{\epsilon} \tag{A.28}$$

where $\vec{\epsilon} = \{\epsilon_1, \ldots, \epsilon_J, \dot{\epsilon}_1, \ldots, \dot{\epsilon}_J\}^\dagger$, $\mathbf{P}(t)$ is a $N \times N$ matrix function (with $N = 2J$), periodic with period T_b.

Floquet theorem 1 *The regular system* $\dot{\vec{\epsilon}} = \mathbf{P}(t) \cdot \vec{\epsilon}$ *where* $\mathbf{P}(t)$ *is a* $N \times N$ *matrix function, periodic with period* T_b*, has at least one non-trivial solution* $x(t)$ *such that*

$$x(t + T_b) = \lambda x(t) \tag{A.29}$$

where λ are the eigenvalues of the matrix defined from the relation

$$\mathbf{\Phi}(t + T_b) = \mathbf{M} \cdot \mathbf{\Phi}(t) \tag{A.30}$$

and $\mathbf{\Phi}(t)$ is a fundamental matrix of the system.

The matrix $\mathbf{M}$ is called the Floquet matrix of the system while its eigenvalues λ are called Floquet multipliers or characteristic numbers of the system.

Floquet theorem 2 *The constant λ of Theorem (1) are independent on the choice of $\mathbf{\Phi}$.*

Floquet theorem 3 *When the matrix $\mathbf{M}$ of Theorem (1) has N distinct eigenvalues, λ_i,$i = 1, 2, \ldots, N$, then (A.28) has N linearly independent normal solutions of the form*

$$\vec{x}_i(t) = \vec{p}_i(t) \cdot \exp(\theta_i t) \tag{A.31}$$

The characteristic exponents θ_i are defined from the equation

$$\exp(\theta_i T_b) = \lambda \tag{A.32}$$

A periodic orbit of the nonlinear system will be linearly stable when the solutions of the linearized equations (A.28), remains bounded.

From the previous analysis and from the Floquet theorems we see that the solution of the linearized system remains bounded when the eigenvalues of the Floquet matrix of the system lie on the unit circle. When the *Jordan canonical form* of the Floquet matrix is not in a diagonal form, then it can be transformed into a block diagonal form. In this case there exists at least one solution of the system which is not bounded but grows as a function of time in a polynomial way. We will consider this case to be linearly stable. We will call this type of solutions of the linearized system marginal modes.

Appendix B

Dynamical systems.

The time evolution of a physical system can be described as a set of ordinary differential equations of the form:

$$\begin{array}{rcl} \dot{x}_1 & = & f_1(x_1, x_2, \ldots, x_N), \\ \dot{x}_2 & = & f_2(x_1, x_2, \ldots, x_N), \\ \vdots & & \vdots \\ \dot{x}_N & = & f_N(x_1, x_2, \ldots, x_N), \end{array} \tag{B.1}$$

where N is the number of degrees of freedom of the system, $\{x_i\}$ are the dynamical variables describing the system and $\{f_i\}$ are some functions of the dynamical variables and the time t. In matrix notation, equation (B.1) can be written in the form:

$$\dot{\vec{x}} = \mathbf{F}(\vec{x}), \tag{B.2}$$

where $\vec{x} = \{x_1, x_2, \ldots, x_N\}^\dagger$ and $\mathbf{F}(\vec{x}) = \{f_1, f_2, \ldots, f_N\}^\dagger$. The functions $\{f_i\}$ are in general nonlinear functions for real systems. The details of $\{f_i\}$ depends on the system.

The system can be described at any time with a point in the N dimensional phase. The time evolution of the system for a certain set of initial conditions can be described with a trajectory in the phase space. This trajectory can be found with the integration of (B.1) or (B.2).

B.1 Fixed points and linear stability.

The time evolution of the system and the trajectory depends on the initial condition. Since the system is nonlinear, for different initial conditions, the trajectory can be a periodic orbit, a quasi-periodic orbit, a chaotic orbit etc. One special case of interest is when there exists points or regions in the phase space, where all the derivatives of (B.1) or (B.2) are zero. These points correspond to steady states of the system and when the initial condition is in a steady state then there is no time evolution of the system. When this points are isolated they are called fixed points of the dynamical systems. The steady state of the dynamical system can be found solving the equation:

$$\begin{array}{rcl} f_1(x_1, x_2, \ldots, x_N) & = & 0 \\ f_2(x_1, x_2, \ldots, x_N) & = & 0 \\ \vdots & & \vdots \\ f_N(x_1, x_2, \ldots, x_N) & = & 0 \end{array} \tag{B.3}$$

or

$$\mathbf{F}(\vec{x}) = \mathbf{0} \tag{B.4}$$

The solution of the above equation can give the steady state or the fixed point $\vec{x}_0$ of the system. The stability of the fixed point and the solution of the dynamical system in the neighbor of the fixed point can be found if we linearize equations (B.1) or (B.2) around $\vec{x}_0$. The linearized equations are of the form

$$\dot{\vec{\epsilon}} = \mathbf{A} \cdot \vec{\epsilon} \tag{B.5}$$

where $\mathbf{A}$ is a $N \times N$ matrix with elements the partial derivatives of the functions $\{f_i\}$ over the dynamical variables $\{x_i\}$

$$\mathbf{A} = \begin{pmatrix} a_{11} & \ldots & a_{1N} \\ \vdots & \ddots & \vdots \\ a_{N1} & \ldots & a_{NN} \end{pmatrix} \tag{B.6}$$

$$a_{ij} = \left. \frac{\partial f_i}{\partial x_j} \right|_{\vec{x}=\vec{x_0}} \tag{B.7}$$

Equation (B.5) can be solved and the solution is of the form

$$\vec{\epsilon}(t) = \exp(\mathbf{A}t)\vec{\epsilon}(0). \tag{B.8}$$

The form of the solution depends on the eigenvalues and the eigenvectors of the matrix **A**. The matrix is real and the eigenvalues can be real or complex numbers. When at least one of the eigenvalues has positive real part, the solution grows exponentially fast in the direction of the phase space denoted by the corresponding eigenvector. In this case the fixed point is unstable and small perturbations will lead the trajectory of the solution away from the region around the fixed point. When all the eigenvalues of **A** have real part less or equal to zero, the fixed point is stable.

Appendix C

Programs

This appendix contains the source code of the programs used for the construction of breathers. These programs can be used, with little modifications, in different models. The modifications that are necessary are related with the on-site and the interaction potential of each model, the lattice geometry, the boundary conditions and other model related parameters. For the eigenvalues and the eigenvectors of the Floquet matrix we use the subroutine from LAPACK library [108] and for the implementation of the Newton method we use the LU decomposition and back substitution subroutines from the Numerical Recipes [107]. These subroutines are not included here. For the compilation and the execution of the program one must use the LUDCMP and the LUBKSB subroutines from [107] and link the program with the LAPACK library. In the case of the LUDCMP and LUBKSB the first lines of the subroutine are slightly modified, the modifications are shown in the following lines.

```
SUBROUTINE LUBKSB(A,N,INDX,B)
INCLUDE 'parameters.f'
real*8 A(NP,NP),B(N),SUM
integer INDX(NP),I,II,J,LL,N
.
.
.

SUBROUTINE LUDCMP(A,N,INDX,D)
INCLUDE 'parameters.f'
PARAMETER (TINY=1.0D-20)
REAL*8 A(NP,NP),VV(NMAX)
REAL*8 D,AAMAX,SUM,DUM
INTEGER INDX(NP),I,IMAX,J,K,N
.
.
.
```

In all the programs all the necessary parameters for the matrix dimensions are in a separate file called "parameters.f". This file is included in every subroutine in order to keep the dimensions of the matrices the same. The file "parameters.f" has the form

file "parameters.f":

```
integer SIZE,SIZE2,MAXWORK,NMAX,NP
PARAMETER   ( SIZE = 200 )
PARAMETER   ( SIZE2 = 400 )
PARAMETER   ( MAXWORK = 1400 )

PARAMETER   (    NMAX = 200 )
PARAMETER   (      NP = 200 )
```

The first program ("newton.f") is used to calculate a single breather or a multibreather in an one dimensional Klein-Gordon lattice with a double well on-site potential. The input file contains all the necessary parameters for the program to work. In the input file there are comments explaining the use of every parameter. Notice that the parameters start on the fourth line of the file, the first three lines are ignored. The program "newton.f" can be used for other potentials with the appropriate modifications in the functions fx, fy, fx2 and fy2. Some of the input variables on this file are ignored by the program "newton.f". The reason for been here is for compatibility of the input file with the input of other programs used for the mobility of breathers as well as the kink construction and mobility.

file "input.dat" for the newton.f program:

```
#
#              for the breather
#
40                                  :  number of cites
20                                  :  center of the breather
1.25                                :  initial position
4.73979999999996                    :  period of the breather
0.631                               :  kmax
0.01                                :  dk
2.0                                 :  petrubation strength
600                                 :  time of simulations
1755                                :  sampling rate
#
#              for the kink
#
25                                  :  number of cites
12                                  :  center of the kink
0.131                               :  coupling
```

```
500                                  :  simulation time
2547                                 :  sampling rate
#
#              extra parameters
#
4                                    :  impurity position
1.0                                  :  impurity mass
1.351                                :  impurity frequency
1.370245098495                       : Displacement of the impurity site
```

Program newton.f:

```
        program main2
        include "parameters.f"
        character*80 junk
        real*8 x(0:SIZE),y(0:SIZE)
        real*8 xinit(0:SIZE),yinit(0:SIZE)
        real*8 alp(SIZE,SIZE),ce(SIZE,SIZE),dlt(SIZE)
        real*8 bet(SIZE,SIZE),de(SIZE,SIZE)
        real*8 vectors(SIZE,SIZE)
        real*8 mass(SIZE)
        real*8 t,dt,kapa,dk,period
        real*8 kmax,dzero
        real*8 imass,wi,despl
        integer iposs
        integer i,n,j,ncent
100        format( e25.16,i4,e25.16)
103        format( e25.16,e25.16)
102        format( i4,e25.16)
101        format()
        open (21,file='breather.out')
```

```
c
c  input data
c
        open (23,file="input.dat")
        read(23,1000) junk
        read(23,1000) junk
        read(23,1000) junk
1000    format ( a80)
        read(23,*) n
        read(23,*) ncent
        do i=0,n+1
           xinit(i)=1.0
           yinit(i)=0.0
        enddo
        read(23,*) xinit(ncent)
        read(23,*) period
        read(23,*) kmax
        read(23,*) dk
c
c       read some junk lines
c
        do i=1,14
          read(23,1000) junk
        enddo
        read(23,*) iposs
        read(23,*) imass
        read(23,*) wi
        read(23,*) despl
        close(23)
c        xinit(iposs)=despl
```

```
        if(n.gt.NMAX/2) then
          write(*,*) "you must decreace the numper of oscilators or"
          write(*,*) "recompile the program with greater NMAX"
c          return
          stop
        endif
c
        do i=1,n
          mass(i)=1.0d0
        enddo
c        mass(iposs)=imass
        dt=4.0d-3
c        dk=0.01d0
c        kapa=dk
        kapa=0.001
        do while( kapa .lt.kmax)
            if( (kapa+dk).gt.kmax) then
               kapa=kmax
            endif
600            continue
            do i=0,n+1
              x(i)=xinit(i)
              y(i)=yinit(i)
            enddo
            do i=1,n
              do j=1,n
                alp(i,j)=0.0
                ce(i,j)=0.0
              enddo
              alp(i,i)=1.0
```

```
            enddo
            t=0.0
            do while(t.lt.period)
                call rk4_s(x,y,t,dt,kapa,n,mass)
                call rk4_s2(alp,ce,x,y,t,dt,kapa,n,mass)
                t=t+dt
            enddo
c
c       Termination contition
c
            sum=0.0
            do i=1,n
              sum=sum + dabs(xinit(i)-x(i))+dabs(yinit(i)-y(i))
            enddo
            write(*,*) kapa,sum
c-------------------------------------------
            do i=1,n
              alp(i,i)=alp(i,i) -1.0
            enddo
            call deval( alp,ce,dlt,xinit,x,yinit,y,n)
            do i=1,n
              xinit(i)=xinit(i)+dlt(i)
            enddo
            if (sum.le.1.0e-11) goto 300
            sum=0.0
            do i=1,n
            sum=sum+dabs( dlt(i) )
            enddo
            if (sum.le.1.0e-14) goto 300
            goto 600
```

```
300            kapa=kapa+dk
              write(*,*) (i,xinit(i),i=1,n)
           enddo
c          write(*,*) kapa
           do i=1,n
              write(21,102) i,xinit(i)
           enddo
           close(21)
c          t=0.0
c          do i=1,n
c            x(i)=xinit(i)
c            y(i)=0.0d0
c            write(22,100) t,i,x(i)
c          enddo
c          write(22,101)
           kapa=kapa-dk
           write(*,*) kapa
           j=0
           do while(t.lt.10.6699999999999d0)
              j=j+1
              call rk4_s(x,y,t,dt,kapa,n,mass)
              t=t+dt
              if(j.gt.40) then
                j=0
                do i=1,n
                  write(22,100) t,i,x(i)
                enddo
                write(22,101)
                endif
           enddo
```

```
        close(22)
c-------------------------------------------------------
c      for the floquet analysis
c-------------------------------------------------------
            do i=1,n
              x(i)=xinit(i)
              y(i)=yinit(i)
              do j=1,n
                alp(i,j)=0.0
         bet(i,j)=0.0
         ce(i,j)=0.0
         de(i,j)=0.0
              enddo
              alp(i,i)=1.0
              de(i,i)=1.0
            enddo
            t=0.0
            do while(t.lt.period)
                call rk4_s(x,y,t,dt,kapa,n,mass)
                call rk4_s2(alp,ce,x,y,t,dt,kapa,n,mass)
                call rk4_s2(bet,de,x,y,t,dt,kapa,n,mass)
                t=t+dt
            enddo
            do i=1,n
              do j=1,n
                alp(i+n,j)=ce(i,j)
         alp(i,j+n)=bet(i,j)
         alp(i+n,j+n)=de(i,j)
              enddo
            enddo
```

```
      call floque(alp,n,vectors)
      open (23,file="eigen.out")
      open (24,file="vectors.out")
      open (25,file="vectors_im.out")
      do i=1,2*n
        write(23,103) alp(i,1),alp(i,2)
      enddo
      close(23)
      dzero=0.0d0
      do i=1,2*n,2
         if (dabs( alp(i,2) ).lt.1.0d-9 ) then
         do k=0,1
         do j=1,2*n
           write(24,102) j,vectors(j,i+k)
           write(25,102) j,dzero
         enddo
         write(24,101)
         write(25,101)
         enddo
         else
           do j=1,2*n
       write(24,102) j,vectors(j,i)
       write(25,102) j,vectors(j,i+1)
    enddo
           write(24,101)
           write(25,101)
         endif
      enddo
  stop
  end
```

```
c   This is a subroutine for solving a system of
c   diferential equations on a latice with first
c   neighbor aproximation
        subroutine rk4_s(x,y,t,dt,kapa,n,mass)
        include 'parameters.f'
        real*8 x(0:SIZE),y(0:SIZE)
        real*8 t,dt,kapa
        integer i,n
        real*8 fx,fy
        real*8 mass(SIZE)
        real*8 kx1(0:SIZE),kx2(0:SIZE),kx3(0:SIZE),kx4(0:SIZE)
        real*8 ky1(0:SIZE),ky2(0:SIZE),ky3(0:SIZE),ky4(0:SIZE)
        real*8 xtmp(0:2),ytmp(0:2)
c
c   periodic boundary conditions
c
        x(0)=x(n)
        x(n+1)=x(1)
        y(0)=y(n)
        y(n+1)=y(1)
c
c  For the first step of the Runke Kuta
c
        do i=1,n
           xtmp(0)=x(i-1)
           xtmp(1)=x(i)
           xtmp(2)=x(i+1)
           ytmp(0)=y(i-1)
           ytmp(1)=y(i)
           ytmp(2)=y(i+1)
```

```
            kx1(i)=dt*fx(xtmp,ytmp,t,kapa)
            ky1(i)=dt*fy(xtmp,ytmp,t,kapa,mass(i))
         enddo
         kx1(0)=kx1(n)
         kx1(n+1)=kx1(1)
         ky1(0)=ky1(n)
         ky1(n+1)=ky1(1)
c
c  For the second step of the Runke Kuta
c
         do i=1,n

            xtmp(0)=x(i-1)+kx1(i-1)/2.0
            xtmp(1)=x(i)+kx1(i)/2.0
            xtmp(2)=x(i+1)+kx1(i+1)/2.0

            ytmp(0)=y(i-1)+ky1(i-1)/2.0
            ytmp(1)=y(i)+ky1(i)/2.0
            ytmp(2)=y(i+1)+ky1(i+1)/2.0

            kx2(i)=dt*fx(xtmp,ytmp,t,kapa)
            ky2(i)=dt*fy(xtmp,ytmp,t,kapa,mass(i))
         enddo
         kx2(0)=kx2(n)
         kx2(n+1)=kx2(1)
         ky2(0)=ky2(n)
         ky2(n+1)=ky2(1)
c
c  For the third step of the Runke Kuta
c
```

```
        do i=1,n

           xtmp(0)=x(i-1)+kx2(i-1)/2.0
           xtmp(1)=x(i)+kx2(i)/2.0
           xtmp(2)=x(i+1)+kx2(i+1)/2.0

           ytmp(0)=y(i-1)+ky2(i-1)/2.0
           ytmp(1)=y(i)+ky2(i)/2.0
           ytmp(2)=y(i+1)+ky2(i+1)/2.0

           kx3(i)=dt*fx(xtmp,ytmp,t,kapa)
           ky3(i)=dt*fy(xtmp,ytmp,t,kapa,mass(i))

        enddo
        kx3(0)=kx3(n)
        kx3(n+1)=kx3(1)
        ky3(0)=ky3(n)
        ky3(n+1)=ky3(1)
c
c  For the fourthd step of the Runke Kuta
c
        do i=1,n

           xtmp(0)=x(i-1)+kx3(i-1)
           xtmp(1)=x(i)+kx3(i)
           xtmp(2)=x(i+1)+kx3(i+1)

           ytmp(0)=y(i-1)+ky3(i-1)
           ytmp(1)=y(i)+ky3(i)
           ytmp(2)=y(i+1)+ky3(i+1)
```

```
      kx4(i)=dt*fx(xtmp,ytmp,t,kapa)
      ky4(i)=dt*fy(xtmp,ytmp,t,kapa,mass(i))

   enddo

   do i=1,n
      x(i)=x(i)+( kx1(i)+2.0*kx2(i)+2.0*kx3(i)+kx4(i) )/6.0
      y(i)=y(i)+( ky1(i)+2.0*ky2(i)+2.0*ky3(i)+ky4(i) )/6.0
   enddo
   return
   end

   subroutine rk4_s2(alp,ce,x,y,t,dt,kapa,n,mass)
   include 'parameters.f'
   real*8 alp(SIZE,SIZE),ce(SIZE,SIZE)
   real*8 x(0:SIZE),y(0:SIZE)
   real*8 x0(0:SIZE),y0(0:SIZE)
   real*8 t,dt,kapa
   integer i,j,k,n
   real*8 fx2,fy2
   real*8 mass(SIZE)
   real*8 kx1(0:SIZE),kx2(0:SIZE)
   real*8 kx3(0:SIZE),kx4(0:SIZE)
   real*8 ky1(0:SIZE),ky2(0:SIZE)
   real*8 ky3(0:SIZE),ky4(0:SIZE)
   real*8 xtmp(0:2),ytmp(0:2)
   do k=1,n
    do j=1,n
      x0(j)=alp(j,k)
```

```
            y0(j)=ce(j,k)
          enddo
c
c   periodic boundary conditions
c
          x0(0)=x0(n)
          x0(n+1)=x0(1)
          y0(0)=y0(n)
          y0(n+1)=y0(1)
c
c  For the first step of the Runke Kuta
c
           do i=1,n
            xtmp(0)=x0(i-1)
            xtmp(1)=x0(i)
            xtmp(2)=x0(i+1)
            ytmp(0)=y0(i-1)
            ytmp(1)=y0(i)
            ytmp(2)=y0(i+1)
            kx1(i)=dt*fx2(xtmp,ytmp,t,kapa)
            ky1(i)=dt*fy2(xtmp,ytmp,t,kapa,x(i),mass(i))
          enddo
          kx1(0)=kx1(n)
          kx1(n+1)=kx1(1)
          ky1(0)=ky1(n)
          ky1(n+1)=ky1(1)
c
c  For the second step of the Runke Kuta
c
          do i=1,n
```

```
          xtmp(0)=x0(i-1)+kx1(i-1)/2.0
          xtmp(1)=x0(i)+kx1(i)/2.0
          xtmp(2)=x0(i+1)+kx1(i+1)/2.0

          ytmp(0)=y0(i-1)+ky1(i-1)/2.0
          ytmp(1)=y0(i)+ky1(i)/2.0
          ytmp(2)=y0(i+1)+ky1(i+1)/2.0

          kx2(i)=dt*fx2(xtmp,ytmp,t,kapa)
          ky2(i)=dt*fy2(xtmp,ytmp,t,kapa,x(i),mass(i))
        enddo
        kx2(0)=kx2(n)
        kx2(n+1)=kx2(1)
        ky2(0)=ky2(n)
        ky2(n+1)=ky2(1)
c
c  For the third step of the Runke Kuta
c
        do i=1,n

          xtmp(0)=x0(i-1)+kx2(i-1)/2.0
          xtmp(1)=x0(i)+kx2(i)/2.0
          xtmp(2)=x0(i+1)+kx2(i+1)/2.0

          ytmp(0)=y0(i-1)+ky2(i-1)/2.0
          ytmp(1)=y0(i)+ky2(i)/2.0
          ytmp(2)=y0(i+1)+ky2(i+1)/2.0

          kx3(i)=dt*fx2(xtmp,ytmp,t,kapa)
```

```
            ky3(i)=dt*fy2(xtmp,ytmp,t,kapa,x(i),mass(i))

          enddo
          kx3(0)=kx3(n)
          kx3(n+1)=kx3(1)
          ky3(0)=ky3(n)
          ky3(n+1)=ky3(1)
c
c  For the fourthd step of the Runke Kuta
c
          do i=1,n

            xtmp(0)=x0(i-1)+kx3(i-1)
            xtmp(1)=x0(i)+kx3(i)
            xtmp(2)=x0(i+1)+kx3(i+1)

            ytmp(0)=y0(i-1)+ky3(i-1)
            ytmp(1)=y0(i)+ky3(i)
            ytmp(2)=y0(i+1)+ky3(i+1)

            kx4(i)=dt*fx2(xtmp,ytmp,t,kapa)
            ky4(i)=dt*fy2(xtmp,ytmp,t,kapa,x(i),mass(i))

          enddo

          do i=1,n
            alp(i,k)=x0(i)+( kx1(i)+2.0*kx2(i)+2.0*kx3(i)+kx4(i) )/6.0
            ce(i,k)=y0(i)+( ky1(i)+2.0*ky2(i)+2.0*ky3(i)+ky4(i) )/6.0
          enddo
        enddo
```

```
        return
        end

c Functions for the runke couta integretion of the
c original equations
c
        real*8 function fx( x,y,t,kapa)
        real*8 x(0:2),y(0:2),t,kapa
        fx= y(1)
        return
        end

        real*8 function fy( x,y,t,kapa,m)
        real*8 x(0:2),y(0:2),t,kapa
        real*8 m
        fy= -(x(1)*x(1)*x(1) -x(1))/m + kapa*(x(0)+x(2)-2.0*x(1) )/m
        return
        end

c -------------------------------------------------------------
c
c Functions for the integration of the
c linearized equations
c
        real*8 function fx2( x,y,t,kapa)
        real*8 x(0:2),y(0:2),t,kapa
        fx2= y(1)
        return
        end
```

```
real*8 function fy2( x,y,t,kapa,tmp,m)
real*8 x(0:2),y(0:2),t,kapa,tmp
real*8 m
fy2=-(3.0d0*tmp*tmp-1.0d0)*x(1)/m+kapa*(x(0)+x(2)-2.0*x(1))/m
return
end
subroutine  deval( alp,ce,dlt,xinit,x,yinit,y,n)
INCLUDE 'parameters.f'
real*8 xinit(0:SIZE),x(0:SIZE)
real*8 yinit(0:SIZE),y(0:SIZE)
real*8 alp(SIZE,SIZE),ce(SIZE,SIZE),dlt(SIZE),d(SIZE)
real*8 alpt(SIZE,SIZE),cet(SIZE,SIZE),sysa(SIZE,SIZE)
integer n,indx(SIZE)
do i=1,n
  do j=1,n
     alpt(i,j)=alp(j,i)
     cet(i,j)=ce(j,i)
  enddo
enddo

do i=1,n
  dlt(i)=0.0d0
enddo
do i=1,n
  do j=1,n
    sysa(i,j)=0.0d0
  enddo
enddo
do i=1,n
 do j=1,n
```

```
           do k=1,n
             sysa(i,j)=sysa(i,j)+alpt(i,k)*alp(k,j)+cet(i,k)*ce(k,j)
           enddo
         enddo
        enddo
        do i=1,n
          do j=1,n
            dlt(i)=dlt(i)-alpt(i,j)*(x(j)-xinit(j) )
     &            -cet(i,j)*(y(j)-yinit(j)  )
          enddo
        enddo
        call ludcmp(sysa,n,indx,d)
        call lubksb(sysa,n,indx,dlt)
        return
        end
c-------------------------------------------------------------
c        eigenvalues
c-------------------------------------------------------------

        subroutine floque(a,n1,vr)
        include 'parameters.f'
        real*8 a(SIZE,SIZE),vl(SIZE,SIZE),vr(SIZE,SIZE)
        real*8 wr(SIZE),wi(SIZE),work(MAXWORK)
        character jobvl,jobvr
        integer info,lda,ldvl,ldvr,lwork,n1,n

        lda=SIZE
        ldvl=SIZE
        ldvr=SIZE
        lwork=MAXWORK
```

```
        jobvl='N'
c        jobvr='N'
        jobvr='V'
        n=2*n1

        call dgeev( jobvl, jobvr,n,a,lda,wr,wi,vl,ldvl,vr,ldvr,
     &              work,lwork,info)
        do i=1,2*n
            a(i,1)=wr(i)
            a(i,2)=wi(i)
        enddo
        return
        end
```

The second program we include here is for the calculation of discrete breathers and multibreathers in a monoatomic as well as in a diatomic FPU lattice with hard or soft interactions. In the input file are defined two masses, in the case of equal masses the system becomes monoatomic while for different masses the system becomes diatomic. The parameters gamma and gamma_0 in the input file are for the interaction potential and for the on-site potential we use for the anticontinuous limit. Negative parameters indicate soft potential while positive parameters indicate hard potential. The last two parameters are used for the breather frequency. The frequency in every step of the Newton method is kept in a constant distance dw from one of the lines shown in figure (6.1). Negative dw means that the breather frequency is bellow the line while positive dw means that it is above. This is done in order to avoid resonances with the phonons. The last parameter indicates one of the lines in figure (6.1), 1 and 2 correspond to the lower and the upper limit of the acoustic band respectively, 3 and 4 correspond to the lower and the upper limit respectively of the optical band. The numbers 5 and 6 correspond to the lower and the upper limit respectively of the optical band divided by 2, 7 and 8 correspond to the lower and the upper limit respectively of the optical band divided by 3 and so on.

file "input.dat" for the fpu.f program:

```
#
#              for the breather
#
40                              :  number of cites
21                              :  center of the breather
0.472179                        : initial position
9.053999999988                  : period of the breather
0.050                           :  kmax
0.0251                          :  dk
1.0                             :  petrubation strength
500                             :  time of simulations
47                              :  sampling rate
16.0                            :  heavy mass  (odd sites)
1.0                             :  light mass  (even sites)
+1.0                            :  parameter gama for the interaction W
+1.0                            :  parameter gama_0 for the onsite V
0.01                            : dw for the breather frequency
10                              : which phonon frequency to follow by dw
```

Program fpu.f:

```
      program main2
c     implicit none
      include "parameters.f"
      character*80 junk
      real*8 x(0:SIZE),y(0:SIZE)
      real*8 xinit(0:SIZE),yinit(0:SIZE)
      real*8 alp(SIZE,SIZE),ce(SIZE,SIZE),dlt(SIZE)
      real*8 bet(SIZE,SIZE),de(SIZE,SIZE)
      real*8 vectors(SIZE,SIZE)
```

```
      real*8 sum
c      real*8 mass(SIZE),dm
      real*8 omega(SIZE),m1,m2
      real*8 t,dt,kapa,dk,period
      real*8 kmax,dzero
      real*8 lamda,dl
      real*8 imass,wi,despl
      real*8 wph(10) , dw,pi
      integer iposs,wintex
      real*8 gamma(SIZE),gamma0(SIZE),g1,g2
      integer i,n,j,ncent
      common gamma,gamma0
100      format( e25.16,i4,e25.16)
103      format( e25.16,e25.16)
102      format( i4,e25.16)
101      format()
      open (21,file='breather.out')
c
c  input data
c
      open (23,file="input.dat")
      read(23,1000) junk
      read(23,1000) junk
      read(23,1000) junk
1000  format ( a80)
      read(23,*) n
      read(23,*) ncent
      do i=0,n+1
         xinit(i)=0.0d0
         yinit(i)=0.0d0
```

```
        enddo
        read(23,*) xinit(ncent)
        read(23,*) period
        read(23,*) kapa
        read(23,*) dl
c
c       read some junk lines
c
        do i=1,3
          read(23,1000) junk
        enddo
        read(23,*) m1
        read(23,*) m2
        read(23,*) g1
        read(23,*) g2
        read(23,*) dw
        read(23,*) wintex
        close(23)
        do i=1,n+1
c          gamma(i)=0.0d0
           gamma(i)=g1
           gamma0(i)=0.0d0
        enddo
        gamma(ncent)=g1
        gamma0(ncent)=g2
        gamma(ncent+1)=g1
c       gamma0(ncent+1)=g2

        if(n.gt.NMAX/2) then
          write(*,*) "you must decreace the numper of oscilators or"
```

```
          write(*,*) "recompile the program with greater NMAX"
          stop
        endif
c
        do i=1,n
          omega(i)=1.0d0/m1
        enddo
        do i=2,n+1,2
          omega(i)=1.0d0/m2
        enddo
        do i=1,n
           write(*,*) i,omega(i),gamma(i),gamma0(i)
        enddo
        dt=1.0d-3
        lamda=0.0001d0
c       dw=0.02d0

        do while( lamda .le. 1.0d0 )
             if( (lamda+dl).gt.1.0d0) then
               dl=dl/3.0d0
               write(*,*) "--------->    dl=",dl
c              dt=1.0d-4
             endif
             do while( (lamda+dl).gt.1.0d0)
                 dl=dl/3.0d0
                 write(*,*) "--------->    dl=",dl
            enddo
            if(dl.le.0.0001) then
               lamda=1.0d0
               dt=1.0d-4
```

```
           endif
c
c   find the phonon frequencies
c   and fixing the breather frequency just bellow the optical band
           call fwph( wph , m1,m2,lamda)
           wbr=wph(wintex)+dw
           period=6.2831853d0/wbr
600           continue
            do i=0,n+1
              x(i)=xinit(i)
              y(i)=yinit(i)
           enddo
           do i=1,n
             do j=1,n
               alp(i,j)=0.0d0
               ce(i,j)=0.0d0
             enddo
              alp(i,i)=1.0d0
            enddo
           t=0.0d0
           do while(t.lt.period)
                call rk4_s(x,y,t,dt,lamda,n,omega)
                call rk4_s2(alp,ce,x,y,t,dt,lamda,n,omega)
               t=t+dt
            enddo
c
c       Termination contition
c
           sum=0.0d0
           do i=1,n
```

```
            sum=sum + dabs(xinit(i)-x(i))+dabs(yinit(i)-y(i))
           enddo
           if(sum.gt.1.0d0) then
              dl=dl/2.0
           endif
           write(*,*) wbr,lamda,sum
c-----------------------------------------------
           do i=1,n
             alp(i,i)=alp(i,i) -1.0d0
           enddo
           call deval( alp,ce,dlt,xinit,x,yinit,y,n)
           do i=1,n
             xinit(i)=xinit(i)+dlt(i)
           enddo
           if (sum.le.1.0e-10) goto 300
           sum=0.0d0
           do i=1,n
           sum=sum+dabs( dlt(i) )
           enddo
           if (sum.le.1.0e-14) goto 300
           goto 600
300           lamda=lamda+dl
           write(*,*)(i,xinit(i),i=1,n)
         enddo
         lamda=1.0d0
       write(21,*) "#  BREATHER PARAMETERS "
       write(21,*) "#  FREQUENCY ",wbr
       write(21,*) "#  LAMBDA    ",lamda
       write(21,*) "#"
       do i=1,n
```

```
          write(21,102) i,xinit(i)
        enddo
        close(21)

c-------------------------------------------------------
c       for the floquet analysis
c-------------------------------------------------------
             do i=1,n
               x(i)=xinit(i)
               y(i)=yinit(i)
               do j=1,n
                 alp(i,j)=0.0d0
                bet(i,j)=0.0d0
                ce(i,j)=0.0d0
                de(i,j)=0.0d0
               enddo
               alp(i,i)=1.0d0
               de(i,i)=1.0d0
             enddo
             t=0.0d0
             do while(t.lt.period)
                   call rk4_s(x,y,t,dt,lamda,n,omega)
                   call rk4_s2(alp,ce,x,y,t,dt,lamda,n,omega)
                   call rk4_s2(bet,de,x,y,t,dt,lamda,n,omega)
                t=t+dt
              enddo
             do i=1,n
               do j=1,n
                 alp(i+n,j)=ce(i,j)
                alp(i,j+n)=bet(i,j)
```

```
   alp(i+n,j+n)=de(i,j)
  enddo
enddo
call floque(alp,n,vectors)
open (23,file="eigen.out")
open (24,file="vectors.out")
open (25,file="vectors_im.out")
do i=1,2*n
  write(23,103) alp(i,1),alp(i,2)
enddo
close(23)
dzero=0.0d0
do i=1,2*n,2
   if (dabs( alp(i,2) ).lt.1.0d-9 ) then
   do k=0,1
   do j=1,2*n
     write(24,102) j,vectors(j,i+k)
     write(25,102) j,dzero
   enddo
   write(24,101)
   write(25,101)
   enddo
   else
     do j=1,2*n
       write(24,102) j,vectors(j,i)
       write(25,102) j,vectors(j,i+1)
    enddo
     write(24,101)
     write(25,101)
   endif
```

```
            enddo
       stop
       end
c
c subroutine for the frequencies of the phonnon band
c
       subroutine fwph( wph, m1,m2,l)
       real*8 wph(8),m1,m2,l
       real*8 delta1,delta2

       delta1=(m1-m2)*(m1-m2)*(2.0*l+1.0-l)**2
       delta2=delta1+16.0*m1*m2*l*l
       wph(2)=( (m1+m2)*(2.0*l+1-l) - sqrt( delta1) )/(2.0*m1*m2)
       wph(1)=( (m1+m2)*(2.0*l+1-l) - sqrt( delta2) )/(2.0*m1*m2)
       wph(4)=( (m1+m2)*(2.0*l+1-l) + sqrt( delta2) )/(2.0*m1*m2)
       wph(3)=( (m1+m2)*(2.0*l+1-l) + sqrt( delta1) )/(2.0*m1*m2)
       do i=1,4
            wph(i)=dsqrt(wph(i))
       enddo

       wph(5)=wph(3)/2.0d0
       wph(6)=wph(4)/2.0d0
       wph(7)=wph(3)/3.0d0
       wph(8)=wph(4)/3.0d0
       wph(9)=wph(3)/4.0d0
       wph(10)=wph(4)/4.0d0

       return
       end
```

```
c   This is a subroutine for solving a system of
c   diferential equations on a latice with first
c   neighbor aproximation
       subroutine rk4_s(x,y,t,dt,l,n,wmega)
       include 'parameters.f'
       real*8 x(0:SIZE),y(0:SIZE)
       real*8 t,dt,l
       integer i,n
       real*8 fx,fy
       real*8 wmega(SIZE),wtmp
       real*8 kx1(0:SIZE),kx2(0:SIZE),kx3(0:SIZE),kx4(0:SIZE)
       real*8 ky1(0:SIZE),ky2(0:SIZE),ky3(0:SIZE),ky4(0:SIZE)
       real*8 xtmp(0:2),ytmp(0:2)
       real*8 gamma(SIZE),gamma0(SIZE)
       common gamma,gamma0
c
c   periodic boundary conditions
c
       x(0)=x(n)
       x(n+1)=x(1)
       y(0)=y(n)
       y(n+1)=y(1)
c
c  For the first step of the Runke Kuta
c
       do i=1,n
           xtmp(0)=x(i-1)
           xtmp(1)=x(i)
           xtmp(2)=x(i+1)
           ytmp(0)=y(i-1)
```

```
            ytmp(1)=y(i)
            ytmp(2)=y(i+1)

           wtmp=wmega(i)

           kx1(i)=dt*fx(xtmp,ytmp,t,l)
           ky1(i)=dt*fy(xtmp,ytmp,t,wtmp,l,i)
        enddo
        kx1(0)=kx1(n)
        kx1(n+1)=kx1(1)
         ky1(0)=ky1(n)
        ky1(n+1)=ky1(1)
c
c  For the second step of the Runke Kuta
c
        do i=1,n

            xtmp(0)=x(i-1)+kx1(i-1)/2.0d0
            xtmp(1)=x(i)+kx1(i)/2.0d0
            xtmp(2)=x(i+1)+kx1(i+1)/2.0d0

            ytmp(0)=y(i-1)+ky1(i-1)/2.0d0
            ytmp(1)=y(i)+ky1(i)/2.0d0
            ytmp(2)=y(i+1)+ky1(i+1)/2.0d0

           wtmp=wmega(i)

           kx2(i)=dt*fx(xtmp,ytmp,t,l)
           ky2(i)=dt*fy(xtmp,ytmp,t,wtmp,l,i)
        enddo
```

```
        kx2(0)=kx2(n)
        kx2(n+1)=kx2(1)
        ky2(0)=ky2(n)
        ky2(n+1)=ky2(1)
c
c  For the third step of the Runke Kuta
c
       do i=1,n

           xtmp(0)=x(i-1)+kx2(i-1)/2.0d0
           xtmp(1)=x(i)+kx2(i)/2.0d0
           xtmp(2)=x(i+1)+kx2(i+1)/2.0d0

           ytmp(0)=y(i-1)+ky2(i-1)/2.0d0
           ytmp(1)=y(i)+ky2(i)/2.0d0
           ytmp(2)=y(i+1)+ky2(i+1)/2.0d0

          wtmp=wmega(i)
          kx3(i)=dt*fx(xtmp,ytmp,t,l)
          ky3(i)=dt*fy(xtmp,ytmp,t,wtmp,l,i)

       enddo
       kx3(0)=kx3(n)
        kx3(n+1)=kx3(1)
        ky3(0)=ky3(n)
        ky3(n+1)=ky3(1)
c
c  For the fourthd step of the Runke Kuta
c
       do i=1,n
```

```
        xtmp(0)=x(i-1)+kx3(i-1)
        xtmp(1)=x(i)+kx3(i)
        xtmp(2)=x(i+1)+kx3(i+1)

        ytmp(0)=y(i-1)+ky3(i-1)
        ytmp(1)=y(i)+ky3(i)
        ytmp(2)=y(i+1)+ky3(i+1)

       wtmp=wmega(i)
       kx4(i)=dt*fx(xtmp,ytmp,t,l)
       ky4(i)=dt*fy(xtmp,ytmp,t,wtmp,l,i)

     enddo

     do i=1,n
       x(i)=x(i)+( kx1(i)+2.0d0*kx2(i)+
    &               2.0d0*kx3(i)+kx4(i) )/6.0d0
       y(i)=y(i)+( ky1(i)+2.0d0*ky2(i)+
    &               2.0d0*ky3(i)+ky4(i) )/6.0d0
     enddo
     return
     end

      subroutine rk4_s2(alp,ce,x,y,t,dt,l,n,wmega)
     include 'parameters.f'
     real*8 alp(SIZE,SIZE),ce(SIZE,SIZE)
      real*8 x(0:SIZE),y(0:SIZE)
     real*8 x0(0:SIZE),y0(0:SIZE)
     real*8 t,dt,l
```

```
      integer i,j,k,n
      real*8 fx2,fy2
      real*8 wmega(SIZE),wtmp
      real*8 kx1(0:SIZE),kx2(0:SIZE)
      real*8 kx3(0:SIZE),kx4(0:SIZE)
      real*8 ky1(0:SIZE),ky2(0:SIZE)
      real*8 ky3(0:SIZE),ky4(0:SIZE)
      real*8 xtmp(0:2),ytmp(0:2)
      real*8 tmp(0:2)
      real*8 gamma(SIZE),gamma0(SIZE)
      common gamma,gamma0
       do k=1,n
        do j=1,n
         x0(j)=alp(j,k)
          y0(j)=ce(j,k)
        enddo
c
c   periodic boundary conditions
c
      x0(0)=x0(n)
      x0(n+1)=x0(1)
      y0(0)=y0(n)
      y0(n+1)=y0(1)
c
c  For the first step of the Runke Kuta
c
       do i=1,n
         xtmp(0)=x0(i-1)
         xtmp(1)=x0(i)
         xtmp(2)=x0(i+1)
```

```
            ytmp(0)=y0(i-1)
            ytmp(1)=y0(i)
            ytmp(2)=y0(i+1)

           tmp(0)=x(i-1)
           tmp(1)=x(i)
           tmp(2)=x(i+1)

           wtmp=wmega(i)

           kx1(i)=dt*fx2(xtmp,ytmp,t,l)
           ky1(i)=dt*fy2(xtmp,ytmp,t,tmp,wtmp,l,i)
         enddo
          kx1(0)=kx1(n)
          kx1(n+1)=kx1(1)
          ky1(0)=ky1(n)
          ky1(n+1)=ky1(1)
c
c  For the second step of the Runke Kuta
c
         do i=1,n

            xtmp(0)=x0(i-1)+kx1(i-1)/2.0d0
            xtmp(1)=x0(i)+kx1(i)/2.0d0
            xtmp(2)=x0(i+1)+kx1(i+1)/2.0d0

            ytmp(0)=y0(i-1)+ky1(i-1)/2.0d0
            ytmp(1)=y0(i)+ky1(i)/2.0d0
            ytmp(2)=y0(i+1)+ky1(i+1)/2.0d0
```

```
          tmp(0)=x(i-1)
          tmp(1)=x(i)
          tmp(2)=x(i+1)

          wtmp=wmega(i)

          kx2(i)=dt*fx2(xtmp,ytmp,t,l)
          ky2(i)=dt*fy2(xtmp,ytmp,t,tmp,wtmp,l,i)
        enddo
         kx2(0)=kx2(n)
         kx2(n+1)=kx2(1)
         ky2(0)=ky2(n)
         ky2(n+1)=ky2(1)
c
c  For the third step of the Runke Kuta
c
        do i=1,n

           xtmp(0)=x0(i-1)+kx2(i-1)/2.0d0
           xtmp(1)=x0(i)+kx2(i)/2.0d0
           xtmp(2)=x0(i+1)+kx2(i+1)/2.0d0

           ytmp(0)=y0(i-1)+ky2(i-1)/2.0d0
           ytmp(1)=y0(i)+ky2(i)/2.0d0
           ytmp(2)=y0(i+1)+ky2(i+1)/2.0d0

          tmp(0)=x(i-1)
          tmp(1)=x(i)
          tmp(2)=x(i+1)
```

```
          wtmp=wmega(i)

          kx3(i)=dt*fx2(xtmp,ytmp,t,l)
          ky3(i)=dt*fy2(xtmp,ytmp,t,tmp,wtmp,l,i)

        enddo
         kx3(0)=kx3(n)
         kx3(n+1)=kx3(1)
         ky3(0)=ky3(n)
         ky3(n+1)=ky3(1)
c
c  For the fourthd step of the Runke Kuta
c
        do i=1,n

           xtmp(0)=x0(i-1)+kx3(i-1)
           xtmp(1)=x0(i)+kx3(i)
           xtmp(2)=x0(i+1)+kx3(i+1)

           ytmp(0)=y0(i-1)+ky3(i-1)
           ytmp(1)=y0(i)+ky3(i)
           ytmp(2)=y0(i+1)+ky3(i+1)

          tmp(0)=x(i-1)
          tmp(1)=x(i)
          tmp(2)=x(i+1)

          wtmp=wmega(i)
```

```
          kx4(i)=dt*fx2(xtmp,ytmp,t,l)
          ky4(i)=dt*fy2(xtmp,ytmp,t,tmp,wtmp,l,i)

        enddo

        do i=1,n
           alp(i,k)=x0(i)+( kx1(i)+2.0d0*kx2(i)+
     &              2.0d0*kx3(i)+kx4(i) )/6.0d0
           ce(i,k)=y0(i)+( ky1(i)+2.0d0*ky2(i)+
     &              2.0d0*ky3(i)+ky4(i) )/6.0d0
        enddo
        enddo
       return
       end

c Functions for the runke couta integretion of the
c original equations
c
       real*8 function fx( x,y,t,l)
       real*8 x(0:2),y(0:2),t,l
       fx= y(1)
       return
       end

       real*8 function fy( x,y,t,w,l,i)
        INCLUDE 'parameters.f'
       real*8 x(0:2),y(0:2),t
       real*8 l
       real*8 w
       real*8 potential1,potential2
```

```
      real*8 gamma(SIZE),gamma0(SIZE)
      common gamma,gamma0
      fy= -w*(1.0d0-l)*potential1(x(1),i )
     &           +l*w*potential2( x(2) - x(1),i+1 )
     &           -l*w*potential2( x(1) - x(0) ,i)

      return
      end
c
c   onsite potential for the newton iteration
c
      real*8 function potential1(x,i)
       INCLUDE 'parameters.f'
      real*8 x
      real*8 gamma(SIZE),gamma0(SIZE)
      common gamma,gamma0
      potential1=x+gamma0(i)*x*x*x
      return
      end
c
c   nonlinear interaction potential
c
      real*8 function potential2(x,i)
       INCLUDE 'parameters.f'
      real*8 x
      real*8 gamma(SIZE),gamma0(SIZE)
      common gamma,gamma0
      potential2=x+gamma(i)*x*x*x
      return
      end
```

```
c ------------------------------------------------------------
c
c Functions for the integration of the
c linearized equations
c
       real*8 function fx2( x,y,t,l)
       real*8 x(0:2),y(0:2),t,l
       fx2= y(1)
       return
       end

       real*8 function fy2( x,y,t,tmp,w,l,i)
        INCLUDE 'parameters.f'
       real*8 x(0:2),y(0:2),t,tmp(0:2)
       real*8 l
       real*8 w
       real*8 ppotential1,ppotential2
       real*8 gamma(SIZE),gamma0(SIZE)
       common gamma,gamma0
       fy2=-w*(1.0d0-l)*ppotential1(tmp(1),i)*x(1)
     &        +l*w*ppotential2(tmp(2)-tmp(1),i+1)*(x(2)-x(1))
     &        -l*w*ppotential2(tmp(1)-tmp(0),i)*(x(1)-x(0))
       return
       end
c
c  derivative ot the onsite potential
c
       real*8 function ppotential1( x,i)
        INCLUDE 'parameters.f'
        real*8 x
```

```
       real*8 gamma(SIZE),gamma0(SIZE)
       common gamma,gamma0
       ppotential1=1.0d0+3.0d0*gamma0(i)*x*x
       return
       end
c
c  derivative ot the nonlinear interaction potential
c
       real*8 function ppotential2( x,i)
        INCLUDE 'parameters.f'
        real*8 x
       real*8 gamma(SIZE),gamma0(SIZE)
       common gamma,gamma0
       ppotential2=1.0d0+3.0d0*gamma(i)*x*x
       return
       end


       subroutine  deval( alp,ce,dlt,xinit,x,yinit,y,n)
        INCLUDE 'parameters.f'
       real*8 xinit(0:SIZE),x(0:SIZE)
       real*8 yinit(0:SIZE),y(0:SIZE)
       real*8 alp(SIZE,SIZE),ce(SIZE,SIZE),dlt(SIZE),d
       real*8 alpt(SIZE,SIZE),cet(SIZE,SIZE),sysa(SIZE,SIZE)
       integer n,indx(SIZE)
        do i=1,n
         do j=1,n
            alpt(i,j)=alp(j,i)
            cet(i,j)=ce(j,i)
         enddo
```

```
        enddo

        do i=1,n
          dlt(i)=0.0d0
        enddo
        do i=1,n
          do j=1,n
            sysa(i,j)=0.0d0
          enddo
        enddo
        do i=1,n
         do j=1,n
           do k=1,n
             sysa(i,j)=sysa(i,j)+alpt(i,k)*alp(k,j)+cet(i,k)*ce(k,j)
           enddo
         enddo
        enddo
        do i=1,n
          do j=1,n
            dlt(i)=dlt(i)-alpt(i,j)*(x(j)-xinit(j) )
     &                        -cet(i,j)*(y(j)-yinit(j)  )
          enddo
        enddo
        call ludcmp(sysa,n,indx,d)
        call lubksb(sysa,n,indx,dlt)
        return
        end
c--------------------------------------------------------------
c        eigenvalues
c--------------------------------------------------------------
```

```
      subroutine floque(a,n1,vr)
      include 'parameters.f'
      real*8 a(SIZE,SIZE),vl(SIZE,SIZE),vr(SIZE,SIZE)
      real*8 wr(SIZE),wi(SIZE),work(MAXWORK)
      character jobvl,jobvr
      integer info,lda,ldvl,ldvr,lwork,n1,n

      lda=SIZE
      ldvl=SIZE
      ldvr=SIZE
      lwork=MAXWORK

      jobvl='N'
c      jobvr='N'
      jobvr='V'
      n=2*n1

      call dgeev( jobvl, jobvr,n,a,lda,wr,wi,vl,ldvl,vr,ldvr,
     &              work,lwork,info)
      do i=1,2*n
          a(i,1)=wr(i)
          a(i,2)=wi(i)
      enddo
      return
      end
```

Bibliography

[1] A. J. Sievers and S. Takeno, Phys. Rev. Lett. **61**, 970 (1988).

[2] J. B. Page. Phys. Rev. B **41**, 7835 (1990).

[3] J.C. Eilbeck, P.S. Lomdahl and A.C. Scott, Physica D **16**, 318 (1985)

[4] T. Dauxois and M. Peyrard, Phys. Rev. Lett. **70**, 3935 (1993).

[5] D. K. Campbell and M.Peyrard , Physica D **18**, 47 (1986).

[6] H. Segur and M. D. Kruskal, Phys. Rev. Lett. **58**, 747 (1987); S. Kitchenassamy, Comm. Pure Appl. Math. **44**, 789 (1991); J. Denzler, Comm. Math. Phys. **158**, 397 (1993).

[7] E. Fermi, J. R. Pasta and S. M. Ulam, Collected papers of Enrico Fermi ed. Segré Vol. II Chicago University Press, 978 (1965).

[8] R. S. MacKay and S. Aubry, Nonlinearity, **7** 1623 (1994).

[9] S. Aubry,Physica D **71**, 196 (1994).

[10] S. Aubry,Physica D **86**, 284 (1995).

[11] S. Aubry,Physica D **103**, 201 (1997).

[12] S. Flach and C. R. Willis, Phys. Rep. **295**, 182 (1998).

[13] S. Aubry, Breathers in nonlinear lattices: Recent results from the concept of anticontinuity, preprint.

[14] S. Aubry, Discrete Breathers in nonlinear lattices: New perspectives in physics and biological physics, submitted to "Nonlinear Science at the dawn of the 21th century, ed. P.L. Christiansen and M. Soerensen, Springer.

[15] J. L. Marin and S. Aubry, Nonlinearity **9**, 1501 (1994).

[16] Ding Chen, S. Aubry and G. P. Tsironis, Phys. Rev. Lett. **77**, 4776 (1996).

[17] G. P. Tsironis and S. Aubry, Phys. Rev. Lett. **77**, 5225 (1996).

[18] Ding Chen, "Spatiotemporal properties of coupled nonlinear oscillators", PhD Thesis, 1996, Univ. of North Texas.

[19] Jose Luis Marin Espanol, "Modos Intrinsecos Localizados en Redes No Lineales", PhD Thesis, 1997, Univ. of Zaragoza.

[20] A. Bikaki, N. K. Voulgarakis, S. Aubry and G. P. Tsironis, Phys. Rev. E **59**, 1234 (1999).

[21] P. Maniadis, G. P. Tsironis, A. R. Bishop and A. V. Zolotaryuk, Phys. Rev. E **60**, 7618 (1999).

[22] P. Maniadis, submitted to Phys. Lett. A (2000).

[23] A. V. Zolotaryuk, P. Maniadis and G. P. Tsironis, to be published Physica B (2001).

[24] P. Maniadis, A. V. Zolotaryuk and G. P. Tsironis, submitted to Phys. Rev. E.

[25] George Kalosakas, "Στατικές και δυναμικές ιδιότητες των πολαρονίων στο ημικλασικό πρότυπο Holstein", PhD Thesis, 1997, Univ. of Crete.

[26] G. Kalosakas and S. Aubry, Physica D **113**, 228 (1198).

[27] S. Flach, C. R. Willis and E. Olbrich, Phys. Rev. E **49**, 836 (1994).

[28] S. Flach, Phys. Rev. E **50**, 3134 (1994).

[29] S. Flach, Physica D **113**, 184 (1198).

[30] T. Cretegny and S. Aubry, Physica D **113**, 162 (1998).

[31] S. Aubry and T. Cretegny, Physica D **119**, 34 (1998).

[32] T. Cretegny, S. Aubry and S. Flach, Physica D **119**, 73 (1998).

[33] Magnus Johansson and Serge Aubry, Nonlinearity **10**, 1151 (1997).

[34] M. Johansson, S. Aubry, Y. B. Gadidei, P. L. Christiansen and K. Ø. Rasmussen, Physica D **119**, 115 (1998).

[35] R. Livi, M. Spicci and R. S. MacKay, Nonlinearity **10**, 1421 (1997).

[36] T. Cretegny, R. Livi and M. Spicci, Physica D **119**, 88 (1998).

[37] J.L. Marin, S. Aubry and L.M. Floria, Physica D **113**, 283 (1998).

[38] J.A. Sepulche, R. S. MacKay, Physica D **113**, 342 (1998).

[39] L.M. Floria, J.L. Marin, S. Aubry, P. J. Martinez, F. Falo and J. J. Mazo, Physica D **113**, 387 (1998).

[40] L.M. Floria, J.L. Marin, P. J. Martinez, F. Falo and S. Aubry, Europhys. Lett. **36**, 539 (1996).

[41] G. Kopidakis and S. Aubry, Physica D **130**, 155 (1999).

[42] G. Kopidakis and S. Aubry, Physica D **139**, 247 (2000).

[43] S. Flach, Energy properties of discrete breathers, preprint (1997).

[44] S. Flach, K. Kladko and R. MacKay, Phys. Rev. Lett. **78**, 1207 (1997).

[45] S. Flach, K. Kladko and S. Takeno, Phys. Rev. Lett. **79**, 4838 (1997).

[46] J. J. Mazo, E. Trias and T. P. Orlando, Phys. Rev. E **59**, 13604 (1999).

[47] E. Trias, J. J. Mazo and T. P. Orlando, Phys. Rev. Lett. **84**, 741 (2000).

[48] P. Binder, D. Abraimov, A. V. Ustinov, S. Flach and Y. Zolotaryuk, Phys. Rev. Lett. **84**, 745 (2000).

[49] D. Abraimov, P. Caputo, G. Filatrella, M. V. Fistul, G. Yu. Logvenov and A. V. Ustinov, Phys. Rev. Lett. **83**, 5354 (1999).

[50] B.I. Swanson, J.A. Brozik, S.P. Love, G.F. Strouse, A.P. Shreve, A.R. Bishop, W.Z. Wang and M.I Salkola, Phys. Rev. Lett. **82**, 3288 (1999).

[51] R. Lai and A. Sievers, Phys. Rev. Lett. **81**, 1937 (1998).

[52] U.T. Schwarz, L.Q. English and A. Sievers, Phys. Rev. Lett. **83**, 223 (1999).

[53] H. S. Eisenberg, Y. Silberberg, R. Morantotti, A. R. Boyd and J.S. Atchinson, Phys. Rev. Lett. **81**, 3383 (1998).

[54] M. Peyrard, Europhys. Lett. **44**, 271 (1998).

[55] D. Hennig and G. P. Tsironis, Phys. Rep. **307**, 333 (1999).

[56] M. Kollmann and T. Bountis, Physica D **113**, 397 (1998).

[57] S. Aubry and G. Abramovici, Physica D **43**, 199 (1990).

[58] S. Aubry, in The IMA Volumes in Mathematics and Applications, eds. R. McGehee and K. R. Mayer, Vol 44, pp 7-54, Springer, (Berlin, 1992).

[59] P. B. Hobbs, *Ice Physics*, Clarendon Press, Oxford 1974.

[60] St. Pnevmatikos, Phys. Rev. Lett. **60**, 1535 (1988).

[61] G. P. Tsironis and St. Pnevmatikos, Phys. Rev. B. **38**, 7161 (1989).

[62] A. V. Zolotaryuk and St. Pnevmatikos, Phys. Lett. A **143**, 233 (1990).

[63] St. Pnevmatikos, G. P. Tsironis and A. V. Zolotaryuk, J. Molec. Liquids, (1989).

[64] G. Kalosakas, A. V. Zolotaryuk, G. P. Tsironis and E. N. Economou, Phys. Rev. E **56**, 1088 (1997).

[65] See, e.g., L. D. Faddeev and L. A. Takhtajan, *Hamiltonian Methods in the Theory of Solitons* (Springer-Verlag, Berlin, 1987).

[66] B. A. Malomed, Physica D **15**, 385 (1985); **27**, 113 (1987).

[67] Yu. S. Kivshar and B. A. Malomed, Rev. Mod. Phys. **61**, 763 (1989).

[68] Fei Zhang, Phys. Rev. E **58**, 2558 (1998).

[69] E. Mann, J. Phys. A: Math. Gen. **30**, 1227 (1997).

[70] St. Pnevmatikos, Yu. S. Kivshar, M. J. Velgakis, and A. V. Zolotaryuk, Phys. Lett. A **173**, 43 (1993).

[71] A. M. Kosevich and A. S. Kovalev, Sov. Phys. JETP **40**, 523 (1972); T. Kawahara, J. Phys. Soc. Japan **35**, 1537 (1973); N. Flytzanis, St. Pnevmatikos, and M. Remoissenet, J. Phys. C **18**, 4603 (1985)

[72] A. Xie, L. van der Meer, W. Hoff and R.H. Austin, Phys. Rev. Lett. **84** (2000) 5435.

[73] For a review see, e.g., J.F. Nagle and S. Tristram-Nagle, J. Membrane Biology **74** (1983) 1.

[74] X. Duan and S. Scheiner, J. Mol. Struct. **270** (1992) 173.

[75] N.D. Sokolov, M.V. Vener and V.A. Savel'ev, J. Mol. Struct. **222** (1990) 365.

[76] A.V. Zolotaryuk, St. Pnevmatikos and A.V. Savin, Physica D **51** (1991) 407.

[77] St. Pnevmatikos, N. Flytzanis and M. Remoissenet, Phys. Rev. B **33** (1986) 2308.

[78] Y.S. Kivshar and N. Flytzanis, Phys. Rev. A **46** (1992) 7972; O.A. Chubykalo, A.S. Kovalev and O.V. Usatenko, Phys. Rev. B **47** (1993) 3153.

[79] O.A. Chubykalo and Y.S. Kivshar, Phys. Rev. E **48** (1993) 4128; **49** (1994) 5906.

[80] G. Huang, Phys. Rev. B **51** (1995) 12 347.

[81] S.A. Kiselev, S.R. Bickham and A.J. Sievers, Phys. Rev. B **48** (1993) 13 508; **50** (1994) 9135.

[82] G. Huang and B. Hu, Phys. Rev. B **57** (1998) 5746; B. Hu, G. Huang and M.G. Velarde, Phys. Rev. E **62** (2000) 2827.

[83] Q. Li, St. Pnevmatikos, E.N. Economou and C.M. Soukoulis, Phys. Rev. B **37** (1988) 3534; T. Fraggis, St. Pnevmatikos and E.N. Economou, Phys. Lett. A **142** (1989) 361.

[84] P. Tchofo Dinda and M. Remoissenet, Phys. Rev. E **60**, 6218 (1999).

[85] M. Eleftheriou, B. Dey and G.P. Tsironis, Phys. Rev. E **62**, 7540 (2000).

[86] V. I. Arnold and A. Avez, Ergodic Problems of Clasical Mechanics App., Vol. 29 (Benjamin, New York, 1968).

[87] J. Moser, Stable and Random Motion in Dynamical Systems, Annals of Mathematical Studies, (Princeton University Press, Princeton, 1973).

[88] M. I. Molina and G. P. Tsironis, Phys. Rev. B **47**, 15330 (1993).

[89] G. P. Tsironis, M. I. Molina and D Hennig, Phys. Rev. E **50**, 2365 (1994). M. I. Molina and G. P. Tsironis, Phys. Rev. Lett. **73**, 464 (1994). M. I. Molina and G. P. Tsironis, Int. J. Mod. Phys. B **9**, 1899 (1995).

[90] E. N. Economou "Green's Function in Quantum Physics" Springer-Verlag, Berlin 1990.

[91] M.J. Ablowitz and J.F. Ladik, Stud. Appl. Math. **55**, 213 (1976)

[92] V.M. Kenkre and D.K. Campbell, Phys. Rev. B **34**, 4959 (1986) G.P. Tsironis and V.M. Kenkre, Phys. Lett. A **127**, 209 (1988); V.M. Kenkre, G.P. Tsironis and D.K. Campbell in: Nonlinearity in Condensed Matter, eds. A.R. Bishop et al. (Springer, 1987).

[93] M.I. Molina and G.P. Tsironis, Physica D **65**, 267 (1993).

[94] B.M. Herbst and M.J. Ablowitz, Phys. Rev. Lett. **62**, 2065 (1989)

[95] G. Kalosakas, G.P. Tsironis and E.N. Economou, J. Phys.: Cond. Mat. **6**, 7847 (1994).

[96] A.S. Davydov and N.I. Kislukha, Phys. Status Solidi B **59**,465 (1973).

[97] R. Scharf and A.R. Bishop, Phys. Rev. A **43**, 6535 (1991)

[98] M. Salerno, Phys. Rev. A **46**, 6856 (1992).

[99] D. Cai, A.R. Bishop and N. Gronbech - Jensen, Phys. Rev. Lett. **72**, 591 (1994)

[100] D. Hennig, N.G. Sun, H. Gabriel and G.P. Tsironis, Phys. Rev. E, **52** 255 (1995).

[101] D. Hennig, K.O. Rasmussen, G.P. Tsironis and H. Gabriel, Phys. Rev. E **52**, 4628 (1995).

[102] G.Kalosakas, P.Maniadis and G.P.Tsironis, Physica Scripta **55**, 523 (1997).

[103] P.L.Christiansen, P.Maniadis and G.P.Tsironis, Physica Scripta **57**, 192 (1998).

[104] M.Jorgensen and P.L.Christiansen, "Self-traping and blow-up in integrable dimers", preprint.

[105] J.C. Eilbeck, G.P. Tsironis and S.K. Turitsyn, Physica Scripta **52** 386 (1995).

[106] N. W. Ascroft and N. D. Mermin, Solid state physics, W. B. Saunders Company, New York n(1976).

[107] Numerical Recipes, The Art of Scientific Computing, Cambridge University Press (1986); Numerical Recipes Book on Line, http://www.nr.com

[108] LAPACK - Linear Algebra PACKage, http://netlib2.cs.utk.edu/lapack/

[109] S. E. Koonin and D. C. Meredith, Computational Physics, Addison-Wesley Publishing, California (1990).

[110] D. W. Jordan and P. Smith, Nonlinear Ordinary Differential Equations, Clarendon Press, Oxford (1987).

[111] .M. Thompson and H.B. Stewart, Nonlinear Dynamics and Chaos, John Wiley and Sons Ltd, New York (1986).

[112] Ali Hasan Nayfeh, Introduction to Perturbation Techniques, John Wiley and Sons Ltd, New York (1993).

[113] Michael Tabor, Chaos and Integrability in Nonlinear Dynamics, John Wiley and Sons Ltd, New York (1989).

[114] Gregory L. Baker and Jerry P. Gollub, Chaotic Dynamics, Cambridge University Press, Cambridge (1990).

[115] J. Froyland, Introduction to Chaos and Coherence, Institute of Physics Publishing, Bristol (1992).

[116] A.R. Bishop and T. Schneider, Solitons and Condensed Matter Physics, Springer-Verlag, Berlin (1978).

[117] A.S. Davydov, Solitons in Moleqular Systems, R Reidel Publishing Company, Dordrecht (1985).

[118] Στέφανος Πνευματικός, Σολιτόνια, τα μοναχικά κύματα, Πανεπιστημιακές Εκδόσεις Κρήτης, Ηράκλειο 1992.

[119] Αναστάσιος Μπούντης, Μη γραμμικές συνήθεις διαφορικές εξισώσεις, Εκδόσεις Γ. Α. Πνευματικού, Αθήνα 1997.

[120] Αναστάσιος Μπούντης, Δυναμικά συστήματα και χάος, Τόμος Α, Εκδόσεις Παπασωτηρίου, Αθήνα 1995.

[121] Αναστάσιος Μπούντης, Δυναμικά συστήματα και χάος, Τόμος Β, Εκδόσεις Πανεπιστημίου Πατρών, Πάτρα 1998.